Heparan Sulfate Mediated Transport of Basic Fibroblast Growth Factor through Extracellular Matrix

by

Christopher J. Dowd

B.E. Chemical Engineering
Vanderbilt University, 1991
M.S.C.E.P. Chemical Engineering
Massachusetts Institute of Technology, 1994

Submitted to the Department of Chemical Engineering
in Partial Fulfillment of the Requirements for the Degree of
Doctor of Philosophy in Chemical Engineering
at the
MASSACHUSETTS INSTITUTE OF TECHNOLOGY
June, 1998

Author_____
Department of Chemical Engineering
May 26, 1998

Certified by._____
Charles L. Cooney
Professor of Chemical and Biochemical Engineering
Thesis Supervisor

Certified by_____
Matthew A. Nugent
Associate Professor of Biochemistry and Ophthalmology
Boston University School of Medicine
Thesis Supervisor

Accepted by_____
Robert E. Cohen
St. Laurent Professor of Chemical Engineering
Chairman, Committee for Graduate Students

Heparan Sulfate Mediated Transport of Basic Fibroblast Growth Factor through Extracellular Matrix

by

Christopher J. Dowd

Submitted to the Department of Chemical Engineering
on May 26, 1998, in partial fulfillment of the
Requirements for the Degree of
Doctor of Philosophy in Chemical Engineering

Abstract

Normal tissue function is dependent on local communication between cells. Extracellular signaling can take the form of secreted soluble growth factors, and the extracellular matrices in which the cells are embedded can regulate this signaling. The goal of this project was to develop mathematical and experimental models of extracellular growth factor transport using a specific extracellular matrix model, Descemet's membrane (DM), and a specific growth factor, basic fibroblast growth factor (bFGF). Experimental evidence suggests that extracellular matrices may act as reservoirs of bFGF through the interaction of bFGF with a specific component of the matrix, heparan sulfate (HS). Our mathematical model of bFGF transport through Descemet's membrane encompassed free diffusion of bFGF through the interstices of the DM matrix, coupled with reversible association of bFGF to the DM HS. In order to obtain values for the critical parameters in the model, the HS from the DM was extracted and purified. The kinetics and thermodynamics of the bFGF/HS interaction were measured. The effective diffusivity of bFGF in the DM was determined under conditions where bFGF could not associate with HS. The results from the biochemical characterization of the DM HS were incorporated into the mathematical transport model in conjunction with the diffusion study results. The process of bFGF transport across the complex DM tissue was found to be well represented by this model. The mathematical model was used to explore various *in vivo* scenarios. These studies demonstrated that the extracellular matrix can act as a highly responsive reservoir of bFGF, and that HS containing matrices can stabilize steep local concentration gradients of the growth factor. This project has laid the groundwork for a quantitative understanding of how extracellular matrices can regulate growth factor activity. As a modulator of cell growth and differentiation, the unregulated activity of bFGF can contribute to tumor growth and blood vessel occlusion. Ultimately, a fundamental, quantitative understanding of the role of ECM in regulating the bioavailability of growth factors could provide insights into the mechanisms of these disorders, and could help in designing therapeutic approaches to modulate endogenous growth factor activity.

Thesis Supervisor: Charles L. Cooney
Professor of Chemical and Biochemical Engineering

Thesis Supervisor: Matthew A. Nugent
Associate Professor of Biochemistry and Ophthalmology
Boston University School of Medicine

This Thesis is Dedicated to
My Grandfather

Robert A. Murphy

Acknowledgements

I'd like to thank my two advisors Prof. Charlie Cooney and Prof. Matt Nugent for their invaluable guidance throughout this work.

The members of the Nugent and Cooney labs provided support, fruitful discussions, and even more entertaining not-so-fruitful discussions: Michael, Gizette, Tom, Kim, John, Jack, Christine, Raju, Steffen, Ranga, Ganesh - Thanks.

The Whitaker Foundation and the NIH Biotechnology Training grant provided the all important funding for this research.

Bill Ryan's technical assistance throughout the project was indispensable, and I'd like to thank Coran-Sholes for generously allowing me to use their glass sand blasting equipment.

Professor Edward Merrill provided critical guidance in producing heparin/polyacrylamide gels. Ken Wright at the MIT High Voltage Research Lab operated the electron beam equipment used to link heparin to the polyacrylamide and provided important technical assistance in this aspect of the project..

I'd like to acknowledge the herd of cattle in northern Texas that each contributed to the project in their own special way.

Janet Fischer and Elaine Aufiero in the graduate student office are the heart of the department. I'd like to thank them both taking care of all the details of my grad school career.

The chemical engineering intramural sports program has given me countless hours of much needed diversion. I'd like to thank each of my teammates for not grudging me all those shots, but after 7 years I think the number (of teammates) might run into the hundreds.

My Ph.D. has not be all work, there's been some skiing, a little basketball, a few SCUBA dives, and an occasional beer. The usual suspects deserve recognition: Fred, Antonia, Matt, Justin, Mark, Karen, Dave....

My parents and sister have been a constant source of support and encouragement , and I owe my present success entirely to them.

Radha, my wife, has done more for me than I could write in this entire thesis, let alone this little corner of text, so I'll leave it at that.

Contents

List of Figures

List of Tables

Chapter 1

Background

1.1 Introduction

The analogy has been made that growth factors make up the alphabet of an intricate cell signaling language [1]. As modulators of cell growth and differentiation, growth factor activity must be tightly regulated to ensure the normal functioning of the organism as a whole. Basic fibroblast growth factor (bFGF) represents a prime example of this phenomenon. bFGF is a particularly potent cytokine that has been implicated in processes which include angiogenesis, wound healing, and embryonic development. *In vitro* and *in vivo* experimental evidence suggests that one control strategy involves an extracellular storage mechanism. Basic FGF is sequestered in a specialized extracellular matrix, the basement membrane, by binding to resident heparan sulfate proteoglycan. The objectives of this project were to elucidate the mechanisms of storage and release of bFGF from basement membrane, and to formulate a mathematical model to describe this system.

The biological problem of bFGF regulation bears a strong resemblance to the classical chemical engineering problem of transport coupled with chemical reaction. This project considered bFGF diffusion through the matrix with reversible binding to the heparan sulfate proteoglycan. The rates of diffusion and reaction were influenced by the properties of the basement membrane, the resident heparan sulfate proteoglycan , and the growth factor itself. Consequently, this simple scenario could only be evaluated and

attacked by understanding the basement membrane, the proteoglycan, the growth factor, and their interactions. This concept provides the structure for the background section in which each of the three elements and their interactions are described.

1.2 The Basement Membrane: Descemet's Membrane

Basement membranes are specialized extracellular matrices (ECM) that form a thin lining along the basal surface of endothelium or epithelium in the vasculature, the nervous system, the dermis, and both smooth muscle and skeletal muscle. These ECMs provide structural support, influence the growth and differentiation of cells resting on them, and act as a permeability barrier.

Basement membranes range in thickness from 0.05 μm to 100 μm [2]. Although they appear amorphous under the light microscope, electron microscopy reveals three layers in most basement membranes: the lamina lucida, the lamina densa, and the lamina recticularis [3]. It is worth noting, however, that studies by Chan et al. [4] and Goldberg and Escaig-Haye [5] raised the possibility that the lamina lucida may be an artifact of the electron microscopy preparation process.

As many as 50 different proteins have been isolated from the basement membrane of the Englebredth-Hoth-Swarm (EHS) tumor, a typical experimental basement membrane model [6]. Basement membrane composition is, to some extent, a function of the cell type, the tissue source, and the stage of tissue development [3]. Despite this apparent complexity, four principle components are present in virtually all basement membranes: collagen IV, laminin, heparan sulfate proteoglycan (HSPG), and nidogen /entactin. Depending on the source of the basement membrane, varying quantities of other proteins and proteoglycans also may be present. Unlike the fibrillar collagens found in tendons and cartilage, collagen IV forms a protein meshwork that acts as a scaffolding for the assembly of the other structural components of basement membranes [7]. The four

major components associate with each other through strong non-covalent interactions, and, as a result, most basement membranes can only be solubilized under harsh denaturing conditions. Table 1.1 summarizes the sizes, the concentrations in the EHS tumor, and the functions of these molecules.

Macromolecule	MW (kD)	Molar Conc. (μM)	Function
Collagen IV	550	11	structural support, network assembly
Laminin	800	13	cell binding, structural
Nidogen (entactin)	150	7	modulates laminin binding
high density HSPG	130	5	Multiple interactions, permeability, growth factor binding
low density HSPG	650	1.4	

Table 1.1 EHS tumor basement membrane composition

The components of the insoluble matrix constitute only a small fraction of the actual mass of the basement membrane; as much as 90% of the basement membrane may be water [8]. HSPGs are macromolecules consisting of heparan sulfate (HS) chains attached to a protein core, and these highly charged HS chains are responsible for hydrating the matrix. Although they represent less than 10 % of the dry weight of the basement membrane, the hydrated HS chains occupy most of the volume. As might be expected, a significant fraction of the water in the basement membrane may be closely associated with the GAG chains [8]. Consequently, not all of the water in the basement

membrane is "free" [8] and the physical meaning of aqueous concentrations must be carefully considered.

Descemet's membrane

Descemet's membrane (DM) is the basement membrane of the corneal endothelium. Descemet's membranes can be as much as 100 μm thick, as compared to 100 nm for the glomerular basement membrane. Consequently, it is one of the few basement membrane that can be dissected from an organism and used intact in diffusion experiments. Figure 1.1 illustrates the location of the DM inside the eye. It is sandwiched between the corneal stroma and the endothelial cell monolayer along the posterior surface of the cornea. The DM provides a substrate for the endothelial cell monolayer and controls molecular traffic between the endothelium and the corneal stroma.

Descemet's membrane has been characterized biochemically [9]. Although it contains type IV collagen [10, 11], the major collagen of Descemet's membrane appears to be a novel type VIII collagen [12, 13]. Immunostaining has confirmed the presence of the other major basement membrane proteins: laminin, perlecan HSPG, entactin, and fibronectin. However, laminin appears to be present in lower levels than in other basement membranes [14]. The ultrastructure of the DM, as determined by electron microscopy of freeze etched membranes, appears to be based on a lamellar hexagonal lattice of 80 nm nodes connected by rods approximately 120 nm long and 25 nm in diameter as seen in Figure 1.2. A finer filamentous system of 5-10 nm thick filaments overlays the entire structure [15]. Similar structures have been observed in other

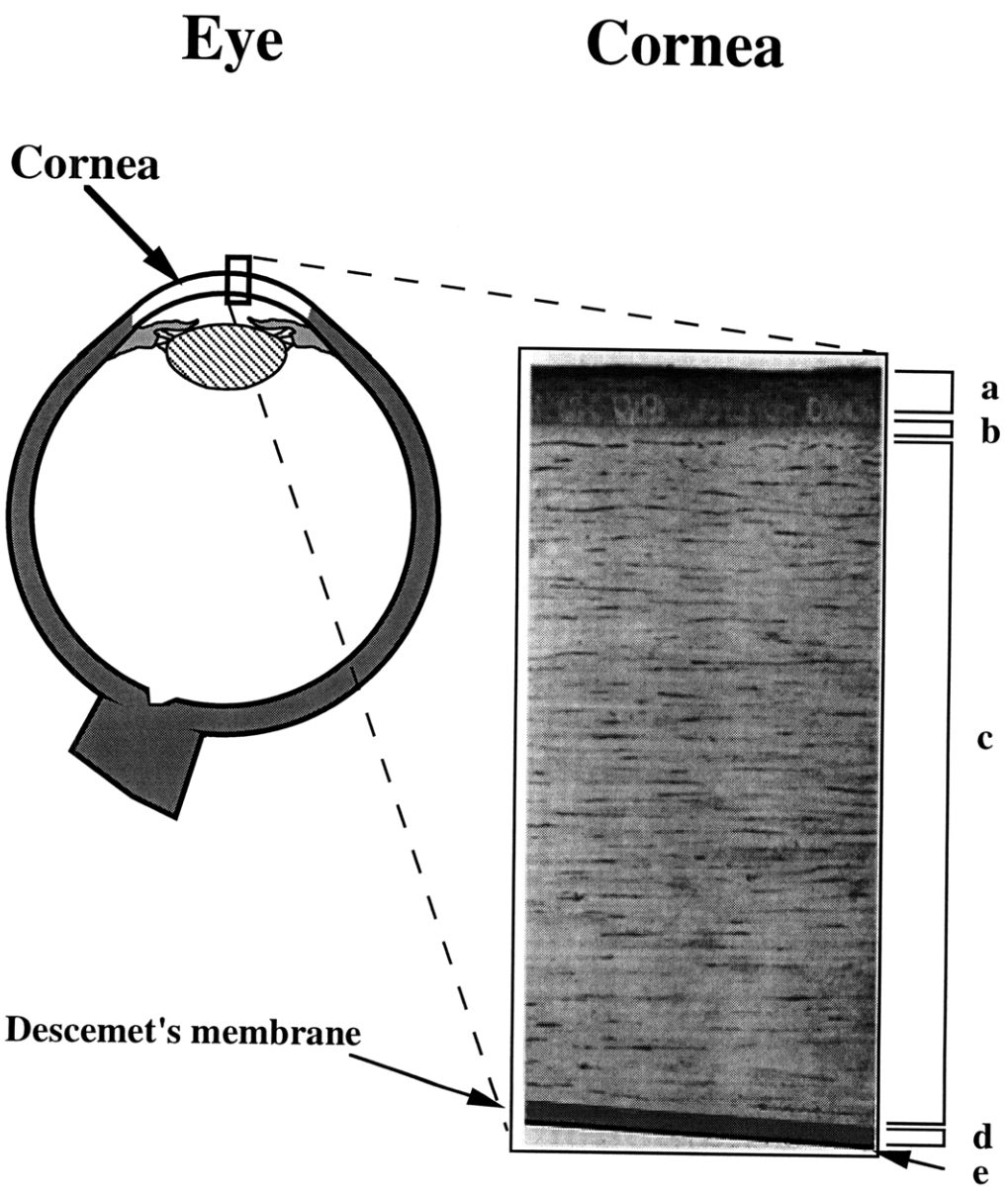

Figure 1.1 Descemet's Membrane: The major layers of the cornea are shown in this 200 x magnification light micrograph of a complete section of the human cornea: epithelium (a), Bowman's layer (b), corneal stroma (c), Descemet's membrane (d), and the endothelium (e). The endothelial monolayer appears as a thin dark line below the thicker Descemet's membrane.

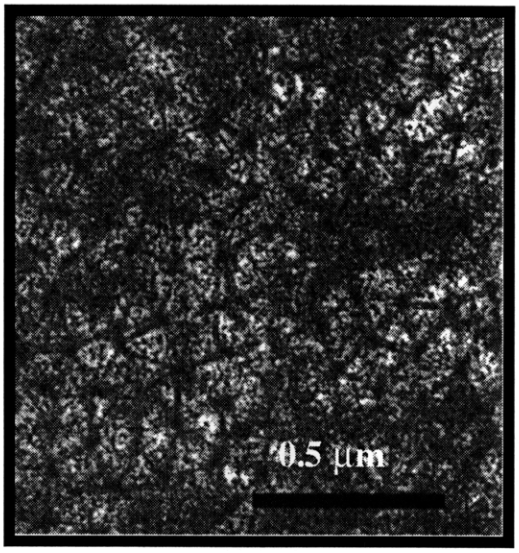

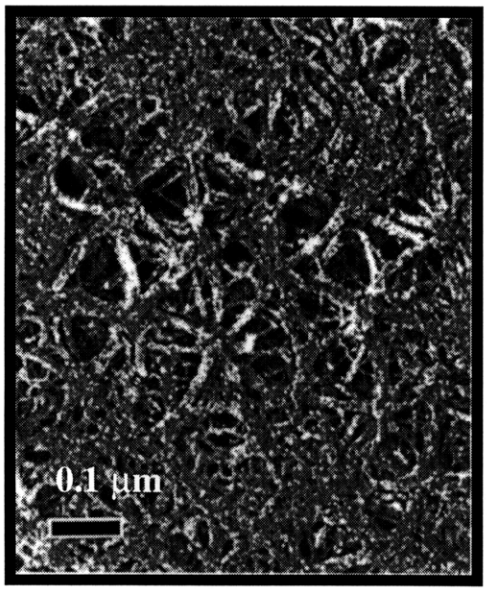

Figure 1.2 DM Ultrastructure: The hexagonal ultrastructure of the DM is revealed in these electron micrographs of freeze-etch replicas (Sawada, 1982).

basement membranes [16]. The acellular nature of the DM, the large comparative size, and the accessibility of the tissue for dissection made it an attractive model extracellular matrix. Furthermore, the DM was the first extracellular matrix shown to be a site for bFGF storage *in vivo* [17], and has been used as a model for the bFGF matrix storage hypothesis.

Basement membranes have a complex architecture arising from the multiple interactions between its protein and proteoglycan components. However, the transport of bFGF through the matrix is probably dominated by bFGF's interaction with the basement membrane HSPG and by its reduced mobility through the dense gel-like network within the basement membrane.

1.3 The Proteoglycan

Proteoglycans consist of one or more glycosaminoglycan (GAG) chains covalently attached to a protein core. The GAG chains are highly charged carbohydrate polymers and have very different physiochemical properties than the core protein. Consequently, proteoglycans are multi-functional macromolecules that are important to physiological processes that range from modulating growth factor activity to providing compression resistance in joints. Heparan sulfate proteoglycans, in particular, are found in virtually all basement membranes [18]. Their ubiquitous nature alone suggests important physiological roles for these macromolecules, and a wealth of experimental evidence supports this supposition. HSPGs have been implicated in atherosclerosis, kidney disease, and Alzheimer's disease; furthermore, the association of growth factors with HSPGs has been connected with angiogenesis, wound healing, and tissue development. Before the larger physiological roles of the basement membrane HSPG can be understood, however, the macromolecule's structure and function must be appreciated.

1.3.1 The Glycosaminoglycans

The glycosaminoglycans are a large family of carbohydrates that include heparin and heparan sulfate in addition to chondroitin sulfate, dermatan sulfate, keratan sulfate, and hyaluronic acid. These carbohydrates are unbranched, acidic, polyanionic chains typically built from a repeated disaccharide sequence of a uronic acid and hexosamine. Figure 1.3 presents the representative disaccharide building blocks for the major non heparin / heparan sulfate GAGs.

Hyaluronic acid differs from the other GAGs in that it has no sulfate groups associated with it. Chondroitin sulfate may be sulfated at the 4 or 6 position of the hexosamine and, in some cases, in the 2 position of the uronic acid, resulting in some structural heterogeneity. All of the GAGs except hyaluronic acid are initially part of a proteoglycan. The GAGs are found primarily as constituents of various extracellular matrices and connective tissues such as skin, bone, arterial walls, synovial fluid, cartilage, and vitreous humor. Their distribution, molecular weight, and composition are dependent on the specific tissue and its state of development [19], [20],[21].

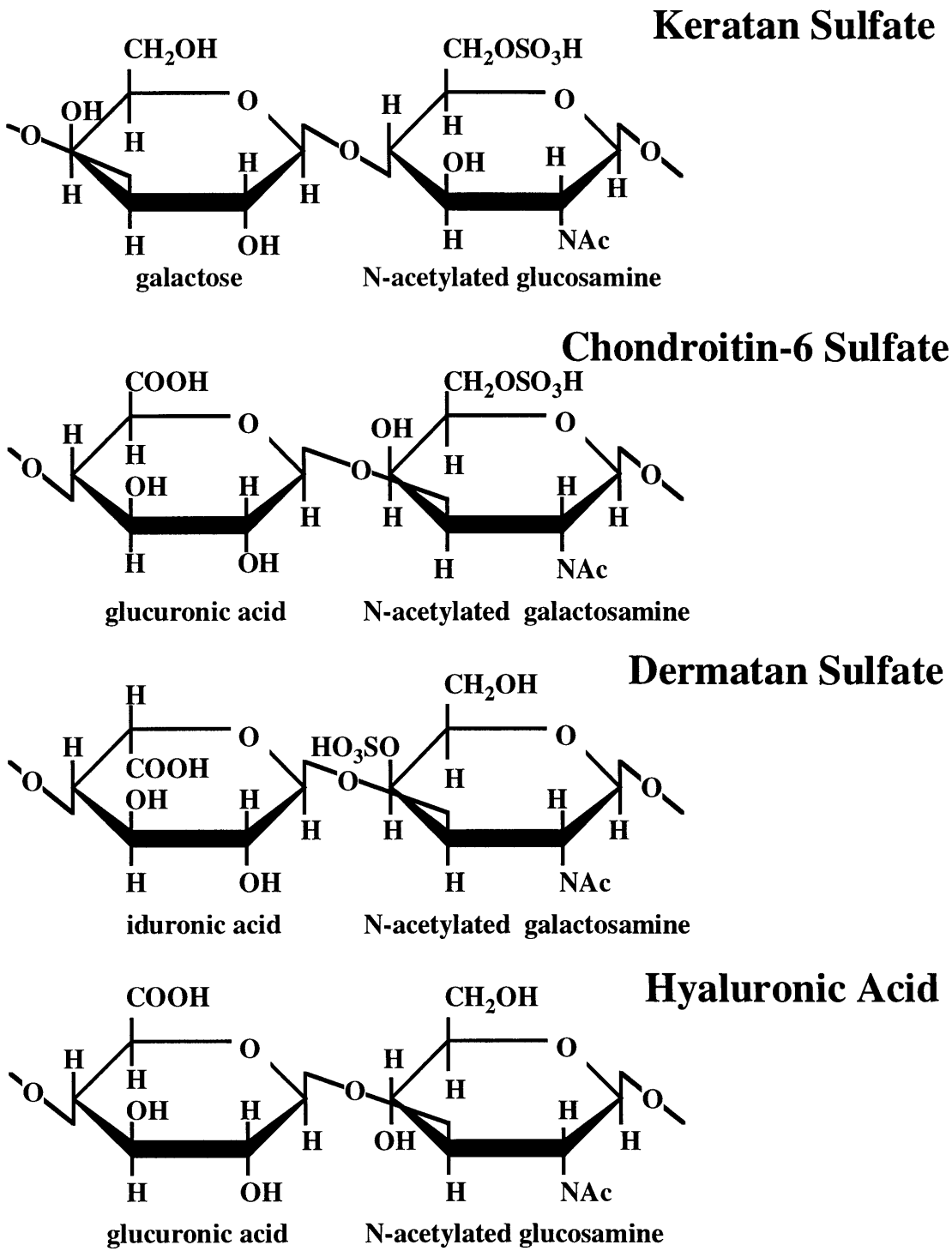

Figure 1.3: GAG Disaccharide Structures

1.3.2 Heparan sulfate vs. Heparin

Heparan sulfate and heparin exhibit the greatest degree of compositional heterogeneity of all the GAGs. Both molecules have common features, but it is important to understand the distinctions that have been made between these GAGs [22]. Figure 1.4 depicts the basic structural units of HS and heparin.

Both HS and heparin contain either iduronic acid (IdoA) or glucuronic acid with a β1-4 linkage to glucosamine (GlcN). The glucosamine may be N-acetylated or N-sulfated, and it may be O-sulfated at position 6 or, rarely, at position 3. Sulfation of the uronic acid is restricted to the 2 position [18]. Four possible forms of the uronic acid (UA) and six forms of the hexosamine have been experimentally identified, resulting in 17 possible UA-GlcN combinations and 10 possible GlcN-UA combinations [23].

HS was initially identified as the fraction of heparin in industrial preparations which lacked anticoagulant activity. Regions of heparin-like structure, however, have been discovered in HS chains, and sequences that confer anticoagulant activity on the HS also have been identified [24]. Heparins have, on average, twice the degree of sulfation of heparan sulfates and have increased levels of both N-and O-sulfation. Trisulfated disaccharides are common in heparin, and iduronic acid is the dominant form of uronic acid. Glucuronic acid predominates in HS, and N-acetylation is more common. Table 1.2 summarizes these differences.

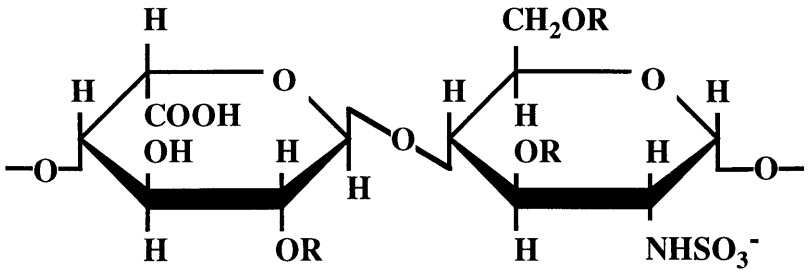

Iduronic Acid **N-Sulfated Glucosamine**

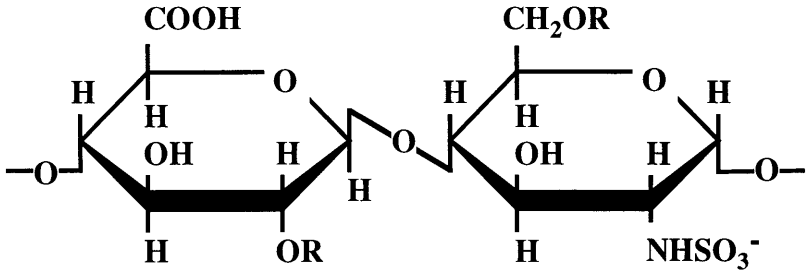

Glucuronic Acid **N-Sulfated Glucosamine**

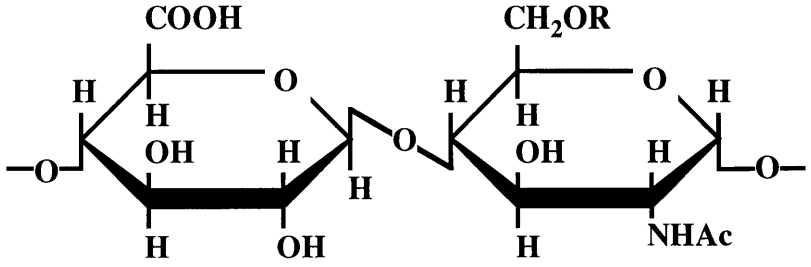

Glucuronic Acid **N-Acetylated Glucosamine**

Figure 1.4: Disaccharide Structures in Heparan Sulfate and Heparin (R=H or SO_3^-)

	heparan sulfate	heparin
dominant uronic acid	glucuronate	iduronate
uronic acid sulfation sites		C2
glucosamine sulfation sites	C6	C6, C3
amine group substituent	acetyl	sulfate

Table 1.2 Generalized comparison of heparin and heparan sulfate structures

A more restrictive biological perspective might classify heparins as the products of the mast cell proteoglycan serglycin, and all other cell membrane and ECM associated heparin-like molecules as heparan sulfate [25]. Bearing these factors in mind, heparan sulfate will be the focus of the remainder of this document.

1.3.3 Structure of Heparan Sulfate

With the recognition of heparan sulfate's physiological importance, increasing amounts of research are being devoted to the mapping of these macromolecules and identifying functionally significant sequences. However, the polydisperse, microheterogeneous nature of heparan sulfate hampers these efforts. Information about the sequence has come largely from degradation studies using specific enzymes and chemical methods. Three endoglycosidases, heparinases I, II, and III, have been isolated from *Flavobacterium heparanum* , and each has a different specificity for heparin/HS disaccharide linkages [26]. In general, heparinase I cleaves between the glucosamine and an iduronic acid residue, heparinase III cleaves between glucosamine and a glucuronic acid residue, and heparinase II cuts nonspecifically between either uronic acid and the glucosamine. Low pH nitrous acid degradation attacks the linkage adjacent to N-sulfated

glucosamines and deaminates in the process. A better understanding of heparan sulfate structure is emerging through the use of these degradative tools [22], [26].

HS fine structure is determined by the substituents of the amine group. Two generalizations can be made: iduronic acid residues are found attached to the C1 carbon of N-sulfated glucosamines, and O-sulfates are found exclusively on disaccharides attached directly to GlcNSO3 [18]. A brief look at the predicted stepwise mechanism of HS synthesis can explain these constraints.

The GAG chains are believed to be synthesized initially as homogeneous chains of unsulfated N-Ac-glucosamine and glucuronic acid attached to a protein core via a carbohydrate linkage region. A series of modifications are performed on the chain with each alteration dependent on the preceding one. Deacetylation/N-sulfation takes place first, and subsequent epimerization of the uronic acid C5 converts glucuronic acid to iduronic acid. Sulfotransferases catalyze the final modifications [27]. The micro heterogeneity in HS arises because these reactions do not proceed to completion. Regions that are N-acetylated tend to lack further modifications [28]. This biosynthetic mechanism produces domains of high and low sulfation. Regions of N-sulfation, high iduronic acid content, and high degrees of O-sulfation are separated by longer stretches of N-acetylated glucosamine/glucuronic acid disaccharide repeats with little sulfation. Turnbull and Gallagher [29] relied on the differing specificities of heparinase I and II to verify this hypothesis. Heparinase I cleaved the GAG in 4 to 5 places, while heparinase III degraded the remaining fragments. Although the overall structural theme in heparan sulfate is one of alternating regions of high and low modifications, significant portions of the molecule have alternating N-sulfated and N-acetylated disaccharides.

The significance of heparan sulfate structure and the distinction between HS and heparin lies in the relevance to protein binding. It is likely that protein binding sites are localized in the modified, highly sulfated regions of the HS chains. These areas have the highest charge density as well as the greatest conformational flexibility due to their

iduronic acid content [21]. Ishihara engineered a cell line to overexpress the enzyme responsible for deacetylation and the transfer of sulfate groups to the nascent heparan sulfate chain. This mutant produced much heparan sulfate with an increased number of highly sulfated regions and contained a high content of 2-O sulfated iduronate. The resulting chains demonstrated a much higher affinity for bFGF [30]. The overall microheterogeneity of the HS chains probably results in a distribution of sites with varying binding affinities for a given protein.

1.3.4 Basement Membrane Proteoglycan

In the last few years, several proteoglycan core proteins have been isolated and cloned. Classification of proteoglycans based on core proteins are now beginning to replace the older system based on the composition of the GAG component. Proteoglycans are important elements of synovial fluid, cartilage, and other ECMs. Likewise, cell surface proteoglycans, particularly HSPGs have important physiological roles. We focus here, however, on the basement membrane proteoglycans.

Both chondroitin sulfate proteoglycans and heparan sulfate proteoglycans are found in basement membranes, but HSPGs appear to be the dominant form. 75% of the GAG produced by EHS tumors is HS. Antibodies made against the core protein of a CSPG from the rat parietal yolk sack have been shown to stain all basement membrane's except the kidney glomerular basement membrane [31]. The bulk of the work performed with basement membrane proteoglycans, however, has centered on HSPGs.

HSPG distribution in basement membranes

Immunostaining of various tissues using antibodies to the major HSPG of the EHS tumor basement membrane, perlecan, have localized HSPGs to the basement membranes of skeletal and cardiac muscle, alveoli and bronchi, and the vasculature [32]. Work by Heremans et al. [33] identified HSPGs in basement membranes of the endothelia

and epithelia of skin, trachea, liver, kidney, placenta, and the umbilical cord. Efforts also have been made to determine the distribution of the proteoglycan within the basement membrane, but the results have been somewhat contradictory. Early work by Kanwar and Farquhar [34] using a cationic dye, ruthenium red, with the glomerular basement membrane suggested that the HS chains of the HSPG were restricted to the lamina lucida. Schittny et al. [35] used antibodies to the proteoglycan and demonstrated uniform staining of Descemet's membrane.

Two studies have examined the HSPG distribution in Descemet's membrane. Schittny et al. [35] observed that sectioned mouse corneas stained with an antibody for the protein core of perlecan and visualized with a secondary antibody containing a fluorescent conjugate showed apparent selective staining of the DM along the edges of the tissue. However, when sections exposed to the specific perlecan antibody were visualized on the electron microscope using protein-A linked to gold, homogenous staining was observed. The authors attribute the differences to experimental artifact in the fluorescent study as a result of the cryofixation. Ljubimov [14] performed a similar fluorescent immunostaining study with perlecan antibodies in the human eye. He observed selective staining of the endothelial face of Descemet's membrane. Given the conflicting results described here, the results of cryofixation followed by fluorescent immunostaining of the DM must be interpreted carefully. Perlecan is probably exists throughout the full thickness of the cornea. However, higher concentrations of this proteoglycan may exist on the endothelial face of the DM.

HSPG forms in basement membranes

Hassell et al. [36] isolated high and low density forms of EHS-HSPG on a CsCl gradient. The high density forms represented several molecular weights, whereas the low density proteoglycan, representing the major HSPG fraction, appeared to consist of core proteins of 350 and 400 kD. The GAG chains were 60 to 70 kD. Antibodies to

the low density form cross-reacted with the high density form, but the reverse was not true. These results suggested that the smaller, high density HSPG might represent proteolytically processed forms of the low density HSPG. A pulse/chase study with EHS-HSPG by Ledbetter et al. [37] indicated that the high density HSPGs were the products of low density HSPG, and work with the glomerular basement membrane HSPG indicated that smaller forms of that proteoglycan arose from a 400 kD precursor [38]. These studies are in contradiction to those by Kato et al. [39] and Paulsson et al.[40] who performed pulse/chase work and characterization studies of the HSPG, respectively. The current reasoning holds that the large low density HSPG is sensitive to proteolytic digestion and is a precursor of some of the high density basement membrane forms, while others probably represent different proteoglycan species.

Perlecan

The HSPG localization studies in different tissues and species mentioned above provided evidence that the 400 kD core protein containing low density HSPG, initially isolated from the EHS, is in fact a ubiquitous basement membrane HSPG in vertebrates [31]. Since its isolation, this molecule has been characterized extensively. Paulsson et al. [40] characterized the proteoglycan with rotary shadowing. This technique revealed a core protein that was 80 nm long containing 6 globular regions and 3 heparan sulfate chains. The sequence of the murine version of this HSPG was published by Noonan et al. [41] and they named the molecule "perlecan". The sequence of the human form followed in papers by Kallunki and Tryggvason [42] and Murdoch et al. [43]. All of these studies depict a large molecule with 5 domains, and homologies to the LDL receptor, the laminin short arm, and N-CAM (neural cell-adhesion molecule). Linkage sites for the HS chains were localized to the N-terminus of the protein.

Heparan sulfate proteoglycans determine many of the gross properties of basement membranes, such as: structure, permeability, charge density, and hydration.

While the heparan sulfate chains appear to be the primary determinants of these properties, the roles of the multidomained perlecan HSPG are only now emerging. On a molecular level, the interaction of the basement membrane heparan sulfate chains with bFGF may be a key step in modulating growth factor activity.

1.4 The Growth Factor

Basic fibroblast growth factor is a member of a larger family of pluripotent cell signaling molecules. The FGF family is made up of at least nine different growth factors that have sequence similarity and that bind heparin. The prototypical molecules of the group, bFGF and acidic FGF (aFGF), were initially isolated from pituitary extracts based on their ability to promote growth in fibroblasts and myoblasts, respectively. The two molecules have a 55% amino acid sequence homology, and have a similar range of activities. aFGF has a much more restricted distribution *in vivo* and is 10 to 100 times less potent than bFGF. aFGF activity, however, is elevated to the level of bFGF when it is associated with heparin [44].

bFGF is a 154 amino acid, 18 kDa, protein with a pI of 9.6. bFGF isolated from human, bovine, ovine, and rat sources demonstrates a 85-95 % homology, suggesting that the entire molecule has functional significance. Initial purifications of bFGF yielded an active, 146 amino acid, 16.5 kD polypeptide. It is now believed that this smaller form is produced by N-terminal cleavage of the nascent 18 kD protein. It is not clear what the physiological significance of this truncated form is, or whether it is actually an artifact of the purification process. Larger forms of the growth factor (196, 201, 210 amino acids) have been identified, as well. They appear to result from the use of an alternate CUG start codon. Although it is found in comparatively high concentrations in the ECM, the striking anomaly in bFGF structure is its lack of a consensus signal

sequence for export of the molecule from the cell [45]. The issue of cellular bFGF release has become the focus of much research, and will be covered later.

1.4.1 Heparin/Heparan Sulfate Interactions

bFGF has a strong affinity for heparin and the heparin-like regions of heparan sulfate. This property has been exploited through the use of heparin Sepharose columns to produce high purity bFGF. A growing body of experimental work suggests that this interaction is critical to the physiological role of bFGF. Consequently, studies have been conducted with heparin and the growth factor to elucidate the nature of this interaction Many of these experiments have been performed using heparin rather than the more biologically relevant heparan sulfate. The presence of heparin-like regions in HS, however, lends credence to the results.

The HS Binding Site on bFGF

The heparin binding site on bFGF has been the subject of much work in an effort to produce peptides that exhibit the properties of the growth factor, or to produce growth factor analogs with different properties. Two potential heparin binding sites were identified from the amino acid sequence of bFGF based on the presence of clustered basic residues. A Lys-Asp-Pro-Lys-Arg sequence was identified at the N-terminus (amino acids 18-22), and an Arg-Ser-Arg-Lys (amino acids 107-110) constituted the second site at the C-terminus [46]. A Cardin -Weintraub consensus sequence of alternating basic (B) and hydropathic residues (X), X-B-B-X-B-X, spanned residues 20 to 28 [47]. The binding of radiolabeled heparin to a series of 25 overlapping synthetic peptide fragments that encompassed the sequence of the 16.5 kD form of bFGF identified residues 24-68 and 103-120 as regions with strong affinity. Smaller fragments of these regions showed some binding also, leading the authors to conclude that the cooperative interaction of several sites could be contributing to the observed affinity [48]. A study employing

various truncated N-and C-terminal recombinant bFGFs demonstrated that the carboxy terminal region was more important to heparin binding than the N-terminal [49]. The replacement of critical arginine and lysines in the carboxy-terminus with glutamine through site directed mutagenesis produced a growth factor with reduced affinity for heparin [50]. These results seem to suggest that while both the N-and C-terminal regions of the molecule can associate with bFGF, a string of basic residues in the C-terminus is essential to high affinity binding.

The structure of bFGF, solved by X-ray crystallography seems to bear this out. A cluster of basic residues (Lys 26, Arg 44, Lys 119, Arg 120, Lys 125, Lys 129, Lys 135) dominated by C- terminal amino acids forms a potential heparin binding site on the surface of the cytokine [51, 52, 53]. Crystal structures of bFGF complexed with a homogeneous preparation of heparin hexasaccharide fragments revealed two binding regions on the growth factor [54]. Asparagine-28, arginine-121, lysine-126, and glutamine-135 formed one site, while lysine-27, asparagine-102, and lysine-136 formed the second site. It should be noted that the amino acid numbering scheme for this crystal structure was off-set by one residue from previous reports [51, 52, 53]. A comparison of the bFGF/heparin complex with crystal structure data of bFGF alone confirmed that bFGF does not undergo a conformational change with binding to heparin. Figure 1.5 shows the heparin binding region on a spacefilling model of bFGF.

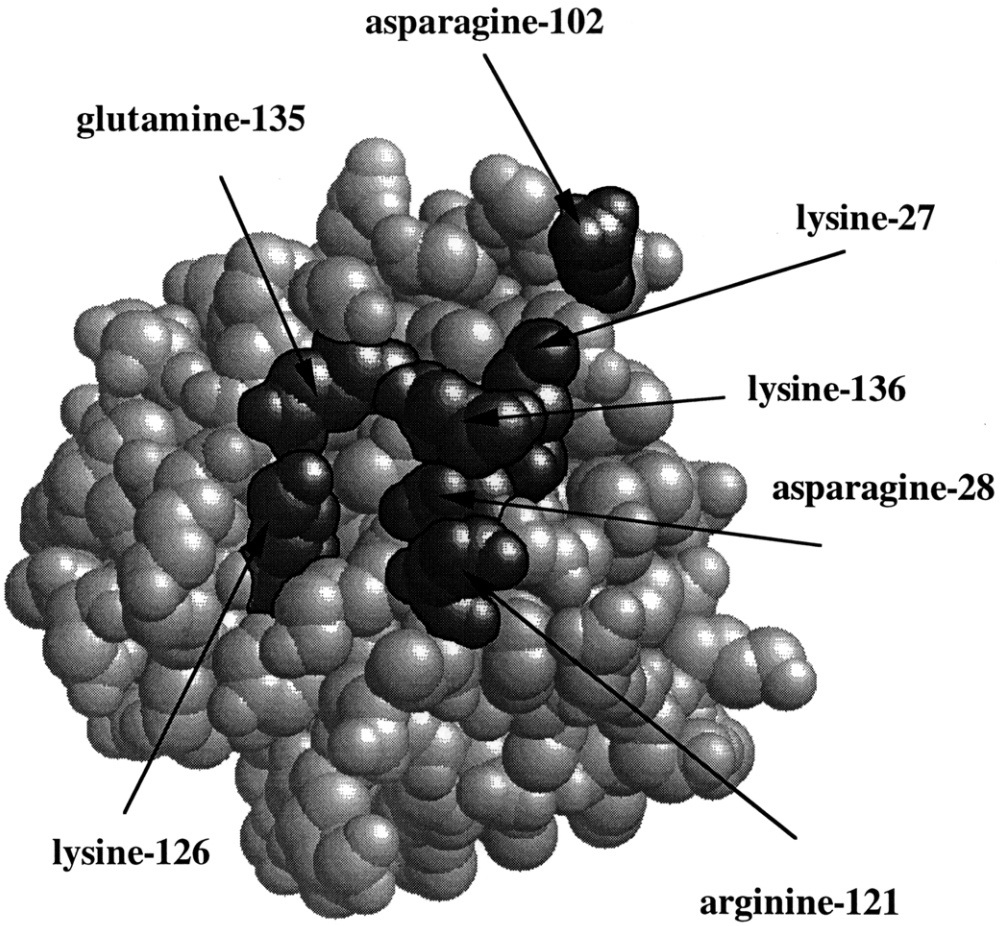

Figure 1.5 Heparin Binding Site on bFGF: The heparin binding site on bFGF was determined by X-ray crystallography of a complex of bFGF with homogeneous heparin hexasaccharides (Faham, 1996). X-ray crystal structure data was obtained from the Brookhaven National Lab Crystal Structure Data Base (Abola et al., 1987), (Bernstein et al., 1977). The visualization was generated using RasMol v2.6 (Sayle, 1995).

bFGF binding site on Heparin /HS

Experiments designed to identify sequences or patterns in HS and heparin that associate with the growth factor typically involve partial enzymatic or chemical digestion of heparan sulfate or heparin followed by fractionation on a bFGF affinity column. Habuchi et al. [55], determined that regions with high $IdoA(2SO_4)GlcNSO_3$ content appear to be critical to the interaction. Turnbull et al. [56] obtained similar results and found that the highest affinity tetradecasaccharide in their preparations contained 74% $IdoA(2SO_3)a1,4GlcNSO_3$, with a 6 SO_4 content of only 1%. The authors concluded that $IdoA2SO_3$ content and fragment size were important to binding. In studies performed with heparin oligosaccharides, similar results were obtained by Ishihara et al. [57] and Tyrrell et al. [58]. bFGF does not recognize a specific sequence in heparin or HS analogous to ATIII; this confirms that a small set of sequence variations do exist with a high affinity for bFGF.

bFGF stabilization by Heparin/HS

The bFGF/GAG interaction appears to both protect and stabilize the growth factor. Initial studies showed that heparin could stabilize the growth factor when it was exposed to heat and acid as well as restore the activity of bFGF that had been stored at -80C [59]. Saksela et al. [60] showed that HS purified from cultured bovine capillary endothelial cells could protect bFGF from destruction by extracellular proteases and plasmin in particular. These results suggest that *in vivo,* binding of bFGF to heparan sulfate could significantly prolong the life of the growth factor. This finding is central to the concept that the ECM acts as a storage site for growth factor, perhaps harboring it until needed. Thus, the ECM may be in the regulatory pathway of growth factor stimulation of cell growth.

1.4.2 Mechanism of Action: Cellular Release and Receptor Interaction

Figure 1.6 is a pictorial representation of bFGF's mechanism of action simplified to four major steps. bFGF is initially released from the cell into the matrix. Step two encompasses the focus of this research, the diffusion, binding, and storage of growth factor in the matrix. Eventually, the growth factor binds to low and high affinity receptors on the cell surface, and it ultimately influences the cell through intracellular mechanisms that are lumped here into step four To understand bFGF transport through the basement membrane, step two, it is important to understand how bFGF may be released from cells into the matrix and how it subsequently interacts with the cell surface receptor once it has left the matrix in steps one, three, and four.

Cellular Release

The absence of a signal sequence on bFGF seems to conflict with several pieces of evidence that suggests it has an extracellular mode of action. It is deposited into the extracellular matrix of cultured cells and into the basement membranes of tissues *in vivo*. Cells possess surface receptors for the growth factor, and anti-bFGF antibodies can block the affects of bFGF. This paradox has prompted research toward determining how this cytokine is released from the cell. Initially, it was proposed that the growth factor might be released attached "piggy back" on nascent heparan sulfate chains. This hypothesis seems unlikely because it still requires that bFGF penetrate an internal cell membrane [61].

The concept that bFGF may be released through lethal or sub-lethal rupture of the plasma membrane has received much attention. A series of experiments by Gajdusek and Carbon [62] with bovine aortic endothelium demonstrated that, *in vitro* , cell lysis or acute injury released up to 50% of the total cell associated growth factor into the ECM. Heparin acted competitively to release bFGF from its binding sites in the

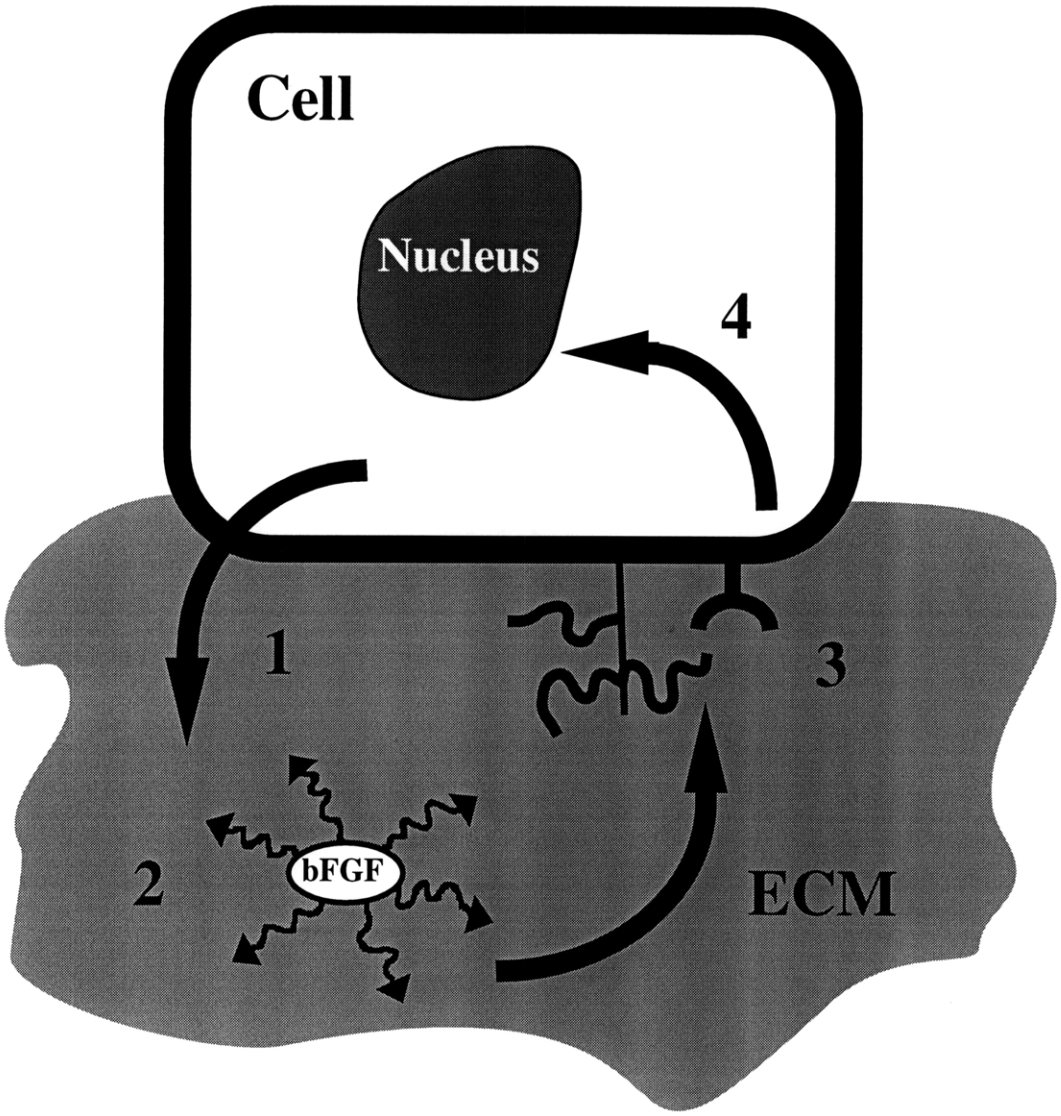

Figure 1.6 bFGF Mechanism of Action: A schematic representation of bFGF's mechanism of action involves (1) cellular release, (2) matrix storage, (3) interaction with the cell surface HSPG and the FGF receptor, and (4) intracellular signal transduction to the nucleus.

matrix; furthermore, heparinase released bFGF from the matrix as well. These observations led them to conclude that HSPGs were the binding sites in the ECM. Lastly, the authors found that a baseline level of 10% of the total growth factor was deposited into the ECM without cell lysis. Work with bovine retina endothelial cells in monolayer showed that bFGF release into medium correlated with cell damage and lysis [63]. McNeil et al. [64] have proposed that bFGF is released through transient disruption of endothelial cell plasma membrane in response to mechanically induced stress. These researchers demonstrated that scraping of the culture released bFGF activity, and that the release did not correlate with cell death or with disruption of the ECM.

Some evidence does exist for a novel secretory pathway for bFGF other than cell death. Irradiation of cultures of bovine, porcine, and human endothelial cells releases platelet derived growth factor activity as well as bFGF [65]. The authors point out that cell death alone cannot account for the quantity of released mitogenic activity, and they conclude that the growth factor must be secreted. They do not, however, address the issue of non-lethal cell rupture. Mignatti et al. [66] were able to correlate the migratory activity of NIH 3T3 transfected with a viral vector expressing bFGF with the amount of bFGF released. The experiments used extremely low cell titers to avoid interference from bFGF released due to cell lysis. The authors showed that reagents that disabled the ER-Golgi pathway for extracellular secretion of the growth factor did affect cell migration. Chemicals that impeded general vesicular endo- and exocytosis did not affect the cells. These results indirectly point to a novel transport mechanism for bFGF.

None of the above experiments conclusively point to only one means of release of bFGF from the cell; there may be multiple release mechanisms. Further research is required to elucidate the most relevant physiological mechanisms of release.

Receptors

A great deal of work has been devoted toward determining the mechanisms of bFGF/receptor interactions. The co-receptor theory holds that binding of bFGF involves low affinity heparan sulfate receptors and high affinity tyrosine kinase receptors. Moscatelli [67] identified approximately 600,000 low affinity heparin-like receptors (Kd of 2 nM) per baby hamster kidney cell, and about 80,000 high affinity sites (Kd of 0.02 nM) on the same cells. He found low and high affinity binding sites on several cell types. In a subsequent study Moscatelli [68] confirmed that receptors were down regulated in response to bFGF. Two separate studies demonstrated that heparan sulfate or heparin is essential to bFGF cell signaling. Rapraeger et al. [69] showed that treatment of Swiss 3T3 fibroblasts with heparinase or chlorate (to block sulfation) reduced binding of bFGF to its high affinity receptor and inhibited the proliferation of these cells in response to bFGF. In a second study [70] CHO cell mutants defective in heparan sulfate production that were transfected with the bFGF receptor did not bind bFGF. The addition of exogenous heparin, however, restored binding. Nugent and Edelman [71] demonstrated that the difference in equilibrium dissociation constant for the high affinity cell surface receptor and the lower affinity HSPG can be attributed to differences in the kinetic off rate constants for the two different binding events, and that the HSPG appeared to stabilize the interaction of bFGF with the cell surface receptor, resulting in a "high affinity" interaction. Fannon and Nugent [72] went on to show that the HSPG sites are not absolutely required for binding, internalization, or stimulation of mitogenic activity.

Extensive characterization work has been performed on the high affinity site. 5 different FGF receptor homologues have been identified: flg, bek, FGFR3, FGFR4, and flg-2. They appear to constitute a new family of tyrosine kinase receptors. A mechanism of action has been proposed for these receptors. Upon binding bFGF, the receptors oligomerize and subsequently undergo autophosphorylation. This activated form of the receptor can then, in turn, phosphorylate several potential substrates. The substrates may

possess catalytic activity that is regulated by phosphorylation, thereby allowing them to initiate a second messenger system which ultimately may be responsible for some of bFGF's functions [73].

1.4.3 Expression and Activity

Since its isolation and characterization, bFGF has been identified in every tissue studied. Its ubiquitous expression is matched by its diverse affects on numerous cell types. The study of this particular growth factor is justified by its wide range of sources and its potential influence on several important physiological processes.

Localization of Expression

bFGF is synthesized by a variety of cells in culture. The prevalence of bFGF in many cell cultures raised questions about the validity of extrapolating *in vitro* data to the *in vivo* situation. Tissue localization studies, however, have found bFGF in many tissues of mesodermal or neuroectodermal origin, including brain, pituitary, retina, corpus luteum, adrenal gland, kidney, placenta, prostate, thymus, bone and the immune system. [74]. These localization studies are described in greater depth in the section on bFGF and the ECM.

In vitro Biological Activities

In vitro, bFGF has manifested a variety of different effects on target cells. Many of the same cell types that secrete the growth factor also are sensitive to it. As a growth factor bFGF is a potent stimulator of DNA synthesis and cell proliferation. In cell culture this activity usually postpones the onset of cell death [75]. bFGF has been shown to be chemotactic for endothelial cells. It also induces cultured endothelial cells to secrete plasminogen activator and collagenase. *In vitro*, bFGF can cause endothelial cells to penetrate collagen gels [45]. The growth factor also promotes and inhibits the

differentiated phenotype in cell cultures, depending on the cell type. Not surprisingly , endothelial cells cultured with bFGF exhibit many of the qualities of their *in vivo* counter parts: contact inhibited growth, differentiated basal and apical surfaces, and production of characteristic proteins [74].

In vivo Biological Activities

The *in vivo* roles of bFGF have been difficult to clarify. bFGF is a potent angiogenic factor in the *in vivo* neovascularization models of the rabbit cornea, the chick chorioallantoic membrane (CAM), and the hamster cheek pouch. Nanogram quantities of the growth factor were capable of inducing new blood vessel growth [44]. The angiogenic properties of bFGF are borne out by the cytokine's abilities, *in vitro*, to promote cell proliferation and chemotaxis, and to enable the cells to invade ECM-like materials in culture.

It seems likely that bFGF plays a major role in tumor pathophysiology. The fact that many cell types that synthesize bFGF also are sensitive to it suggests that the growth factor could be involved with cell transformation. Three members of the FGF family, hST, int-2, and FGF-5 are, in fact, oncogene products. bFGF's angiogenic properties also could ensure blood vessel growth into the tumor, a vital step in tumor development. The tumor could produce the growth factor itself, or free it from storage sites in the surrounding tissue [76]. In fact, studies by Hori et al. [77] and Pesenti et al. [78] both demonstrated the importance of bFGF to the neovascularization of tumors and, as a consequence, to an increase in tumor size.

bFGF's ability to induce cell proliferation also implicates it as a likely candidate in the wound healing process. The growth factor has been detected in focal brain injuries, and it also has been found to enhance the healing of corneal epithelium and endothelium [44].

Basic fibroblast growth factor appears to modulate several varied biological processes. Its interaction with heparin and heparan sulfate is well documented, and this relationship is probably critical to its activity. The potential mechanisms by which bFGF is released from the cell and interacts with its cell surface receptor have been described. A glaring gap in this overview remains: how does bFGF interaction with basement membrane HSPG participate in the regulation of bFGF's activity?

1.5 ECM Modulation of bFGF Activity

This section illustrates how bFGF / HS interactions in the environment of the basement membrane regulate bFGF action. Experimental evidence is presented supporting the following contentions: bFGF is deposited into the ECM and binds to resident HSPG, bFGF localized to the ECM can influence cell functions over an extended period of time, bFGF can be released through enzymatic degradation of ECM, and ECM can control the availability of growth factor. bFGF interacts specifically with the HS chains of HSPGs in the basement membrane. However, the regulation of bFGF activity stems directly from the fact that the HSPGs are anchored to the basement membrane through non-covalent interactions with other basement membrane components and through physical entrapment. The basement membrane, then, provides a unique environment for the interaction of bFGF with HS, and it is in this sense that we refer to the basement membrane regulation of bFGF activity.

Several studies have established that bFGF was deposited in basement membranes and into the ECMs produced by the same cells in culture. Baird and Ling [79] showed that radioiodinated bFGF is bound by the ECM secreted beneath cultured bovine capillary and vascular endothelial cells, and could be subsequently released with 3 M salt solutions. Pretreatment of the matrix with either heparin, heparinase I, or heparinase III, but not other GAGs or GAG-lyases, markedly reduced the binding. Furthermore, they

purified acidic and basic FGF from extracts of the ECM that had not been previously exposed to growth factor. In a similar study [80], a bFGF-like activity was isolated by heparin Sepharose chromatography from the ECM deposited by cultured bovine corneal and aortic endothelial cells. The molecule was identified as bFGF based on 1) having a molecular weight of 18,400, 2) tight binding to heparin Sepharose, 3) cross-reactivity to bFGF antibodies, and 4) mitogenic activity for aortic and capillary endothelial cells. The layer of cells was removed by lytic and non-lytic methods, but in either case, the same amount of bFGF was isolated from the ECM. These data suggest that the bFGF was actually deposited by the cells and was not an artifact of the preparation process. Globus et al. [81] also reported the isolation of both bFGF and aFGF activity from bovine bone cell cultures. Bashkin et al. [82] characterized the binding of bFGF to cultured bovine endothelial cell ECM as having a Kd of 610 nm. They found that binding was effectively inhibited by heparitinase and that sulfation of heparin was critical to its binding inhibiting properties. These studies provide strong evidence that bFGF is synthesized and deposited in the basement membrane produced by various cell lines, and, more specifically, that interactions with a heparin-like molecule are responsible for the binding.

Several *in vivo* studies corroborated the *in vitro* work described above. Jeanny et al. [83] demonstrated that radiolabeled bFGF and aFGF bound to bovine embryonic eye basement membranes. Minimal bFGF binding was registered when the basement membrane was treated with heparin, implicating a heparin-like molecule in the binding site. Folkman et al. [17] went one step further in analyzing the basement membranes of mature bovine corneas. They were able to isolate bFGF from bovine Descemet's membrane, localize it visually through immunofluorescence, and release it with heparin. A study utilizing the basement membrane of the Englebredth-Hoth-Swarm (EHS) tumor confirmed that bFGF bound to a low density heparan sulfate proteoglycan with a Kd of 30 nM, and that it did not bind to other basement membrane components [84]. The results of the *in vitro* and *in vivo* experiments clearly indicate that bFGF is

deposited into basement membrane, but these studies did not address the ability of ECM sequestered bFGF to influence cells or the potential mechanisms of bFGF release.

Presta et al. [85] showed that the ECM laid down by fetal bovine aortic endothelial cells contained a bFGF activity that was capable of inducing plasminogen activator (PA) activity in the cells growing on it. This activity was attributed to ECM sequestered bFGF, because it was detected after the cell cultures had been rinsed with a low salt buffer to remove soluble bFGF. Rinsing the cultures with a high salt buffer (2M) removed bFGF from the ECM sites and abolished the PA-inducing activity. Introducing heparin or heparan sulfate to the medium, after the salt wash, actually reduced the observable PA activity. The authors hypothesized that the bFGF was being released by a heparinase activity secreted by the cells, and that exogenous heparin or HS competed with the ECM HS for the enzyme. However, soluble heparin may have competed for bFGF with the cell surface receptors, resulting in decreased PA expression. Rogelj et al. [86] took a different approach to the same problem by using ECM secreted by corneal endothelial cells and by PF-HR-9 mouse endodermal carcinoma cells. The corneal endothelial cells produce an ECM that is mitogenic for capillary endothelial cells, but the PF-HR-9 cells, which do not synthesized bFGF, produce a non-mitogenic ECM. Anti-bFGF antibodies eliminated the mitogenic activity of the corneal endothelial ECM, while a mutant PF-HR-9 expressing bFGF promoted endothelial cell proliferation.

The issue of the long term bioavailability of growth factor deposited in the basement membrane was addressed by Flaumenhaft et al. [87]. Their experiments showed that bovine capillary endothelial cells exposed to growth factor for 10 to 30 minutes, and then rinsed of soluble bFGF, were stimulated to produce PA to the same extent as were cells continuously exposed to the growth factor. Treatment of the culture with high salt, incubation of the bFGF in the presence of heparin, and exposure of the ECM to heparinase all abolished this activity. Thus, together these *in vitro* and *in vivo* studies demonstrate that the ECM can function as a long-term bFGF storage site.

More recent research in this area has focused on the role of heparinases and proteases in the release of growth factor from the ECM. Vlodavsky et al. [88] reported that heparinases could release bFGF from cultures of bovine corneal endothelia and from Descemet's membrane as well. Likewise, Saksela and Rifkin [89] explored the capacity of plasminogen activator to free active growth factor via plasmin formation. A study by Ishai-Michaeli et al. [90] investigated the abilities of thrombin to release endogenous and exogenous bFGF.

bFGF Transport through Basement Membranes

bFGF transport through basement membranes has been addressed in two papers. Flaumenhaft et al. [91] demonstrated enhanced movement of bFGF through agarose, fibrin gels, and cell monolayers when the growth factor was preincubated with heparin. They proposed that when bFGF's binding site was occupied by heparin, it did not interact with anionic sites in the gel and, consequently, had a larger radius of diffusion. Dabin and Courtois [92] explored the diffusion of bFGF through artificial basement membranes prepared from matrigel, an extract from the EHS tumor basement membrane. They found that although increased concentrations of HSPG did slow the passage of bFGF, it was still able to transverse the membrane. They did not, however, see increased diffusion through the matrix when heparin was added to bFGF. The authors concluded that the basement membrane could play a regulatory role in bFGF activity by controlling the bioavailability of the growth factor.

How is bFGF activity regulated by basement membrane? No definitive answer exists to this question, but a picture has emerged from the studies cited above [93] [94]. bFGF is deposited into the basement membrane where it interacts with the heparan sulfate chains of HSPG. This association stabilizes bFGF and protects it from proteolytic degradation. bFGF could diffuse out of the basement membrane at a rate dictated by the concentration of bFGF sites in the membrane, the avidity of bFGF for membrane HS, the

diffusivity of bFGF, and the nature of the surrounding tissue. These release mechanisms would likely be coupled to the concentration of cell surface receptors and the rates of receptor uptake through a cell surface / ECM bFGF equilibrium. In the event that neighboring tissue is physically damaged, as in a wound, comparatively large quantities of bFGF would be released from the disrupted cells and basement membranes. The intact basement membrane surrounding uninjured cells could function to buffer this bolus of bFGF. The normal turnover of basement membrane components would also release bFGF from the matrix. Furthermore, as a part of the wound healing response, basement membrane structure could be altered with proteases and heparinases.

Chapter 2

Theory

2.1 Introduction

A growing body of literature has implicated heparan sulfate in basement membranes as a key regulator of bFGF transport. Furthermore, it has been proposed that these basement membranes act as a reservoir for bFGF. It is not clear how this reservoir functions, and a quantitative model of the system would greatly enhance our understanding of the physiology of this important growth factor. We proposed a model that encompassed the diffusion of bFGF through the matrix in conjunction with reversible binding to heparan sulfate sites in the matrix as represented by the following equations:

$$\frac{\partial b}{\partial t} = D_{eff}\frac{\partial^2 b}{\partial x^2} - \frac{\partial c}{\partial t} \qquad 2.1$$

$$\frac{\partial c}{\partial t} = k_{on} h b - k_{off} c \qquad 2.2$$

$$h_{tot} = h + c \qquad 2.3$$

$$K = \frac{b}{b_{bulk}} \qquad 2.4$$

Equation 2.1 reflects the diffusion of free solute bFGF (b) through a membrane with an effective diffusivity of D_{eff}. The second term on the right-hand side accounts for loss of free solute through the formation of a complex (c) with heparan sulfate sites in the matrix. The association of bFGF with these HS sites (h) is embodied in equation 2.2 as a reversible reaction with on and off rate constants k_{off} and k_{on}. Equation 2.3 stipulates that the total number of HS sites (h_{tot}) is constant. Lastly, the concentration of free solute in the membrane is related to the bulk concentration at the membrane interface through a partition coefficient (K). This chapter concerns itself with the development of these equations for diffusion and binding in a hydrogel membrane and with their experimental implications.

2.2 Diffusion in Gels

Hydrogels are macromolecular networks formed from chemically crosslinked or physically crosslinked hydrophilic polymers. The polymers would dissolve in the aqueous environment were it not for the presence of these crosslinks. Descemet's membrane is a collagenous hydrogel with much of the hydration provided by the charged proteoglycans. Solute diffusion through DM can be represented by the diffusion equation derived from Ficks law. However, the diffusivity is not the free solution diffusivity. The polymer network of the hydrogel can significantly influence the diffusion of solutes through the gel and an effective diffusivity is employed to account for these differences. In addition to theses general issues, other specific characteristics of our DM system need to be considered. Specifically, the glycosaminoglycans in the DM give it an overall negative charge, while bFGF has an overall positive charge at physiological pH. Electrostatic interactions could also potentially influence diffusion. Thus, the partition coefficient for bFGF into the DM may not be unity. Numerous researchers have attempted to relate the effective diffusivity and partition coefficients of a particular solute in a given gel to measurable solute and gel properties.

2.2.1 Effective Diffusivity in Gels

Measurement of diffusivities of solutes in polymer solutions initially suggested the following general relationship for effective diffusivity as a function of polymer concentration (c_p) and the free solution diffusivity (D_o)[95]

$$D_{eff} = D_o \exp(-\alpha c_p^{\nu}) \tag{2.5}$$

where the coefficients α and ν are dependent on the hydrogel and solute.

Ogston et al. [96] developed a stochastic jump model to account for the reduced diffusivities observed for solutes in polymer solutions. In this approach the size of a random step taken by a solute molecule is altered by the presence of polymer rods, as:

$$D_{eff} = D_o \exp\left[-\phi^{1/2}\frac{r_s}{r_f}\right] \tag{2.6}$$

where the effective diffusivity is a function of the free solution diffusivity (D_o), the volume fraction of fibers (ϕ), the solute radius (r_s), and the polymer fiber radius (r_f). This equation is of the general form described above. However, it is a purely geometric derivation, and it does not take into account the hydrodynamic drag forces that are exerted on solutes by the polymer chains. Peppas et al. [97] developed a similar theory for highly swelled membranes, but it too does not account for hydrodynamic effects.

Phillies et al. [95] developed a hydrodynamic scaling model for diffusion in polymers that accounts for interactions between the solute and polymer. Phillips et al. [98] used an effective medium approach that also accounted for hydrodynamic effects:

$$D_{eff} = D_o \left[\frac{1}{1 + (r_s^2/k)^{1/2} + \frac{1}{9}(r_s^2/k)} \right] \qquad 2.7$$

where k is the Darcy permeability of the membrane. This derivation is based on the Stokes-Einstien equation. However, rather than calculating the friction coefficient of a sphere moving in Navier-Stokes flow, Brinkman's equation is used instead. This equation was found to over-predict values of D_{eff}/D_o, and Brady modified the approach to include the effects of the tortuosity of the polymer matrix [99].

Work by Johnson et al. [100] with charged agarose gels and charged proteins in buffers with varying ionic strengths suggests that electrostatic effects do not have a significant impact on the effective diffusivity when compared to the phenomena described above.

2.2.2 Partitioning in hydrogels

The polymer fibers also restrict the solvent space that a solute molecule can occupy in a gel. Ogston [101] analyzed this phenomenon in a random suspension of fibers. He determined the fraction of solvent volume in the gel unavailable to the solute and this leads to the expression for partition coefficient below:

$$K = \exp\left[-\phi \left(1 + \frac{r_s}{r_f} \right)^2 \right] \qquad 2.8$$

where r_f is the fiber radius, r_s is the solute radius, and ϕ is the volume fraction of fibers. Fanti and Glandt [102] used density functional theory to predict partition coefficients at much higher solute concentrations. While their analysis confirmed the validity of Equation 2.8 in the limit of infinite solute dilution, significant deviations occurred at the higher solute concentrations. Partition coefficients can also be affected by electrostatic effects.

Work with negatively charged agarose gels and negatively charged proteins demonstrates that at low ionic strengths, where charge effects are most pronounced, the partition coefficients were as much as three times lower than for high ionic strengths [100].

2.2.3 Models versus Reality

The goal of section 2.2 was to highlight the key parameters governing diffusion in gels. Descemet's membrane is a hydrogel. However, it is also a much more complex structure than the models on which the equations in section 2.2 are based. Ultrastructure studies of the DM have revealed that it is composed of fibers and meshwork of several different length scales [15]. The DM is deposited and continuously remodeled over the course of an organism's lifetime, and displays structural anisotropy across its thickness. Furthermore, the glycosaminoglycans are probably responsible for much of the hydration of this extracellular matrix. No model of gel diffusion has been able to capture the complex interplay between the highly crosslinked collagen meshwork, and the flexible, hydrated glycosaminoglycan chains.

2.3 Diffusion with Reversible Binding

The combination of equations 2.1 and 2.2 is a classic problem in chemical engineering. The characterization of the bFGF/HS interaction as a simple association dissociation reaction deserves clarification. As detailed earlier, the heterogeneous structure of HS probably does not present a single class of binding sites for bFGF. However, typical equilibrium binding isotherms can be described quite well with a single average K_d. In studies with heparin, the stoichiometries as larger as five bFGF molecules per heparin chain have been observed. Our analysis of the interaction of bFGF and DM HS assumes that ,on average, only a single site is present per HS chain. This assumption is supported by the fact that HS chains have been shown to have substantially fewer binding sites than

heparin chains. Furthermore, the results of kinetic studies with bFGF and heparin or heparan sulfate in the literature are well represented by the kinetic model presented here.

The literature regarding bFGF association with extracellular matrix components deals almost exclusively with the HSPG component of the matrix. Consequently, our model regards the bFGF/HS association as the dominant interaction bFGF experiences in the DM. However, it is likely that bFGF is capable of binding to other components in the matrix to some extent. Lastly, irreversible adsorption of denatured bFGF to experimental elements as well as the membrane itself, was accounted for in all of these studies.

2.4 Measuring Transport in Descemet's Membrane

In this work the transport of bFGF across the DM was measured experimentally using a diffusion chamber apparatus. In order to determine the effective diffusivity of bFGF, in some of the experiments the association of bFGF with DM HS was blocked. Consequently, in the following sections we discuss diffusion through a membrane with and without binding to sites in the membrane.

2.4.1 Diffusion Without Binding

Figure 2.1 is a schematic of a standard diffusion cell for making diffusion measurements. Here, a thin membrane is bounded on either side by well mixed source and sink chambers that are of much larger volume than the membrane itself. At t=0 a solute is introduced to the source chamber, and allowed to diffuse across the membrane. In the scenario depicted here, the thickness of the membrane is much less than the membranes diameter, so the only concentration gradient that will exist will be in the x-direction through the membrane.

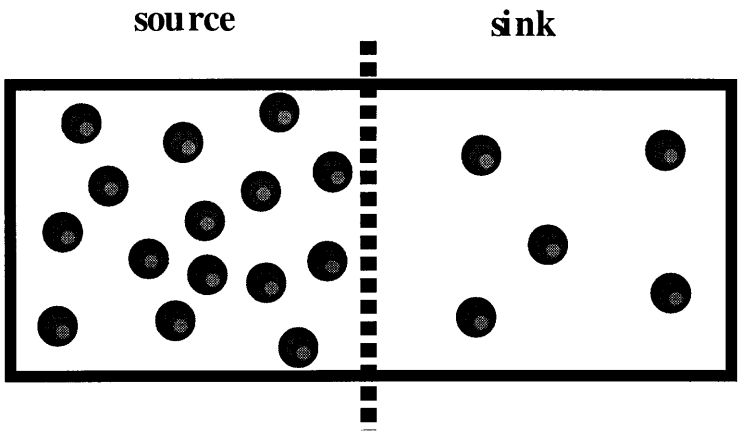

Figure 2.1 Diffusion Chamber Schematic

Diffusion across the membrane is represented by the diffusion equation:

$$\frac{\partial b}{\partial t} = D_{eff}\frac{\partial^2 b}{\partial x^2} \qquad 2.9$$

The membrane has no solute in it initially. The source and the sink are large enough that during the time course of the experiment their concentrations do not change appreciably. The source concentration is set at b° and the sink concentration is set to 0. The following solution for the solute profile in the membrane results [103]:

$$b = Kb^\circ\frac{l-x}{l} + \frac{2}{\pi}\sum_{n=1}^{\infty}\frac{-Kb^\circ}{n}\sin\frac{n\pi x}{l}\exp\frac{-D_{eff}n^2\pi^2 t}{l^2} \qquad 2.10$$

where l is the membrane thickness and K is the partition coefficient for solute in the membrane.

Daynes used this equation and the following approach to measure the diffusion of gases through latex rubber [104]. Although the concentration in the sink has been specified to be 0, in fact, a small amount of solute will cross into the sink chamber, but the concentration in the sink will remain negligible when compared to the source chamber.

Hence, the flux into the sink can be computed by applying Ficks law to equation 2.10 at the interface of the membrane and source solution (x=l). Multiplying by the diffusion area (A) then gives the moles per second of solute entering the sink chamber:

$$\frac{KAD_{eff}b^{\circ}}{l}\left[1+2\sum_{n=1}^{\infty}(-1)^{n}\exp\frac{-D_{eff}n^{2}\pi^{2}t}{l^{2}}\right]=V_{\sin k}\frac{db_{\sin k}}{dt} \qquad 2.11$$

where V_{sink} is the volume of the sink chamber.

As can be seen in the equation above, the rate at which solute leaves the membrane must be equal to the rate at which it accumulates in the sink. The concentration of solute in the sink at any time, t, is obtained by integrating equation 2.11. With no solute in the sink initially, the result is:

$$b_{\sin k}=\frac{AD_{eff}Kb^{\circ}t}{lV_{\sin k}}-\frac{AlKb^{\circ}}{6V_{\sin k}}-\frac{2AlKb^{\circ}}{\pi^{2}V_{\sin k}}\sum_{n=1}^{\infty}\frac{(-1)^{n}}{n^{2}}\exp\frac{-D_{eff}n^{2}\pi^{2}t}{l^{2}} \qquad 2.12$$

By retaining 3-4 terms of the summation, this equation can be used to analyze diffusion experiment data using commercial curve fitting software. However, at long enough times, the summation term becomes insignificant, and equation 2.12 reduces to:

$$b_{\sin k}=\frac{AD_{eff}Kb^{\circ}}{lV_{\sin k}}\left(t-\frac{l^{2}}{6D_{eff}}\right) \qquad 2.13$$

It should be noted that at very long times, the lag time itself will become insignificant.

Equation 2.13 represents the constant, pseudo-steady state flux through the membrane, and the accumulation of solute in the sink is linear with time. The x-intercept, or "lag" time is the time required for a pseudo-steady state linear concentration gradient to establish itself inside the membrane.

This equation provides two means for analyzing the results of a diffusion chamber experiment to determine the diffusivity of solute in the membrane. The slope of the line provides the diffusivity (D) with knowledge of the area for diffusion (A), the sink chamber volume (V), the source concentration (c°), the thickness of the membrane (l), and the partition coefficient (K). This strategy is referred to as the steady state approach. The x-intercept of the line provides the diffusivity when the membrane thickness is known and is referred to as the lag-time method. The advantage to measuring diffusivities based on the lag time is that only the membrane thickness need be known. The disadvantage of the lag time technique is that, depending on the experimental system, the lag time may be very short. Furthermore, the low initial concentrations of diffusing solutes must by measured accurately. This inaccuracy must be balanced against the larger number of parameters that must be measured, with their associated errors, to determine the diffusivity with the steady-state approach. The steady state approach was used to analyze data in this study.

2.4.2 Diffusion with Reversible Binding

The significance of the reversible binding to the diffusion process depends on the concentration of sites and the kinetics of the interaction. No analytical solution exists for the complete set of equations 2.1 - 2.4. They must be evaluated numerically. However, under certain conditions the equations can be simplified to a form that does have an analytical solution. While this simplification is not valid for the DM diffusion problem, this solution is an excellent tool to test numerical solutions to the more general case, and it is useful for understanding the general behavior of diffusion/binding problems.

2.4.3 Fast, Reversible Binding to Unsaturable Sites

Equation 2.1 - 2.4 can be simplified greatly if the binding events occur much more rapidly than diffusion, and if the binding sites do not saturate with solute. If the binding events take place on a much shorter time scale than diffusion, then the relevant

species will be at local equilibrium at each point in the membrane. This condition is satisfied when the Dahmkholer numbers for binding and release are much greater than 1.

$$Da_{on} = \frac{l^2 k_{on} h_{tot}}{D_{eff}} >> 1 \qquad Da_{off} = \frac{l^2 k_{off}}{D_{eff}} >> 1 \qquad 2.14$$

Under these circumstances, the equilibrium dissociation constant (K_d) is sufficient to describe the reaction.

$$K_d = \frac{k_{off}}{k_{on}} = \frac{bh}{c} \qquad 2.15$$

If the concentration of complex is always much less than the total concentration of available sites, then the concentration of sites (h) in equation 2.15 can be reasonably approximated by the total concentration of sites (h_{tot}), and equation 2.15 can be rewritten:

$$\frac{\partial c}{\partial t} = \frac{h_{tot}}{K_d}\frac{\partial b}{\partial t} \qquad 2.16$$

With this simplification, the equations for diffusion and binding can be reduced to a single equation:

$$\frac{\partial b}{\partial t} = \frac{D_{eff}}{\left(1 + \frac{h_{tot}}{K_d}\right)}\frac{\partial^2 c}{\partial x^2} \qquad 2.17$$

This equation can now be treated as in the development of the lag time analysis with the following result:

$$b_{\sin k} = \frac{AD_{eff}b^{\circ}}{lV_{\sin k}}\left(t - \frac{l^2}{6D_{rxn}}\right) \qquad 2.18$$

$$D_{rxn} = \frac{D_{eff}}{\left(1 + \frac{h_{tot}}{K_d}\right)} \qquad 2.19$$

The two different diffusivities arise when the flux of solute at the interface is derived. The D_{rxn} term is used to describe the effective diffusivity within the membrane itself, but at the interface, D_{eff} determines the flux of solute out of the membrane.

It is evident from equation 2.19 that increases in the concentration of binding sites or increases in the affinity of those sites for solute (decreasing K_d) can significantly increase the lag time. However, the constant, pseudo-steady state flux is not altered by the binding event. Once the association/dissociation reactions have reached their equilibrium in the membrane, diffusion proceeds independent of those events. The lag time is not simply the time it takes to saturate all the binding sites, that is an impossibility in this derivation since it is assumed that c is always much greater than h_{tot}. The diffusion reaction problem with Descemet's membrane is also characterized by faster reaction than diffusion. However, the high affinity of bFGF for sites in the matrix dictates that most of the heparan sulfate sites in the membrane will be occupied. This more complex problem still demonstrates the same features described above.

Two important experimental implications arise from this analysis, 1) the effective diffusivity of bFGF cannot be determined from the lag time in cases where binding to the DM HS is allowed, and 2) the effective diffusivity can be determined from the slope of equation 2.19 once a pseudo-steady state has been reached.

Chapter 3

Project Overview

3.1 Objectives and Approach

The goals of this study were to develop a mathematical model of growth factor transport through extracellular matrix, to develop an experimental system to obtain critical parameters for the mathematical model, and, ultimately to validate, the mathematical model using the experimental system.

bFGF was selected as a model growth factor because of it was physiologically relevant and because its association with the heparan sulfate in basement membrane extracellular matrix appeared to regulate its bioavailability. Descemet's membrane was an attractive model basement membrane because it was comparatively large, it was possible to remove it intact from the eye, and because it provided one of the initial *in vivo* models for the bFGF/ECM storage hypothesis. Our subsequent experimental approach was intimately linked to the mathematical representation of the transport processes. The initial equations from chapter 2 described the process of bFGF diffusion through the DM with reversible association to the DM HS chains:

$$\frac{\partial b}{\partial t} = D_{eff}\frac{\partial^2 b}{\partial x^2} - \frac{\partial c}{\partial t} \qquad 3.1$$

$$\frac{\partial c}{\partial t} = k_{on} hb - k_{off} c \qquad 3.2$$

$$h_{tot} = h + c \qquad 3.3$$

$$K = \frac{b}{b_{bulk}} \qquad 3.4$$

The experimental program was aimed directly at obtaining the critical parameters for the diffusion/binding model. The biochemical characterization of Descemet's membrane (Chapter 5) was conducted in order to determine the total concentration of HS in the membrane, equilibrium and kinetic data for the HS bFGF interactions, and overall properties of the membrane. Effective diffusivities of bFGF under different conditions in Descemet's membrane were determined through diffusion chamber experiments that are detailed in Chapter 7. The numerical solution to these equations employing data obtained in Chapters 5 and 7 is then described in Chapter 9. Chapter 6 discusses the issue of limiting bFGF adsorption to experimental surfaces and Chapter 8 focuses on work with heparin/polyacrylamide hydrogels as synthetic basement membranes.

3.2 Motivation

The extracellular regulation of bFGF activity is important to a variety of different physiological processes. While the factors that govern bFGF passage through basement membranes are numerous, we would not expect all of them to be equally important to the overall mechanism of transport. The critical elements in the process can be identified by building mathematical models that incorporate the potentially important elements and comparing the model's predictions to empirical studies. In this way, a framework for understanding the interplay of key matrix/growth factor parameters can be developed. The power of a mathematical model based on the underlying physio-chemical

properties of a particular growth factor/matrix system ultimately lies in its predictive capabilities.

A mathematical model of bFGF transport through basement membrane would provide a framework for developing rational approaches to delivery of bFGF therapeutically, and would aid in understanding how the interaction of bFGF with embryonic HSPGs can direct certain aspects of development. Furthermore, a wide variety of proteins interact with the various components of the extracellular matrix. The results of this study will lay the groundwork for understanding a host of physiological and pathophysiological processes that depend on matrix regulation of the transport of various proteins and enzymes through extracellular matrix.

bFGF's intimate association with the wound healing process and its capacity to stimulate new blood vessel growth have made it an attractive potential therapeutic agent for pathologies ranging from gastrointestinal ulcers, heart disease, to neuronal injury. In all these cases, the method of drug delivery is critical. Intravenous administration of bFGF results in rapid clearance of the growth factor from the blood stream [105]. Local delivery of bFGF through a controlled release device provides the most efficient means of placing the growth factor where it is needed most [105]. However, intelligent design of these controlled release systems depends on a knowledge of how the growth factor will distribute itself through neighboring tissues and the rate at which it will move through these tissues. A model of how bFGF diffuses through actual tissue would provide critical initial estimates for designing release systems.

bFGF and its relatives play critical roles in embryonic development. bFGF has been implicated in patterning of the chick limb bud [106] and other members of the FGF gene family have been tied to mesoderm induction in *Xenopus laevis* [107]. Furthermore, HSPGs are also critical elements in various developmental pathways. For example, Yurchenco et al [108] performed immunolocalization studies on developing rat embryos and reported that perlecan expression was closely tied with the development of the

vasculature. Given the established role of bFGF in angiogenesis, their results suggest that perlecan and bFGF may act together to modulate the development of the murine vasculature. A basic model of bFGF movement through the HSPG rich extracellular matrix of a developing embryo could provide critical insights into the highly regulated pathways that govern cell proliferation and differentiation during embryogenesis.

Numerous diseases, including cancer and cardiovascular disease, are characterized by uncontrolled cell proliferation. As a modulator of cell growth and differentiation, the unregulated activity of bFGF can contribute to tumor growth and smooth muscle hyperplasia leading to blood vessel occlusion. A fundamental, quantitative understanding of the role of ECM in regulating the bioavailability of growth factors could provide insights into the mechanisms of these disorders, and could help in designing therapeutic approaches to modulate endogenous growth factor activity.

Extracellular matrices throughout an organism consist of structural elements, such as collagen and proteoglycans, and diffuseable enzymes and growth factors that can reversibly bind to these structural components. The vast majority of research in extracellular matrix biology has been geared toward identifying the myriad components of the ECM, determining their function in the matrix, and characterizing their interactions with each other and the cells in their environment. This work is obviously critical to understanding the role of ECMs in health and disease, but it is incomplete. The complex interplay of these biomolecules is modulated, in part, by their concentrations, binding affinities, and the diffusivities of the mobile species. These parameters must be evaluated for ECM systems, and their interrelationships must be defined through mathematical models based on the physics and the chemistry of these systems. A full understanding of how extracellular matrices influence the growth and differentiation of the cells with which they are associated will emerge only when these aspects of ECM biology are taken into account.

Chapter 4

Materials and Methods

4.1 General Techniques

The following abbreviations will be found throughout this section 50 mM phosphate buffered 150 mM NaCl pH 7.4 (PBS), bovine serum albumin (BSA), PBS with 1 mg/mL BSA (PBS-BSA), glycosaminoglycan (GAG), 50 mM Tris (TRIS (hydroxymethyl) aminomethane buffered 150 mM NaCl pH 7.4 (TBS), fluorescein isothiocyonate (FITC).

4.1.1 Trichloroacetic Acid Precipitation

Trichloroacetic acid precipitation was employed as a standard method to resolve ^{125}I proteins from disassociated radiolabel. Stock solutions (50 mL) of trichloroacetic acid (TCA), bovine serum albumin (BSA), and potassium iodide (KI) were prepared: 1) 10 mg/mL BSA in deionized water, 2) 100% wt/vol TCA in deionized water (50 g / 50 mL), and 3) 10 mM KI in water (0.083 g/ 50 mL water). 100 µL experimental samples were routinely collected and subjected to TCA precipitation by adding: 1.4 mL PBS or saline, 100 µl 10 mg/mL BSA , and 200 µl 10 mM KI. 250 µl of cold 100% TCA was then added, and the solution was vortexed vigorously to ensure complete mixing of the TCA. The total volume was not important as long as these volume ratios were maintained. The samples were placed on ice for 10 minutes to ensure complete protein precipitation.

The precipitate was pelleted in a microcentrifuge at 12000 x g for 5 min. Larger flat bottom gamma counting cuvettes were placed in 15 mL centrifuge tubes , containing tissue pads in the conical section, and centrifuged for 10 minutes at 3,000 rpm (1800 x g) in a model PR-J centrifuge (International Centrifuge, Needham, MA). The supernatant was removed, the pellet was washed with 14% TCA, allowed to incubate for 10 minutes at 4 °C, and the centrifugation was repeated. The resulting pellet was retained as the protein fraction.

4.1.2 Dimethylmethylene Blue GAG Quantification Assay

A modification of the dimethylmethylene blue (DMB) colormetric assay [109] was used to determine concentrations of GAG. DMB binds irreversibly to GAG chains, resulting in an adsorption shift in the DMB that is proportional to the amount of GAG in the sample within a certain concentration range. The DMB reagent was prepared with 16 mg DMB, 2.37 g NaCl, 3.04 g glycine, and 0.77 mL 12 N HCl, and brought up in 1.0 L deionized H_20. This solution was stirred for approximately one hour until no particulates were visible, and then it was filtered through a 0.22 μm sterile filter to remove undissolved DMB. If the DMB is not given sufficient time to dissolve, the filtration step will remove most of the DMB from the solution.

Concentrations of GAG in a sample were determined by comparison to a standard curve made with a series of known concentrations of GAG and their corresponding DMB absorbance readings. The GAG standard curve was prepared with the dominant GAG in the sample since the DMB assay has varying sensitivities to the different GAGs. With 1.0 mL of DMB solution, the sample volume maximum was 700 μL. The minimum amount of GAG detectable by this assay was 0.2 μg/sample, and above 4 μg/sample, the DMB becomes increasingly insensitive to higher GAG concentrations. Given the above guidelines, a typical standard curve for a 40 μl sample ranged from 5 to 100 μg/mL and contained 5 standard concentrations in duplicate, not

including a blank for zeroing the spectrophotometer. The standards were read as described below, and then the concentration in μg/mL was plotted versus absorbance at 525 nm. This data was fit to a straight line, and the resulting equation was used to determine unknown sample concentrations.

Samples were added to cuvettes taking care not to scrape the optical surfaces. 1 mL of DMB solution was added to the cuvette without frothing, and the DMB was mixed by inverting the cuvette twice. The absorbance at 525 nM was read immediately as it decayed over time. The DMB interaction with GAGs is based in part on a charge-charge association, consequently high concentrations of salt disrupted the interaction and significantly reduced the sensitivity of the assay. High concentrations of protein (1 mg/mL) slowed the DMB association with the GAG. Ultimately, nearly the same sensitivity was achieved. However, the DMB was incubated with the GAG for several hours until the absorbance failed to rise.

4.1.3 Bradford Coomassie Blue Protein Assay

The Bradford Coomassie blue colormetric dye binding assay [110] was used to determine protein concentrations in solution. The Coomassie blue binds to protein with a concomitant shift in its absorbance that is proportional to the concentration of protein within a certain concentration range. Concentrations of protein in a sample were determined by comparison to a standard curve made with a series of known concentrations of protein and their corresponding Coomassie blue absorbance readings. The standard curve was prepared in duplicate with BSA in the sample buffer in the range of 1 to 10 μg/mL BSA. 1 mL of each sample was added to each test tube. The samples were diluted into the 1-10 μg/mL protein range. If no estimate was available for the sample concentration, several dilutions were prepared to obtain one in the assay's protein range. One mL of each dilution was added to each test tube, and 250 μl of the Bradford Reagent (BioRad, Hercules, CA) was added to all of the test tubes. Samples and standards were

mixed thoroughly in the test tubes before being added to the cuvette. The samples and standards absorbances were read at 595 nm, and the sample concentration was determined from the standard curve. The color was stable for several hours.

4.1.4 Bolton Hunter Iodination of bFGF

A modified Bolton-Hunter procedure for radio-iodinating bFGF and heparan sulfate [71] was used in this study. The Bolton-Hunter approach does not involve free ^{125}I. The iodine is covalently attached to a larger molecule that reacts with an amine group to form a covalent bond to the target protein. Consequently, the inhalation hazard of gaseous ^{125}I is dramatically reduced. However, proper safety precautions must be followed throughout this experiment to avoid serious radioactive contamination. All operations were conducted under a fume hood, with a lab coat, and 2 pairs of gloves. The solvent carrier in the Bolton Hunter Reagent (NEN, Boston, MA) was evaporated with a very low flow of nitrogen. 1.4 µl of stock bFGF (8.6 mg/mL) was added to 40 µl of 100 mM NaPO4 buffer, pH 8.5. 30 µl of this solution, in turn, was added to the dried down Bolton Hunter reagent, and incubated on ice for 2.5 hours. The reaction was quenched with 200 µl 0.2 M glycine for 45 minutes on ice. Upon completion of the quenching step, 20 µl of 0.5% gelatin was added as a carrier, and the volume was brought up to 500 µl with 250 µl of gel filtration buffer (50 mM Tris-HCl, 0.05% gelatin, 1 mM dithiothreotol, 0.3 M NaCl, pH 7.5, sterile). Two 5 µl samples were removed for TCA precipitation to determine the specific radioactivity of the bFGF. The free Bolton Hunter reagent was removed from the ^{125}I-bFGF with a PD-10 gel filtration column that was gravity fed with the gel filtration buffer described above. The flow rate was approximately 1 mL/min, and 0.5 mL fractions were collected. Two microliters of each fraction were assayed for radioactivity with a gamma counter, and the ^{125}I-bFGF void peak was pooled. Two 5 µl samples were removed for TCA precipitation. The bFGF activity and concentration were determined from the initial concentration, the 2 sets of precipitation data, and a measured

reaction yield of 70%. The biological activity and the ability of ^{125}I-bFGF to bind HS were confirmed by measuring the ability of ^{125}I-bFGF to promote endothelial cell proliferation and by measuring ^{125}I-bFGF binding to cell surface HSPGs and HS in solution.

4.2 Descemet's Membrane Characterization

4.2.1 Immunostaining DM for Confocal Microscopy

Immunostaining of freshly isolated corneas with an antibody raised against EHS perlecan was performed to confirm the presence of HSPG in bovine DM. Corneas from mature cows were cut out of the eye with curved surgical scissors and immediately frozen in liquid nitrogen. The corneas were mounted and sectioned longitudinally into 8 μm thick sections with a cryostat. The sections were mounted on microscope slides and stored a -70°C until they were needed.

Although the supplier suggests incubating the sections with 200-250 μL of 15,000 U/mL hyaluronidase (Sigma H3631, 7500 U/mg) to aid in exposing epitopes, experiments with and without the enzyme, pre-treatment revealed no difference in staining. All the slides were washed in a 3% BSA/PBS solution for 10-15 minutes. The primary anti-HSPG antibody (Upstate Biotechnology, Anti-HSPG antibody from mouse-rat hybridoma) stock solution was at 1.1 mg/mL and was diluted to 10 μg/mL in 2.6 mL of 1% BSA/PBS. 200 μl of the primary antibody solution were added to each slide and were incubated overnight in a humid tray at 4°C. The following morning, all the slides were rinsed two times with PBS, and incubated 10 min in 3% BSA/PBS.

The secondary antibody, a goat anti-rat rhodamine conjugate (Vector Labs, Burlington, CA) was used at 50x dilution in 1% BSA/PBS. 300 μl were added to each slide, and the slides were incubated for 1 hour at room temperature. The slides were then rinsed two times with PBS and 4 - 5 drops of Slow Fade, anti-fade reagent (Molecular

Probes, Eugene, OR) was added to each slide for 5 minutes, followed by 4 more drops of anti-fade reagent. The sections were covered with a coverslip, and the edges were sealed with nail polish.

The immunostains were imaged with a Leica upright laser scanning confocal microscope with an argon ion laser having an output power of 2-50 mV. Successive scans were made in 1 μm "slices" through the membrane and stored on an optical disc.

4.2.2 Gel Electrophoresis and Western Blot of Collagenase treated Perlecan

Perlecan degradation by collagenase preparations was assessed with gel electrophoresis followed by Western blotting of perlecan samples treated with collagenase and untreated controls. The perlecan core protein containing HSPG for this study was isolated from bovine aortic endothelial cells by Dr. K. Forsten [111]. 10 μl of perlecan (168 μg/mL GAG) was added to 20 μL of 2.5 mg/mL collagenase D (low protease activity, Boehringer Manheim) in 50 mM Tris buffer, 150 mM NaCl, pH 8.0 buffer and was incubated at 37 °C for 6 hours. Controls without perlecan and without collagenase were also treated. The collagenase was inactivated by boiling at 100 °C for 3 min following the incubation.

SDS -polyacrylamide gel electrophoresis (5% running gel, 3.5% stacking gel) was used to analyze collagenase digested and control non-digested perlecan. Bio-Rad Prestained SDS PAGE molecular weight standards were used for size calibration.

All samples were pre-treated with final concentrations of 0.015 U/mL of heparinase I , heparinase III, and chondroitinase ABC (Seikagaku America, Rockville, MD) to remove all GAG chains from the proteoglycan so that the core proteins could be resolved with SDS PAGE. Gel bands were transferred to Immobilon-P Transfer Membranes (Millipore, Bedford, MA). Five percent non-fat dry milk (Carnation) in PBST (phosphate buffered saline, 0.1% Tween) was used as the blocking buffer.

Membranes were incubated with anti-heparan sulfate proteoglycan (anti-perlecan) at a final concentration of 1 μg/mL in PBST containing 1% non-fat dry milk for 1 hr at 37°C. Membranes were washed 5 times with PBST; once for 15 min, four times for 5 min. The membranes were then hybridized for 1 hr 37°C with anti-rat IgG, horseradish peroxidase linked whole antibody (1.5 μl in 5 mL PBST, containing 1% milk), and washed 5 times with PBST as before. The membranes were then exposed for 1 min to the Renaissance reagents, Chemiluminescence Oxidizing and Enhanced Luminol (NEN, Boston, MA). The action of horseradish peroxidase on these reagents generated light, and the bands were visualized by autoradiography on hyperfilm autoradiography film (Amersham, Buckinhamshire, England).

4.2.3 Descemet's Membrane Dissection

Descemet's membranes were obtained by dissection of fresh adult bovine eyes. Thirty to forty eyes were ordered from Pel-Freeze (Rogers, Arkansas) for shipping overnight in wet ice. The dissection began with the removal of the cornea. A cut was made into the limbus of the eye, and the cornea was removed by cutting along its periphery with curved scissors. The cornea was then placed endothelium face up on the knob of a bell jar lid (Figure 4.1). The knob was a glass sphere with a curvature very similar to the bovine eye, so the cornea presented a smooth, unwrinkled working surface. The endothelium was removed by repeated wiping with a tissue followed with PBS rinses.

Descemet's membrane was actually removed with a Teflon spatula approximately 1.5 mm thick, 10 cm long, and 1.5 cm across. One end to the Teflon was cut at a very sharp angle, and the edge was trimmed with a scalpel to conform to the curved shape of the corneal mount.

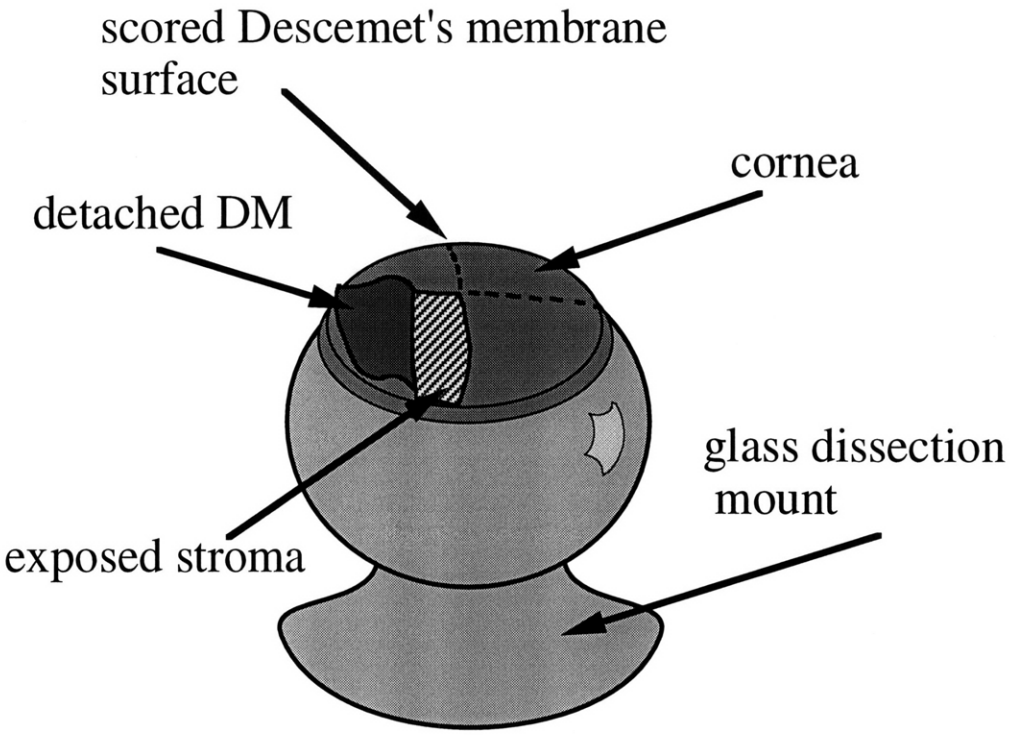

Figure 4.1 Membrane Dissection Procedure: The dissection of Descemet's membrane from the cornea involves: 1) excising the cornea, 2) placing it endothelium face up on a glass dissection mount, 3) removing the endothelium 4) scoring the DM surface, and 5) gently teasing the DM away from the corneal stroma.

The Teflon tool was used to score the surface of the cornea into quarters. The objective was to tear the Descemet's membrane without cutting into the stroma itself. The DM was then wetted with PBS. The exposed edge of the DM was gradually teased away from the stroma using the Teflon tool. This operation is illustrated in Figure 4.1. Upon removal, the DM was placed in a vial with storage buffer. Membrane sections from the same eye were placed in the same vial and stored in the refrigerator for as long as 3 months with not noticeable change in properties. However, in most cases, membrane were used several weeks after dissection.

4.2.4 Descemet's Membrane Water Content

The water content of Descemet's membrane was determined by incubating the DM in a solution containing radioactive urea and fluorescently labeled high molecular weight dextran, and then comparing the total volume accessible to urea to the total volume accessible to a high molecular weight dextran. The urea provided the total aqueous volume, while the dextran provided the membrane excluded volume. Experiments were performed in duplicate.

Eight to ten membranes from mature cow eyes were diced using a razor blade in a glass dish while the membranes were kept moist with 0.5 mL of PBS. They were placed in a pre-weighed 2 mL micro centrifuge tubes with conical bottoms, and brought up to a volume of 1 mL of PBS. Approximately 100,000 cpm of [^{14}C]urea in 10 µl and 10 µl of 0.25 mg/mL 2 million molecular weight FITC Dextran were added to each tube. The tubes were tightly capped, vortexed vigorously, and weighed full. They were incubated at 4°C for 3 days with daily vortexing. Two 200 µl samples were removed for fluorescence spectroscopy, and two 50 µl samples were removed for beta counting from each tube. The fluorescence and gamma counts of the stock solutions of FITC Dextran and urea, respectively, were also measured. Based on the known initial volume and specific activity of the urea, and the specific activity in the membrane suspension, the total

volume accessible to urea was determined in each tube. This calculation was repeated with the fluorescence data to determine the extra-membrane volume. The difference represented the membrane aqueous volume.

The wet weight of the membrane was also measured. Small holes (approx 1 mm in diameter) were punched in the bottom of the membrane containing centrifuge tube using a 22 gauge needle. One hole was punched in the cap with an 18 gauge needle, and the centrifuge tube was fitted into a pre-weighed gamma counter tube. The two tubes were spun at 500 rpm for approximately 1 min. The final weights of the gamma counting tube and the membrane centrifuge tube yielded the amount of surface water removed and the membrane wet weight, respectively.

Membrane dry weights were measured after first passing 5 mL of deionized water over the membrane preparation in the tube with the perforated bottom to remove BSA and dissolved salts. The tube was then frozen in liquid nitrogen or the -70°C freezer, lyophilized overnight, and weighed.

4.2.5 β-Eliminative Dissolution of DM

β-eliminative dissolution of the DM was performed to release the entrapped HS chains [112]. One hundred mature bovine eyes were obtained from Pel Freez and were dissected as described above. The membranes were collected in a pre-weighed 50 mL centrifuge tube and were subjected to 3 buffer changes into deionized water. They were then frozen in the -70°C freezer and lyophilized. The total membrane dry weight was determined from the final weight of the dried membranes and centrifuge tube.

Forty milliliters of 1 M NaBH4, 0.05 M NaOH reaction buffer was prepared and added to the dried membranes in a 250 mL round bottom flask. This solution was mixed at 37°C for 24 hours. The solution was neutralized through very slow addition of small volumes of glacial acetic acid. The digested membrane solution was then dialyzed first into 1.0 liter of 1.0 M urea in PBS in a 3500 MWCO Spectrapor dialysis membrane

(Spectrum Medical Industries, Los Angeles, CA). After equilibration, the buffer was changed to 4.0 M urea in PBS. This crude HS extract was subsequently analyzed and purified with ion exchange chromatography.

4.2.6 GAG Composition Assay

This assay relied on selective degradation of GAGs by specific lyases to determine the composition of a given GAG mixture. Table 4.1 lists the specific lyases used in this assay and their sources.

Standard curves were prepared for each of the three GAGs (heparan sulfate, keratan sulfate, and chondroitin sulfate) in the range 10 - 100 µg/mL in 100 mM Tris buffer adjusted to the appropriate pH as listed in the table below in a volume of 100 µl.

Enzyme	Substrate	Aliquot Conc	Working Conc	Buffer pH
Chondroitinase ABC	dermatan and chondroitin sulfates	1.0 U/mL	0.1 U/mL	8.0
Keratanase II	keratan sulfate	0.1 U/mL	0.01 U/mL	5.9
Heparinase III / I	heparan sulfate / heparin	100 U/mL	10 U/mL	7.0

Table 4.1 GAG Lyases for Composition Assay

The GAG sample was diluted to 400 - 500 µg/mL with deionized water if the samples had concentrations higher than 500 µg/mL. GAG samples below 250 µg/mL were concentrated prior to analysis. 70 µl of appropriate buffer was added to 20 µl sample in a tube containing 10 µl enzyme. The heparinase sample was digested with a 50:50 mixture of heparinases I and III. For reduced sample volume these volumes can all

be halved. Each sample was digested with each of the enzyme preparations, and a control was included for each sample in which the pH 7 buffer and 10 µl of deionized water were used. All samples were digested for 3 hours at 37°C and their GAG content was determined using the dimethylmethylene blue assay (DMB).

Each enzyme degraded it's particular GAG substrate in the sample, resulting in a decrease in the overall absorbance as determined by the DMB assay. The slopes of the standard curves prepared for each GAG type related these decreases in absorbance to decreases in GAG concentration. The GAG concentration decreases observed for each enzyme with a particular sample were then totaled, and the percent of each specific GAG type was defined as the ratio of the concentration reduction for that enzyme to the sum total concentration drop for all the enzymes.

4.3 Descemet's Membrane HS Isolation and Characterization

The β-eliminative dissolution of the DM resulted in a solution containing high concentrations of protein and comparatively low GAG concentrations. The majority of the protein was removed from the preparation using anion exchange chromatography which selects for the highly negatively charged GAG chains. The HS was isolated from the other GAG's in the preparation by selectively degrading those GAG species with specific enzymes and then performing a second anion exchange chromatography step. The purified HS was characterized in terms of its molecular weight and affinity for bFGF.

4.3.1 Preparative Anion Exchange Chromatography for DM GAG purification

Anion exchange chromatography was used to purify GAG chains from the digested DM preparation. A Pharmacia 1 cm diameter glass column with two end adapters was used with Fast Flow Q sepharose anion exchange media (Sigma). The packed column bed height was 3.5 cm for a total volume of 2.7 mL. The column was equilibrated

with 50 mL 4 M urea in PBS. The digested membranes were loaded in two batches of 45 mL and 47 mL at 1 mL/min, with a 40 mL equilibration with 4M urea PBS run in between the loads.

The column was washed with 30 mL of 0.3 M NaCL 4 M urea PBS at 1 mL/min. It was eluted with a linear salt gradient of 11 mM NaCl / mL at a flow rate of 4.5 mL/min (0.3 M NaCl to 1 M NaCl). Fractions of 0.6 mL were collected, and every third one was analyzed for GAG content using the DMB assay. The column was cleaned with 33 mL of 2.2 M NaCl PBS urea. The second batch was washed with 0.3 M NaCL as before, but it was eluted at a slightly higher salt gradient of 23 mM/mL and a flow rate of 1.5 mL/min (0.3 M NaCl to 1.5 M NaCl). A GAG peak with a large shoulder eluted from each column. The corresponding peaks were pooled from each run and were each dialyzed into PBS pH 5.7 in a 3500 MWCO Spectrapor membrane (Spectrum Medical Industries, Los Angeles, CA)

4.3.2 Keratanase and Chondroitinase treatment of DM GAG

Fresh Keratanase II (Seikagaku America, Rockville, MD) was prepared at 0.1 U/mL in PBS pH 5.7. 300 µl was added to 33 mL of pooled GAG from the first peak eluted from the Q sepharose column. The enzyme and GAG were incubated at 37°C for 3 hours. The GAG concentration was measured by DMB before and after the digestion and compared to pilot study results to ensure that the reaction had gone to completion. The pH of the digest was adjusted to pH 8.0 for the Chondroitinase ABC digestion with 0.53 mL 10 N NaOH, and the 400 µL of Chondroitinase ABC (Seikagaku) at 5 U/mL was added to the solution. Enzymatic digestion was carried out for 4 hours at 37°C, and the GAG concentration was checked with the DMB assay at the beginning and end of the digestion.

4.3.3 Final Q Sepharose Purification of DM HS

A 1 cm diameter Pharmacia column with two adapters was poured with 0.7 mL of Fast Flow Q sepharose for a final bed height of 0.9 cm. The column was equilibrated with 37.5 mL phosphate buffer pH 6.0 at 1 mL/min. The keratanase/chondroitinase treated samples were loaded at 1 mL/min, washed with 10 mL of 0.15 M NaCl PBS, and then washed with 17 mL of 0.3 M NaCl PBS at the same flow rate. The column was eluted with a salt gradient of 8 mM NaCl/mL at a flow rate of 2.5 mL/min (0.3 to 0.7 M NaCl). Fractions were collected and assayed for their GAG content with the DMB assay. The HS peak was pooled, dialyzed exhaustively into deionized water through a 3500 MWCO membrane, lyophilized, and stored.

4.3.4 Gel Filtration Chromatography with CL6B media

The molecular weight of Descemet's membrane heparan sulfate and the molecular size distribution of FITC Dextrans were both estimated using CL6B gel filtration media in a 1.5 cm ID Econo column (BioRad, Hercules, CA) based on comparisons with published calibration standards for GAGs [113] and calibration with commercial Dextran molecular weight standards (Sigma, St Louis, MO). All buffers were prepared beforehand with deionized water and were subsequently degassed under vacuum to reduce the likelihood of bubble formation during column pouring. TBS pH 7.4 with 150 mM NaCl was used to run and equilibrate the column. The CL6B media was available preswollen in 20% ethanol buffer with other preservatives. This buffer was exchanged with the running buffer and fines in the media were removed.

Column pouring was begun by closing the stopcock at the bottom outlet of the column, attaching the pouring reservoir to the column top, and filling the column with equilibration buffer. The gel filtration media in the graduated cylinder was completely suspended and poured into the column reservoir as the bottom stopcock was opened. The

column was packed at 2.5 mL/min for 1 hour to a final bed height of 20 cm. 8 mL of fluid dead volume was left above the column bed.

The column was loaded with sample by draining the fluid down to the gel bed, pipetting 0.5 mL of sample onto the bed surface, allowing that to enter the column, adding 8 mL of dead volume to the bed, and then starting the flow. Fraction collection was begun as the flow was started. The column was typically run with a gravity feed at 1 mL/min. Free [^{35}S]sulfate was run through the column to measure the included volume, and high molecular weight FITC Dextran was used to measure the column void volume. The [^{35}S] was detected using a scintillation counter, while the FITC dextran was detected by a fluorescent spectrophotometer with an excitation filter of 485 nm and an emission filter of 530 nm.

4.3.5 Heparin/Heparan Sulfate Binding Constant Measurement

Binding constants of bFGF to heparin and heparan sulfate were measured using a 5 mL G75 Sephadex (Pharmacia, Uppsala, Sweden) column to rapidly separate bFGF-heparin/heparan sulfate complexes from unbound bFGF. 2 g of Sephadex G-75 were dissolved in 40 mL PBS and swelled at 90°C for 3.5 hours. The gel slurry was degassed for 1 hour under vacuum. 7.5 mL of the gel slurry was added to 50 mL PBS, and this solution was poured through a funnel into a 5 mL syringe with a stopcock at the bottom. A cap with a rubber seal was attached to the open mouth of the syringe-column. An 18 gauge needle was attached to a 30 mL syringe without the plunger. The 30 mL syringe functioned as the buffer reservoir for the column. The reservoir and column were connected as a unit directly above a fraction collector.

All experiments were conducted at 4°C. A series of heparan sulfate concentrations was prepared from the lyophilized DM heparan sulfate. 2 µl of ^{125}I-bFGF was added to 230 µl of HS solution and allowed to incubate for 1.5 hours on ice. The solution concentration of bFGF was 2 nM and the heparan sulfate ranged from

approximately 10 pM - 150 nM. Two 10 µl aliquots were taken of this solution to determine the concentration of bFGF in the column load. The column was pre-equilibrated with 30 mL of PBS-BSA, and then drained down to the bed surface. 200 µL of bFGF-HS solution was added to the column, and then drained to the bed. 1 mL PBS-BSA was added to the surface of the bed, and the column was filled with 30 mL PBS-BSA. The flow was started through the column as the fraction collector was activated. Thirty-five, 5 drop, fractions were collected and counted for radioactivity. The entire process of loading the solution till the start of sample collection took approximately 1.5 min. The flow rate through the column averaged about 1.6 mL/ min.

The data was fit to a single site equilibrium binding model for bFGF and HS with the following equation:

$$\theta = \frac{h}{K_d + h} \qquad 4.1$$

The concentration of bFGF/HS complex was determined from the void volume peak, the concentration of free HS (h) was the difference between the initial HS concentration and the complex concentration, and the fractional saturation of bFGF (θ) was the ratio of complex concentration to the initial concentration of unbound bFGF. The equilibrium binding constant (K_d) was obtained from a least squares fit using the Levenberg-Marquardt algorithm performed with KaleidaGraph (Synergy Software, Reading, PA).

4.3.6 Kinetics of bFGF/ Descemet's Membrane Heparan Sulfate Interaction

Kinetic studies designed to measure both on and off rate constants were based on the Sephadex G-75 size exclusion chromatography described in equilibrium binding studies (4.3.5).

<u>On Rate Constant (k_{on}) Measurement</u>

All experiments were conducted PBS-BSA to limit nonspecific protein adsorption. bFGF at 2 nM was incubated with approximately 10 nM DM heparan sulfate

at 4°C for various time points (2-30 minute range) and then the peak was resolved on a sephadex G-75 column as described in section 4.3.5.

Off Rate Constant (k_{off}) Measurement

bFGF at 2 nM was allowed to equilibrate with approximately 10 nM DM heparan sulfate at 4°C for a minimum of 1 hour. Unlabeled bFGF was added to this solution at a concentration of 16.4 μM to compete the ^{125}I-bFGF off the heparan sulfate, and samples were incubated for varying amounts of time (4 -20 min range). The complex was resolved on a sephadex G-75 column as described earlier.

4.4 Diffusion Studies With Descemet's Membrane

4.4.1 Membrane Mounting

Membrane dissection was described above. Membranes used in diffusion studies were not all used immediately and required a storage buffer to prevent microbial growth and membrane degradation over time. The storage buffer was typically prepared in 50 mL volumes. The base buffer was PBS with 0.1 % sodium azide. In addition, the buffer contained protease inhibitors: 1 μg/mL of pepstatin, 0.5 μg/mL leupeptin, and 1 mM NEM. 1 mL of storage buffer was added to 4 mL glass vials.

Figure 4.2 is an illustration of the diffusion chamber apparatus used in these experiments. The two diffusion half cells were purchased from Crown Glass (Somerville, NJ). The membrane mounts were produced by sand-blasting holes of defined diameter (0.65 cm diameter for 2 bolt holes and 0.5 cm diameter for the membrane hole) and position from 3 x 1.5 inch microscope slides. The entire assembly was held in position using a Crown Glass diffusion cell clamp bolted to a Lucite base.

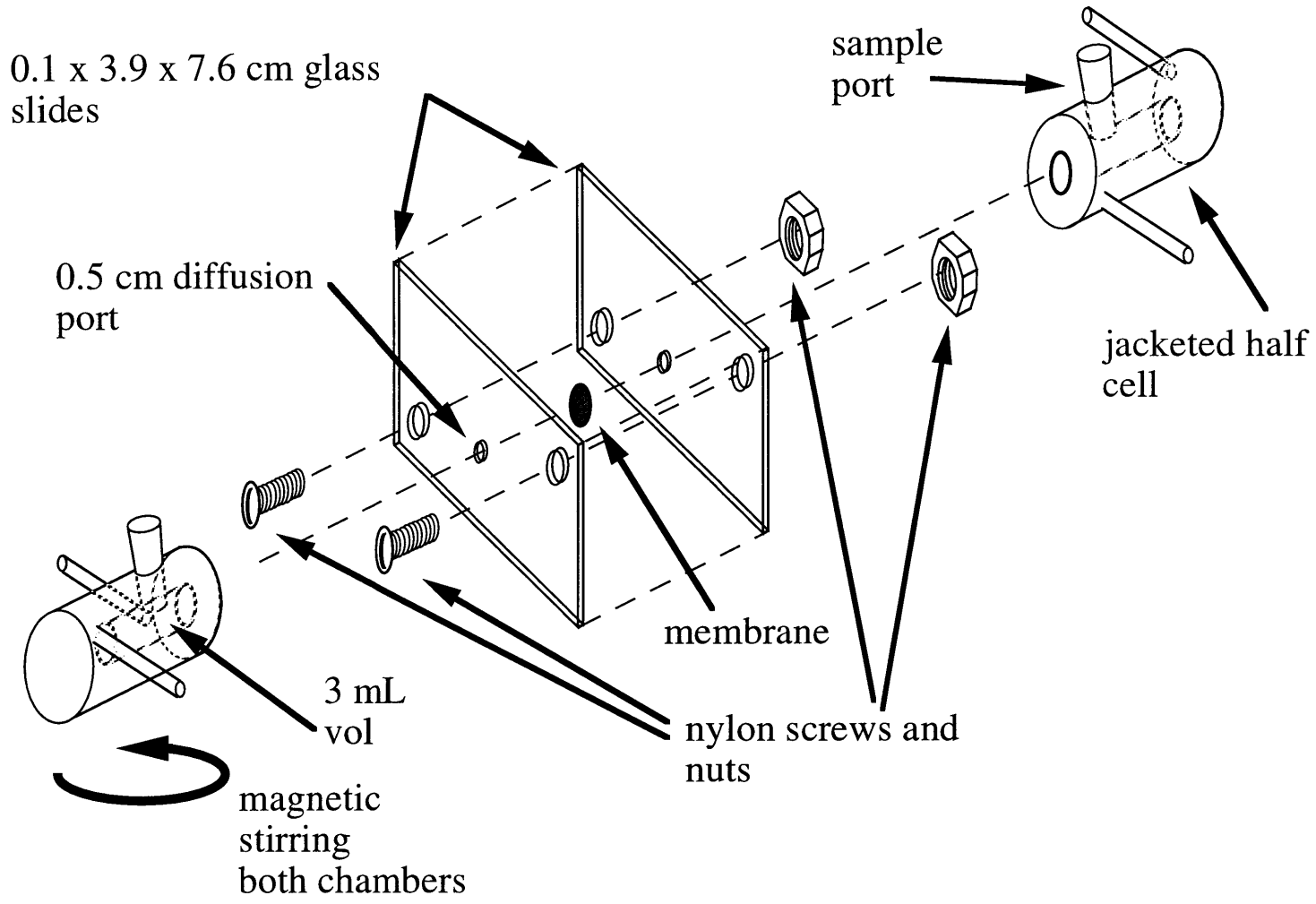

Figure 4.2 Diffusion Apparatus: The diffusion chamber apparatus consists of two diffusion chambers placed on either side of the 2 glass slide mounts that hold the membrane in place. Both chambers are mixed with magnetic stir bars.

The same procedure was followed for mounting Descemet's membranes and the Durex DV membranes using in the mixing studies. A bead of vacuum grease was applied around the face of each of the diffusion cells. 2 nylon thumb screws were placed in the bolt holes of one of the membrane mounts. The membrane itself was carefully positioned over the 0.5 cm diameter hole in this membrane mount using cotton swabs, and excess water was removed from the glass surface. The second mounting plate then was gradually lowered into place, and the nylon nuts were tightened evenly over the protruding screws. A drop of PBS-BSA was applied to each face of the exposed membrane to prevent it from drying-out and the membrane was observed under a dissecting microscope for any obvious holes created during dissection or mounting. The mounted membrane was placed over one of the diffusion cells and gently pressed to distribute the grease. This process was repeated for the second chamber, and the entire apparatus was positioned in the metal-Lucite clamp. The clamp bolt was tightened only until resistance was felt. 3 mL of 0.22 μm filtered PBS-BSA was added to each chamber and the apparatus was placed on the stir plate in a 4°C cold room. The plate stirring rate was set to setting 4, corresponding to a stir rate of 500 rpm. The following morning the chamber was observed for any leaks in the grease seal that may have developed overnight.

4.4.2 Mixing Studies with Urea

The diffusion of [^{14}C]urea across Millipore Durex DV membranes (0.65 μm pore size) was measured in the diffusion apparatus with and without the membrane slide mounts. Experiments were conducted at stirring speeds of 260 and 1180 rpm in PBS at 4°C. [^{14}C]urea (NEN, Boston, MA) was introduced to the source chamber, 200 μl samples were removed from the sink chamber and replaced with PBS over the course of a 4 hour experiment. The source chamber concentration was determined with 20 μL samples. Five samples were taken from the source chamber over the course of the experiment and the samples were not replaced.

4.4.3 FITC Dextran Membrane Integrity Study

High molecular weight FITC Dextran was used to assess the integrity of Descemet's membrane. 50 mg/mL solutions of FITC Dextran (Sigma) having average molecular weights of 148 kD and 38 kD were prepared in PBS. Descemet's membranes from 3 eyes were dissected and mounted in 3 diffusion chambers following the protocols listed in section 4.4.1. Six hundred microliters of buffer was removed from the source chamber of each of the diffusion chambers and 300 µl of each Dextran preparation was added to the source to initiate each experiment. At time points of 24, 52 and 94 hours, 500 µl samples were taken from the sink chambers and 10 µl samples were taken from the source chambers. Corresponding volumes of PBS were used to replace the amounts removed from each chamber.

The samples were chromatographed on a CL6B gel filtration column 1.5 cm in diameter and 19 cm long. All columns were pre-equilibrated with 50 mL of PBS, and run at flow rates of approx. 2 mL/min following a procedure similar to the one used for molecular weight determination of heparan sulfate (section 4.3.4). After removing 10 µl from the sink to determine the total column load, the remaining volume was loaded on the column. For source chamber runs, 2 µl of source sample was added to 500 µl of PBS and the resulting volume was loaded onto the column. Fractions were collected in 1 minute intervals. Two hundred microliters of each fraction was read in a fluorescent spectrophotometer with an excitation filter of 485 nm and an emission filter of 530 nm. To determine the amount of fluorescent Dextran loaded on the column, 10 µl of the sink load was read with 200 µl PBS, and 2 µl of the source load was read with 200 µl PBS.

4.4.4 Partition Coefficients

Descemet's membranes were dissected as described above (section 4.2.3) and diced until the larger pieces were approximately 1 mm^2. USB micro-columns were

incubated in PBS-BSA and then weighed dry. Roughly 0.1 g of membrane were added to each column and allowed to incubate in PBS-BSA while being constantly inverted at 4°C for 12 hours. Non-heparin binding ^{125}I-bFGF and ^{125}I-IL1β were prepared as described above. The wet mass of the membranes was determined by centrifuging the columns for 30 sec at 50 x g to remove excess solution and then measuring the total mass. Five hundred microliters of the solutions containing ^{125}I-bFGF or ^{125}I-IL1β were added to the membranes in the columns and incubated at 4°C with constant rotation. The centrifugation step was repeated. Both the membrane containing columns and their incubation solutions were counted in a gamma counter and weighed. The volume of incubation solution was determined by mass difference. A PBS-BSA solution was run through the membrane containing columns at 4°C at a flow rate of 1 mL/min and 2 mL fractions were collected. These fractions were then counted in a gamma counter. The partition coefficient was determined from the known membrane volume (V_{mem}), the total amount of elutable radioactivity from the membranes (γ_{mem}), the volume of incubation solution (V_{bulk}), and the total cpm of the incubation solution (γ_{bulk}).

$$K = \frac{\left(\frac{\gamma_{mem}}{V_{mem}}\right)}{\left(\frac{\gamma_{bulk}}{V_{bulk}}\right)} \qquad 4.2$$

4.4.5 Diffusion Chamber Coating

Applying a hydrophilic coating to the diffusion chambers and membrane mounts was a prerequisite for all diffusion experiments with proteins. The chambers and membrane mounts were soaked in 6 N HCl overnight and then washed exhaustively with deionized water. The coating solution was prepared with 25 mL 3-glycidoxypropyltrimethoxysilane (Aldrich), 225 mL of deionized water, and 62.5 µl of 1 M HCl to adjust the solution pH to 3.5. The silane reacts with water and was opened and

used in the hood. It was used immediately after solvation. The chambers and slides were coated for 6 hours at 90 °C, including a 1 hour warm-up period to prevent the chambers from shattering. Following the coating, the chambers were rinsed thoroughly with deionized water and placed in a dry box for storage.

4.4.6 Heparin Sepharose Purification of bFGF

Heparin sepharose CL6B was dissolved in deionized water to form a 1:2 gel to water slurry. A 100 µl column was poured using USB compact reaction columns and 1 L of PBS was run over the column overnight. The following morning, the column was equilibrated with approximately 30 mL of chilled PBS-BSA buffer. A 100 µl aliquot of ^{125}I-bFGF diluted with 200 µl PBS-BSA was added to the column after two 2 µl samples had been removed for TCA precipitation and the column had been drained to the bed surface. The column with bFGF was maintained in suspension on ice for a 10 minute incubation period. 30 mL of chilled 0.5 M NaCl PBS were then passed over the column to remove free label and unbound bFGF. After draining the column to its bed surface, 300 µl of 3.0 M NaCl in 1 mg/mL PBS was added to the gel, and incubated on ice for another 10 minutes. The eluant was removed by centrifuging the sample into a 2 mL centrifuge tube at 12000 rpm for 30 seconds, and its volume was determined using a 1 mL graduated pipette. In experiments conducted in a high salt buffer, the centrifugation step was omitted, and the bFGF was eluted with 4 x 200 µl volumes of 3.0 M NaCl. Two, 2 µl, samples were removed for TCA precipitation. The final concentration of bFGF was determined from the initial known concentration of bFGF and the 2 TCA precipitations.

4.4.7 Sephadex G-25 (PD-10) purification of bFGF and IL1β

Neither ^{125}I-IL1β nor ^{125}I inactive bFGF bind heparin; however free label must be removed from these preparations. In these cases, a pre-packed PD-10 column containing Sephadex G-25 gel filtration media was used to remove the free label in a

procedure similar to the one employed during Bolton Hunter labeling of bFGF (section 4.1.4). The PD-10 column was mounted on a ring stand, and an 18 gauge needle connected to the barrel of a 30 mL syringe was inserted into the cap of the PD-10 column. The column was equilibrated with 30 mL of chilled PBS-BSA buffer. The syringe and column cap were then removed from the column, and the column was allowed to drain down to it's frit. The IL1β or bFGF was brought up to a volume of 500 µl and 2 x 2 µl samples were removed for TCA precipitation. The remaining volume was added to the surface of the column frit and allowed to drain into the column itself. One and a half milliliters of PBS-BSA was then added to the bed, the cap and syringe were attached, the syringe was filled with 30 mL of PBS-BSA, and flow to the column was begun. Ten drop fractions were collected in 7x100 mm culture tubes, and 2 µl of each fraction was read in the gamma counter. The peak that eluted in the void volume of the column was then pooled. Two samples of 2 µL each were removed for TCA precipitation and the remainder was used in the diffusion experiment.

4.4.8 Diffusion Time Course Studies

bFGF or IL1β

Prior to initiating each diffusion study, the buffer in the sink chamber was replaced in case any trace amounts of radioactivity had leached off the chamber walls during the overnight equilibration. For experiments using native bFGF, the contents of the source chamber were replaced with a phosphate buffer lacking salt. The salt for the source chamber came entirely from the loaded bFGF. In all other studies the contents of the source chamber were replaced with a buffer identical to the one found in the sink chamber. Over the course of the experiment, 200 µl sample were removed from the sink chamber and the time was noted. This volume was replaced with PBS-BSA. The source chamber was sampled at 20 µl volumes much less frequently, and this volume was not

replaced. All samples were then subjected to TCA precipitated to quantitate the radioactive protein as described previously.

bFGF or IL1β in 3.0 M NaCl experiments

The protocol for these studies was the same as described in the sections above with the following exceptions. The Descemet's membranes were incubated overnight in the 3.0 M NaCl PBS 1 mg/mL in the diffusion cells. The buffers in both chambers were replaced with fresh 3.0 M NaCl PBS-BSA. The non-salt phosphate buffer was not used. After sampling from the sink chamber, the removed volume was replaced with the 3.0 M NaCl solution.

Protamine Sulfate experiments

Descemet's membrane were preincubated for 3 days in 10 mg/mL protamine sulfate before they were mounted in the diffusion chamber. The protocol for bFGF purification was not altered. All buffers used during the diffusion study were the same as described above except they all contained 10 mg/mL protamine sulfate.

Unlabeled bFGF experiments

100 μg of unlabeled bFGF was added to the experiment simultaneously with the ^{125}I-bFGF. The unlabeled bFGF was not pre-purified on heparin sepharose. The large amount of unlabeled bFGF would have required a much larger heparin sepharose column, and the resulting high salt eluant would have introduced too much salt to the diffusion cell. The percent active bFGF was determined to be 55% based on measurements with a bFGF ELISA kit (R&D Systems, Minneapolis, MN) following the manufacturer's procedures. The resulting concentration of active bFGF was approximately 1 μM.

4.4.9 bFGF Heparin Binding Assay

A 500 µl heparin sepharose column was poured in a USB micro reaction column and equilibrated in PBS-BSA. 2 mL of the sink chamber or 20 µL from the source chamber was allowed to drain over the heparin sepharose. The column was then washed with 5 mL 0.5, 1.0, and 3.0 M NaCl PBS-BSA solutions, 5 fractions of each were collected, and the radioactivity of the samples was measured in a gamma counter.

4.4.10 Determining DM thickness

The thickness of the membrane is a critical parameter in the diffusion process. The thickness of each membrane was measured after each diffusion experiment by taking advantage of its natural tendency to curl over on itself. Using a light microscope at 200x magnification the membrane was viewed in cross-section and photographs were taken. Membrane thicknesses were determined based on a calibrated micrometer photographed at the same magnification. Based on 26 individual diffusion experiments with Descemet's membrane the average membrane thickness was 40 µm with a standard deviation of 8 µm. The total thickness variation in a given membrane averaged 14 µm.

4.4.11 Descemet's Membrane Thickness Variation in High Salt

Changes in membrane thickness in response to shifting salt concentrations must be distinguished from regional variations in the actual membrane thickness. This was accomplished by designing an observation chamber that permitted the same area of the membrane to be viewed under a microscope (Nikon Diaphot) for the duration of the experiment. A 4x10 mm rectangle was excised from a 3 x 6 cm sheet of 1.5 mm thick neoprene rubber. A portion of Descemet's membrane was placed in this rectangular hole and sandwiched between two microscope slides. The slides were clamped in place and 18 gauge needles were forced into the open rectangle at opposing corners, and the entire

apparatus was fixed in position on a microscope stage. Buffer (PBS-BSA) was pumped into the chamber and the membrane was allowed to equilibrate for 2 hours. After this time period, pictures (Tmax 100 film, Eastman Kodak Co, Rochester, NY) were taken of a particular region of the membrane to provide a reference thickness at a magnification of 200x. The buffer was then switched by pumping 3.0 M NaCl PBS-BSA over the membrane. The conductivity of the effluent was monitored to ensure that the membrane had completely equilibrated with salt. The DM was incubated in this solution for 12 hours, and pictures were taken of the identical reference region. Changes in membrane thickness were determined by measuring the change in thickness in the photographs.

4.5 Polyacrylamide Glycosaminoglycan Gels

4.5.1 Production of GAG Acrylamide Gels: Electron Beam Treatment

Gels were cast between two glass plates held together with either an acetate or low density polyethylene (LDPE) spacer. Acetate spacers were 125 μm thick, while the LDPE spacers were 250 μm thick. PBS, bis/acrylamide stock solution (30% bis/acryl at 37.5:1 acrylamide:bis-acrylamide) (BioRad, Hercules, CA), and heparin stock solution (Heparin Grade IA, from porcine intestinal mucosa) (Sigma, St Louis, MO) were added to produce a final concentration of 10% bis/acrylamide and heparin concentrations ranging from 0.4 to 5 mg/mL. A 10% w/v solution of ammonium persulfate (BioRad) and 6.6 M N,N,N',N' tetramethylethylenediamine (TEMED) (BioRad, Hercules, CA) were added in the respective ratios of 1:2000 and 3:1000 to initiate polymerization. The polymerizing solution was poured between the glass plates and a layer of deionized water was layered over the surface. Polymerization was complete after 1 hour. The gels were removed from the glass plates and transferred to a PBS buffer containing heparin at the concentration found in the gel. The gel was allowed to equilibrate in this solution overnight.

The following morning the gels were transported to the electron-beam facility (MIT High Voltage Research Lab) where they were exposed to a high energy electron

radiation beam from a Van de Graaff generator with an overall energy output of 2.5 megaelectronvolts. Gels were exposed to total dosages ranging from 1.5 to 4.5 MRads. The gels were then punched into 11 mm diameter discs and allowed to incubate in a PBS solution to remove unbound heparin. The buffer was changed at various time points over a 2 week period for a total of 4 buffer changes until the GAG content in the buffer was below the threshold of detection by DMB (200 ng/mL). The GAG content of the gels was measured by uronic acid assay.

4.5.2 Uronic Acid Assay for Heparin Content of Gels

The uronic acid content of gels was measured using a modification of the assay developed by Bitter and Muir for the quantification of GAGs based on their uronic acid content [114].

All samples were prepared in aqueous saturated benzoic acid where possible. A standard curve was prepared using glucuronolactone (Sigma, St Louis, MO) in the 4-40 μg/mL range and heparin controls (30 and 100 μg/mL). Depending on sample volume, 3 or 5 mL of the 0.025 M sodium tetraborate in concentrated sulfuric acid solution was added to kimax screw cap test tubes.

All operations were conducted under a fume hood wearing gloves and lab-coat. Immediately before adding the sample, the sulfuric acid in the kimax tubes was frozen by immersing it in liquid nitrogen for approximately 1 minute. It was important that the acid be frozen, since an enormous amount of heat was generated when the aqueous sample was mixed with the acid. The sample (0.5 or 1 mL) was immediately added to the frozen acid, vortexed lightly, and placed on ice. As more samples were added to the ice, they were periodically revortexed. The acid and sample must be completely mixed and must always be kept on ice to avoid overheating during the mixing process. When the uronic acid content of gels was measured, the gel or gels were added to the kimax tube first. The kimax tube was weighed before and after the addition of the gel to obtain an estimate of the

gel volume, and aqueous saturated benzoic acid solution was added to the tube to bring the volume up to 1 mL. This sample was then frozen solid in liquid nitrogen, and 5 mL of borax acid solution was added to the frozen sample.

After the samples had been mixed completely, they were heated in the oven for 10 min at 100 °C. Placing the samples in a heating block in the oven ensured rapid and efficient heat transfer to the samples. During experiments conducted with heparin-polyacrylamide gels, the gels were incubated in the acid for 2 hours to allow for complete diffusion of acid into the gel and for diffusion of degraded GAG out of the gel. One hundred microliters (200µl for 1 mL samples) of 0.125% carbazole in methanol was then added to all samples, and they were vortexed vigorously for complete mixing. The color was developed by heating the samples for 10 min at 100 °C, and their absorbance was read at 530 nm. The color was stable for at least 16 hours. Absorbance measurements were made in disposable cuvettes.

4.5.3 bFGF Binding to GAG/acrylamide Gels

Gel discs 1.1 cm in diameter containing no GAG, 200 µg/mL heparin, and 400 µg/mL chondroitin sulfate were incubated in 1 mL of PBS-BSA for 6 hours at 4 °C, and then 13 ng of ^{125}I-bFGF was added to the solution. The discs were incubated with bFGF for 12 hours, and were then subjected to a series of washes for 2 hours each with 0.5 M and 1.0 M NaCL PBS-BSA. These washes were followed by a 4 hour wash with 3.0 M NaCl PBS-BSA, and finally, an overnight incubation with 4 M guanidine HCL in 3.0 M NaCl PBS-BSA. All washes and gels were then counted in a gamma counter to determine their ^{125}I content.

4.5.4 Electron Beam Treatment of Soluble Heparin

A stock solution of heparin (4 mg/mL Fraction Ia from porcine intestinal mucosa) was prepared and aliquoted into glass vials. All but one of the vials were

exposed to the electron beam, each vial receiving a different exposure (1.5, 3.0, or 4.5 MRads). The heparin preparations were diluted to approximately 12 nM (0.6 μg/mL) and incubated with 3 nM ^{125}I-bFGF for 1 hour at 4°C. The solutions were then chromatographed on a 5 mL Sephadex G-75 column as described in section 4.3.5.

4.5.5 Diffusion Studies with Polyacrylamide Gels

Polyacrylamide gels were punched into 13 mm discs and transferred to the slide mounts using a section of Saran Wrap (Dow). Diffusion experiments were conducted exactly as described for Descemet's membrane except the polyacrylamide gel was used instead. Sections 4.4.4, 4.4.5, and 4.5.7 describe the protocols.

Chapter 5

Characterization of Descemet's Membrane

5.1 Introduction

The fundamental hypothesis of this study is that DM HS influences bFGF transport through Descemet's membrane. Characterizing Descemet's membrane, with particular regard to DM heparan sulfate, was a necessary first step in this analysis. The biochemical composition and ultrastructure of Descemet's membrane has been explored by a number of researchers [9, 15, 115]. The presence of perlecan, the major basement membrane HSPG, has been confirmed by immunostaining [14, 116], but no study to date has purified and characterized Descemet's membrane heparan sulfate. The concentration of HS in the membrane and its affinity for bFGF are particularly important variables in the diffusion reaction model. Other researchers have characterized both the concentration of HS in various tissues, and the affinity of bFGF for HS from various sources. However, these parameters vary a great deal depending on the HS source; for example, measurements of bFGF/HS equilibrium binding constants have ranged over 3 orders of magnitude for HS from various tissues and cultured cell lines. Consequently, it was essential that the HS from actual DM be purified and characterized.

This chapter describes the isolation and purification of HS from basement membrane. In order to obtain a molar tissue concentration of HS, the molecular weight

distribution of the chains as well as the membrane water content had to be measured. The purified HS was used to determine the equilibrium dissociation constant for bFGF and heparan sulfate, and the kinetics of the interaction were explored also.

5.2 Membrane Isolation

In order to study the Descemet's membrane, a method was needed to obtain morphologically pure samples. As discussed earlier, Descemet's membrane is bordered by the corneal stroma and the corneal endothelium. The corneal endothelium is a monolayer of cells, and it is readily removed from the membrane by a series of wipes with cotton swabs or tissue followed by rinsing with PBS, as confirmed by microscopic observation of the cornea and DM. It is much more difficult to dissociate the DM from the stroma. Any dissection that involves merely pulling or cutting the stroma away from the DM will invariably leave significant amounts of stroma associated with the membrane. These stromal layers swell in aqueous solution once the tissue has been disrupted as seen in Figure 5.1a, below. The stroma, *in vivo*, is formed from tightly packed lamella. However, the swelling causes those layers to separate, creating the much more loosely arranged structure seen in the figure.

A series of dissection approaches were tried, ranging from pulling the DM away with forceps to using a specialized surgical cyclodyalisis tool to separate individual stromal layers. Ultimately, we developed a simple technique for obtaining comparatively large sections of stromal free membrane for use in diffusion experiments and in the studies described here. The technique is described in detail in section 4.2.3. The cornea was excised using a pair of curved surgical scissors to cut along the cornea's periphery. It was placed on a curved surface with its endothelium face up, and the endothelial cell layer was removed by repeated wiping with a tissue and rinsing with PBS.

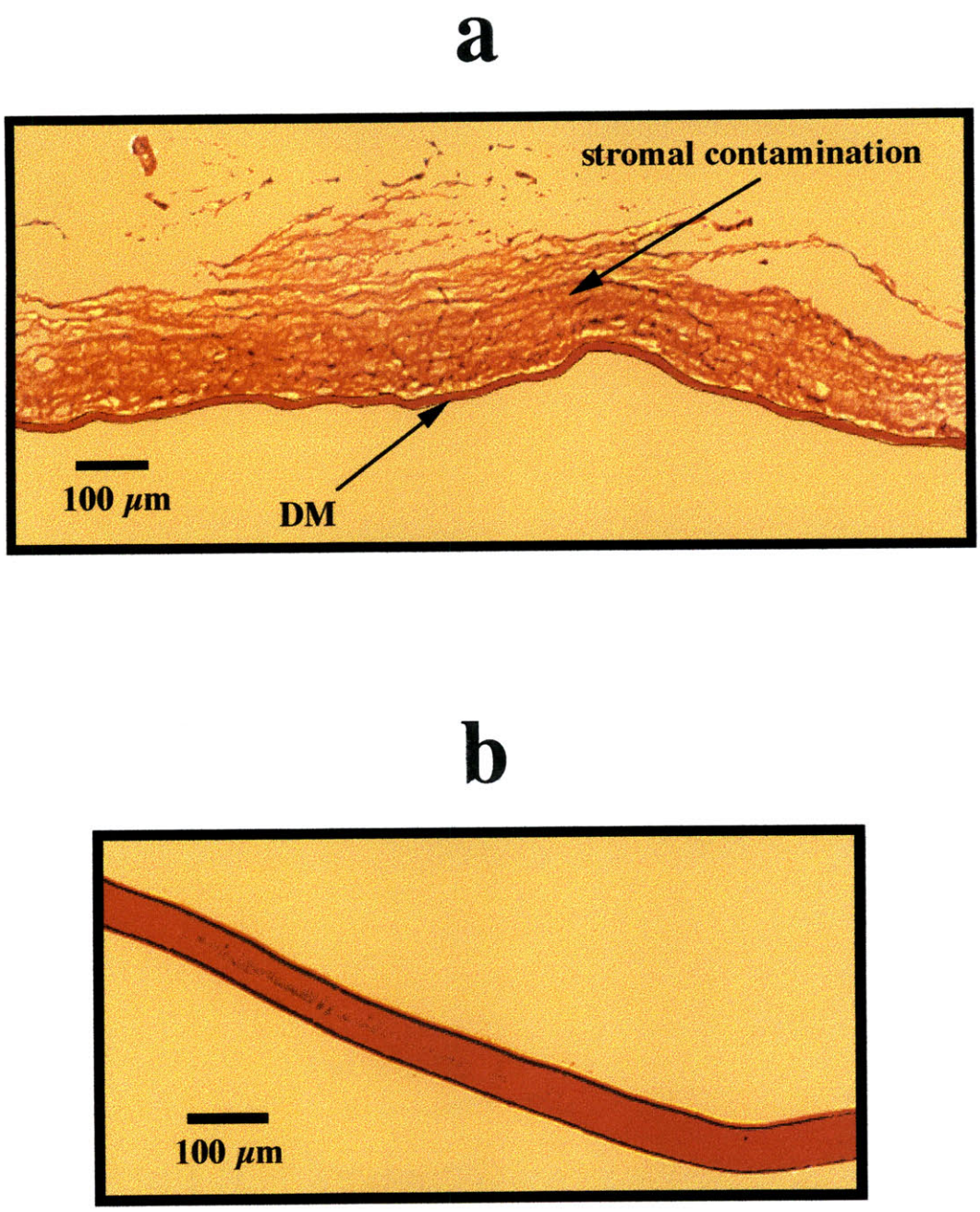

Figure 5.1 Descemet's Membrane Dissections: (a) A crude dissection of a calf Descemet's membrane has a large amount of swollen corneal stroma still associated with the DM. (b) Dissection of a mature cow DM employing the refined dissection tecnique shows no evidence whatsoever of stroma. Both specimens were fixed in formaldehyde, imbedded in parafin, sectioned, and stained with PAS, a typical basement membrane stain. Note, also, that the endothelial cell monolayer has been colmpletely removed from both specimens.

The surface of Descemet's membrane was then scored with a scalpel, and using a curved Teflon spatula, the membrane was teased slowly away from the stroma. The success of this method depended a great deal on the thickness of the membrane. Descemet's membrane thickens with age in both cows and humans [117, 118]. The thick membranes from older animals are much more easily removed. Therefore, in all our studies, DM from adult cows (over three years old) were used. Figure 5.1 b shows a fixed, sectioned portion of membrane stained with the periodic acid schiff (PAS) technique, a typical basement membrane stain [119]. All traces of either stroma or endothelium are absent.

The thickness of bovine Descemet's membrane varies across a given membrane. The thinnest region is in the center of the cornea, and it thickens progressively toward the edges. This increase in thickness is paralleled by the cornea itself. The average thickness for membranes used in this study was 40 ± 8 μm.

5.3 Isolation of Descemet's Membrane Heparan Sulfate

5.3.1 Immunolocalization of Perlecan HSPG to Descemet's Membrane

We conducted immunolocalization studies with an antibody to perlecan, the major extracellular matrix heparan sulfate proteoglycan, to confirm its presence in the bovine DM and to determine its distribution in Descemet's membrane. It is believed that most of the HS is associated with this proteoglycan, and the HS should mirror the proteoglycan membrane distribution. Whole corneas from mature cow were frozen and sectioned into 4 μm thick slices and exposed to a perlecan antibody. This primary antibody was recognized, in turn, by a secondary antibody conjugated to fluorescent probe, fluorescein isothiocyanate (FITC). The sections were visualized and recorded using a confocal laser scanning microscope. Confocal fluorescent microscopy has the advantage over standard fluorescent microscopy in that the confocal microscope can be focused to a single plane less than a micron thick within the object of interest.

In Figure 5.2, it is clear that the perlecan is restricted to Descemet's membrane with negligible background staining of the stroma. Significant amounts of perlecan were also detected in Bowman's membrane, the extracellular matrix that separates the stroma from the corneal epithelium. Ljubimov [14] reported that, in human eyes, perlecan appears to be localized to the endothelial face of the DM. Upon first inspection, a similar staining pattern was evident in the bovine DM. However, in this study, the endothelium was not removed prior to freezing and sectioning. It is likely that the freeze thaw destroyed the endothelial cell layer, but we attribute the higher staining levels on the endothelial surface to formerly cell associated perlecans. The confocal microscope can be used to image regions within the tissue 0.3 μm thick. A series of images was generated by moving through the 8 μm slice of cornea in 1 μm increments. The three images in the figure represent views from the top surface, the center, and the bottom surface. Both the upper and lower surfaces show more uniform staining patterns, while the central region shows perlecan only on the periphery. The antibody molecules probably cannot penetrate into the central region of the membrane, and, as a result, staining appears localized to the edges of the membrane. We concluded that the distribution of perlecan, and hence, HS, was uniform through the bulk of the DM based on these results.

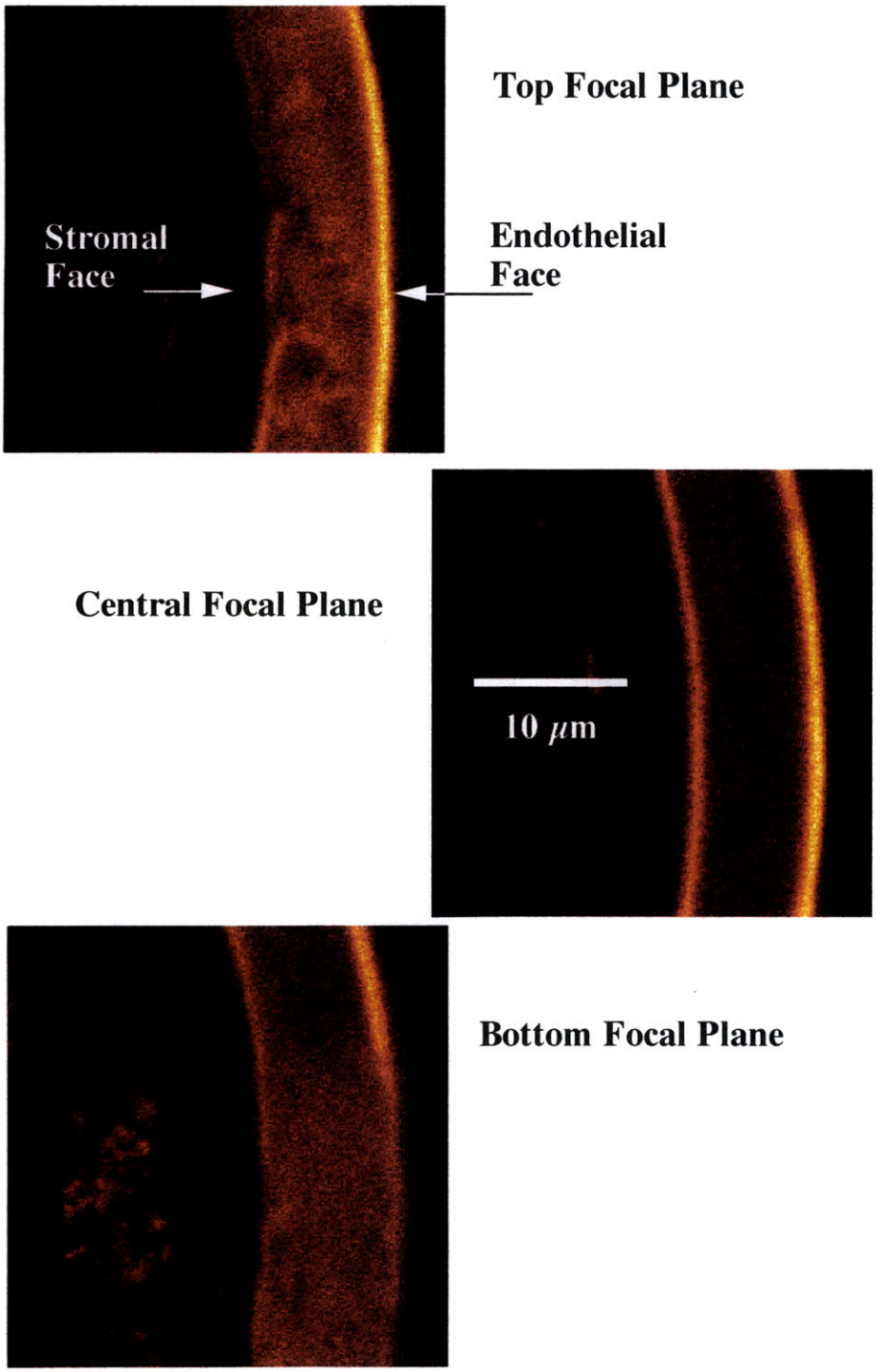

Figure 5.2 Perlecan HSPG Immunostain of DM: Whole corneas were frozen, sectioned, and immunostained for the perlecan HSPG. Using the confocal microscope, three images of a single stained corneal section were generated at different optical planes within the sample: the upper surface, the section center, and the lower surface. Preferential staining of the endothelial face was attributed to HS rich endothelial cell residue. The peripheral staining seen in the central image was attributed to restricted diffusional access of the immunoglobulin staining agents to the interior of the membrane.

5.3.2 Extraction of HS from Descemet's Membrane

High Salt/ Denaturant extraction

Initial efforts at extracting heparan sulfate proteoglycan from Descemet's membrane relied on traditional techniques involving high salt and high concentrations of denaturants such as urea and guanadinium hydrochloride [120]. Despite the clear presence of perlecan in the immunostain results, almost no HS was detected in four separate extraction experiments. The low yields could have been due in part to the fact that these Descemet's membrane preparations had significant stromal contamination. The high percentage of keratan sulfate would significantly reduce the percentage of heparan sulfate in the sample. However, although the swollen stroma appeared to make up close to 90% of the volume of dissections as determined by the fixed, sectioned, and stained sections, we estimated that the DM represented 50% of the dissection's mass. Consequently, heparan sulfate should still have been present at much higher concentrations than was evident in our assays if it was present in the extracts. Another possibility was that the large HSPG was physically entrapped in the tight collagen VIII meshwork that dominates the architecture of Descemet's membrane. This theory was supported by the observation that significant amounts of the HSPG were evident in immunostains of the extracted membrane. Based on this hypothesis we shifted our strategy toward dissolution of the membrane followed by subsequent recovery of the HSPG.

Collagenase Digestion of Descemet's membrane

Since the major structural component within the membrane is the collagen network [10, 11], we attempted to release the HSPG by digesting the collagen matrix with enzymes. In fact, isolation of HSPG from the EHS tumor basement membrane is dependent on growing the tumor in lathyritic mice that have poorly crosslinked collagen. Preparations of collagenase from *clostridium histolyticum* were very effective in

dissolving the matrix. However, as seen in the Western blot in Figure 5.3, the collagenase preparation also rapidly degraded the perlecan core protein. Untreated perlecan, isolated from the conditioned media of cultured bovine aortic endothelial cells [111], appeared as a high molecular weight doublet. However, after 3 hours of treatment with 2.5 mg/mL collagenase, the only immunoreactive band was a perlecan fragment at the bottom of the gel. This experiment could not be used to determine whether the collagenase itself digested the perlecan or whether some other proteases in the preparation were responsible. In a paper by Whitelock [121] published after these studies were performed, it was demonstrated that collagenases degraded perlecan. Furthermore, when ^{35}S radiolabeled HS was incubated with and without collagenase and then passed over a Q sepharose anion exchange column, more radioactivity was present in the flow through of the collagenase containing sample. Degraded GAG fragments bind weakly to Q sepharose media, and hence, appear in the column flow-through. This result suggested that contaminating heparinase activity was also present in the collagenase. Given this information we turned toward a specific chemical approach to liberate the HS chains from the matrix, reductive beta-elimination.

β-eliminative cleavage of HS from the core protein with alkaline sodium borohydride

Beta-eliminative cleavage of GAG chains from the proteoglycan core protein is routinely used to release the GAG chains from the protein core for subsequent analysis, including molecular weight determination [112]. In control studies with heparin, the elimination reaction was carried out for 24 hours without significant reduction in the heparin concentration as measured by the dimethylmethylene blue (DMB) dye binding assay. Since the DMB assay is based on charge-charge interaction, this result implied that no significant desulfation of the heparin occurred during the incubation. Membranes were isolated as described above with no detectable stromal contamination.

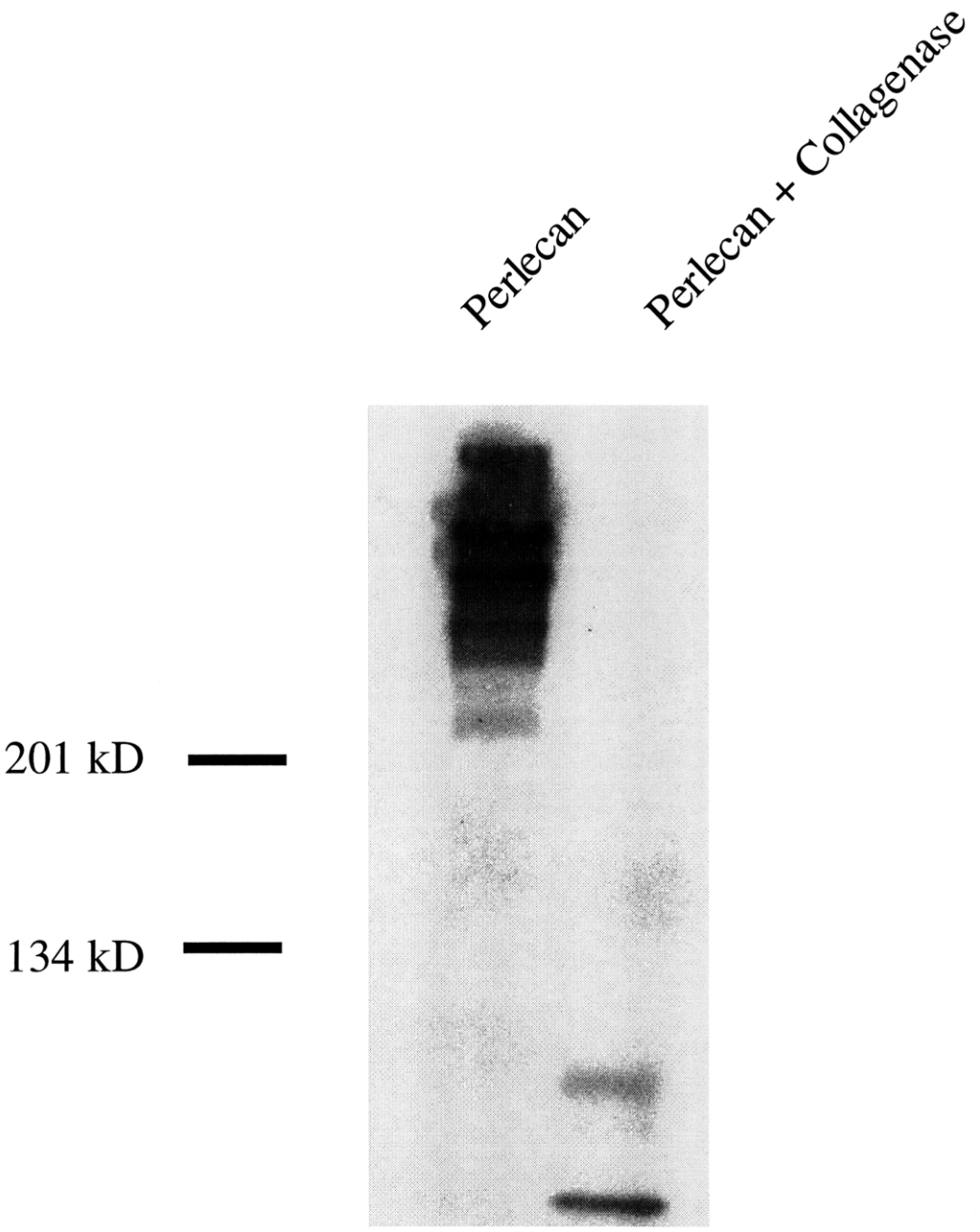

Figure 5.3 Western Blot of Collagenase Degradation of HSPG: [^{35}S] perlecan treated with collagenase and a control without collagenase were subjected to SDS PAGE and a Western blot with anti-perlecan antibodies. Both samples were treated with heparinase prior to electrophoresis to remove HS chains to allow the core proteins to enter the gel. The control perlecan shows a characteristic high molecular weight doublet, while the sample subjected to collagenase treatment shows only low molecular weight degradation products.

They were incubated in a 1 M sodium borohydride solution with 50 mM NaOH at 37 °C for 24 hours. The membranes were completely solubilized by this treatment. The solution was neutralized and dialyzed. The amount of GAG was determined by the DMB assay, and the Bradford coomassie blue assay was used to determine protein content. GAG composition was determined by selective enzymatic degradation. Table 5.1 summarizes the results from two independent extractions and provides a comparison with two kidney basement membranes.

GAG	extract 1	extract 2	ave	TBM	GBM
Heparan Sulfate	37%	44%	41%	90%	85%
Keratan Sulfate	51%	50%	50%	0%	0%
Chondroitin Sulfates	12%	6%	9%	10%	15%

Table 5.1 GAG composition of degraded DM as determined by the selective enzymatic degradation assay is compared to the composition of the bovine kidney glomerular basement membrane (GBM) and the tubular basement membrane (TBM) [122].

The kidney basement membranes have no detectable levels of keratan sulfate. However, the corneal stroma is rich in keratan sulfate. The higher levels of keratan sulfate in Descemet's membrane may represent the influence of stromal cells on DM synthesis.

It was difficult to assess the efficiency of the beta-elimination step in releasing HS chains from the membrane. Given the duration of the incubation and the fact that the membranes themselves were dissolved by the treatment, it is likely that the yield was quite high. An estimate of 50% recovery suggested an overall GAG concentration in the membrane of about 3 mg/mL and a HS concentration of about 1 mg/mL.

5.3.3 Purification of DM HS

Measurements of DM HS association with bFGF and measurement of the HS molecular weight distribution require pure preparations of heparan sulfate. We used ion exchange chromatography to separate the highly negatively charged GAGs from contaminating proteins. This step does not significantly purify the heparan sulfate from the other glycosaminoglycans. We employed two enzymatic degradation steps to remove contaminating GAGs. The purification scheme is summarized in the flow sheet in the following Figure 5.4.

The Q sepharose column accomplished a 100 fold reduction in the total amount of protein in the extract. The chromatogram of the first Q sepharose column is shown in Figure 5.5. After a 0.3 M NaCl wash to remove weakly bound protein and GAG, a linear NaCl salt gradient from 0.3 to 1.5 M NaCl was passed over the column. The two major peaks were assayed for their GAG composition, and these values are shown in Table 5.2.

GAG	Peak 1 composition	Peak 2 composition
Heparan Sulfate	62%	13%
Keratan Sulfate	20%	81%
Chondroitin Sulfates	18%	6%

Table 5.2 Composition of Q-Sepharose Elution Peaks

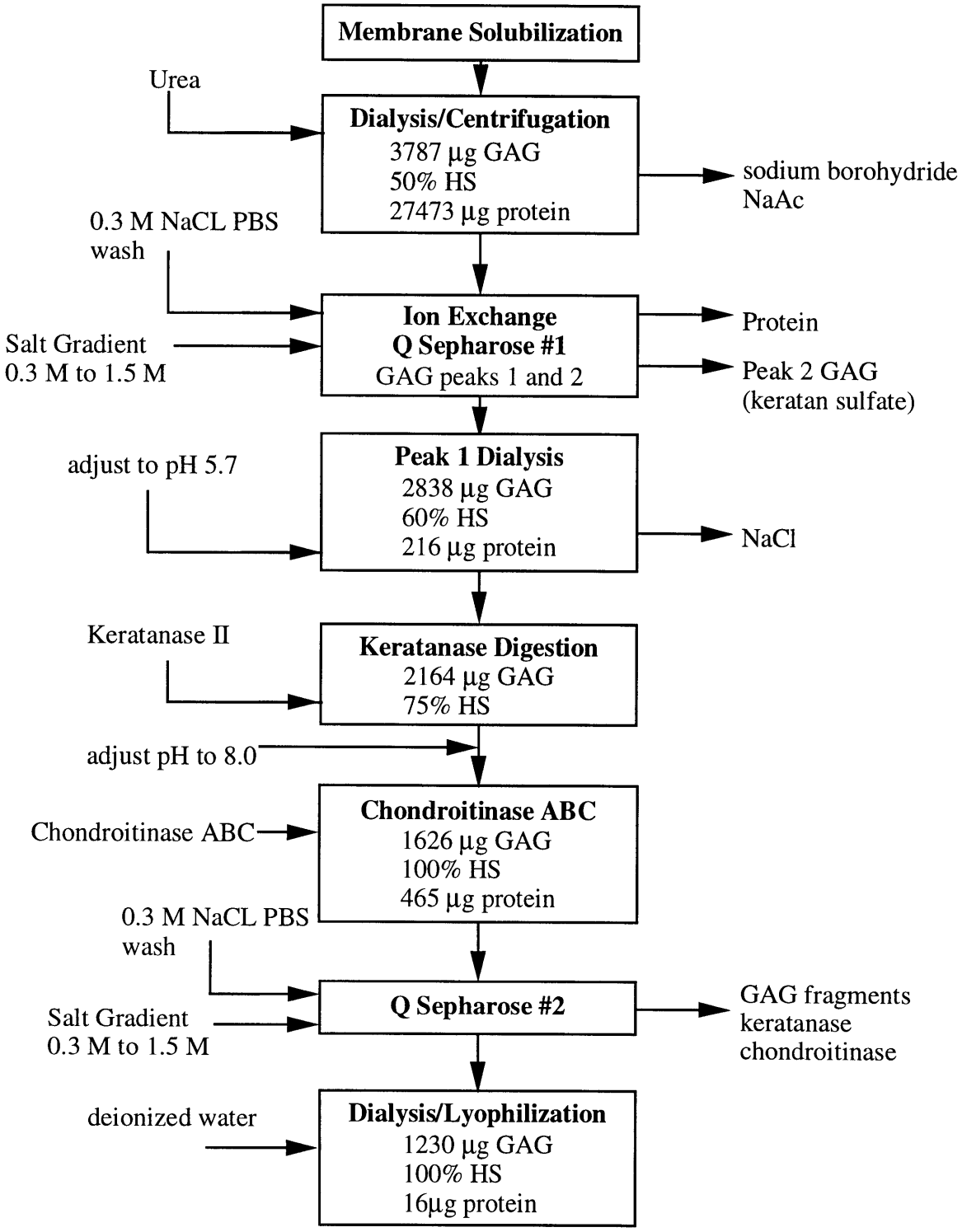

Figure 5.4 HS Purification Flow Sheet: The purification of heparan sulfate from Descemet's membrane was based on ion exchange chromatography applied in conjuction with selective enzymatic degradation of contaminating GAGs. The final product had approximately 1% protein by mass and no detectable contaminating GAG.

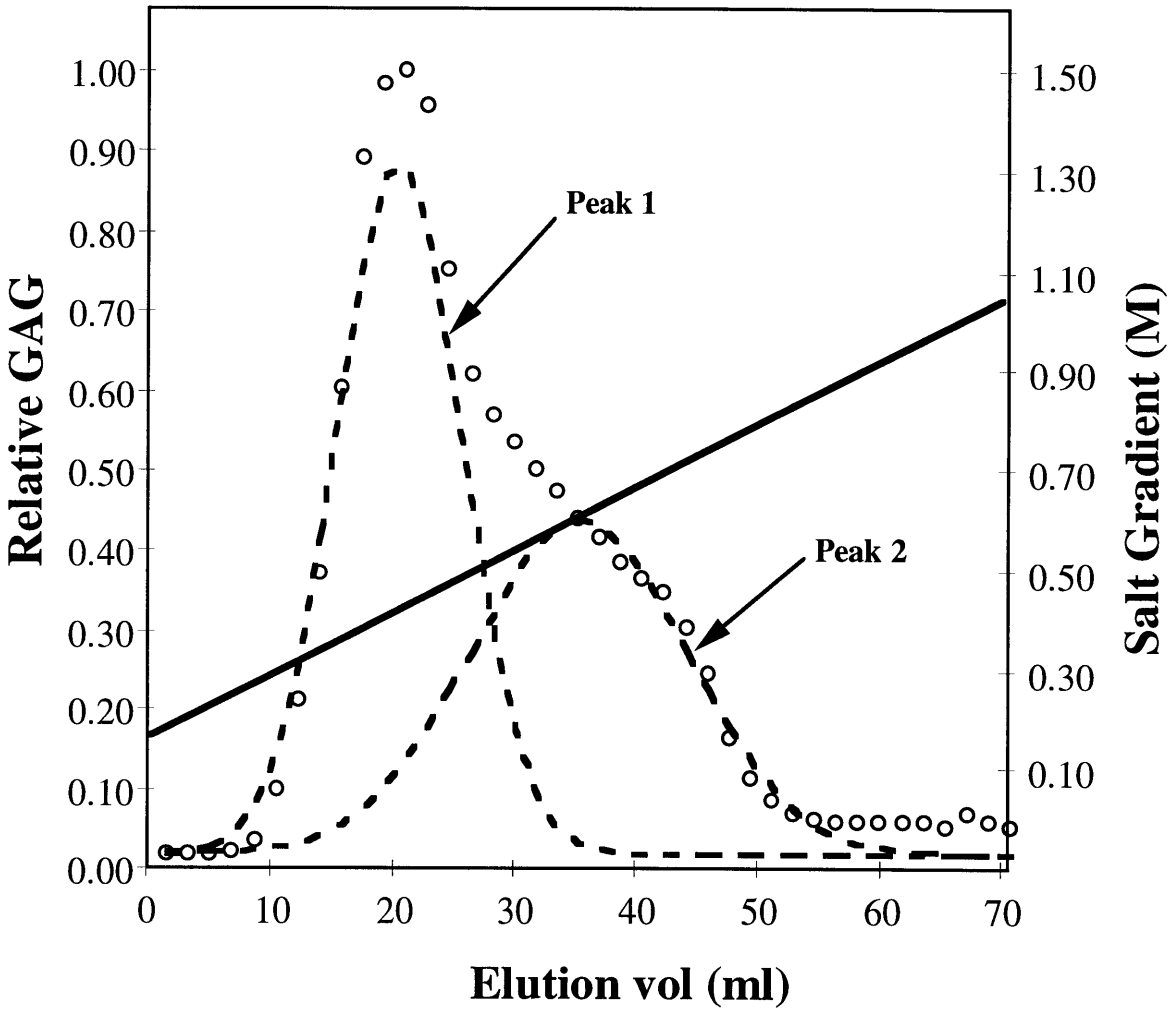

Figure 5.5 Initial Q-sepharose Chromatogram: The crude DM extract was subjected to Q-sepharose gradient chromatography to remove protein and partially resolve HS from other GAGs. Two overlapping peaks were evident in the chromatogram. The open circles are representative of relative GAG concentration as determined by the DMB assay. The solid line is the salt gradient. The dashed line represents a best fit deconvolution of the eluted GAG into two gaussian peaks.

The first peak was rich in HS, and was used in subsequent purifications. The second peak was predominantly keratan sulfate, suggesting that DM keratan sulfate has a significantly higher charge density than HS from the same source.

The anion exchange column was followed by successive enzymatic degradations with keratanase II and chondroitinase ABC. These enzymes selectively degrade keratan sulfate and the chondroitin sulfates, respectively. The purity and specificity of both enzyme preparations had previously been evaluated, and those experiments confirmed that the enzymes contained minimal heparanse contamination. Pilot studies were also conducted with smaller amounts of enzyme and DM GAG to ensure that the target GAG would be completely degraded. After the enzyme treatments, the extract contained significant amounts of GAG fragments, as well as the chondroitinase and the keratanase. These contaminants were removed with a second Q sepharose step as shown in Figure 5.6. This chromatogram confirmed that the higher charge density GAGs had been effectively cleared from the sample. Enzymatic compositional analysis showed no detectable contaminating GAG and approximately 1 % protein by mass. The purified HS was dialyzed and lyophilized for future use.

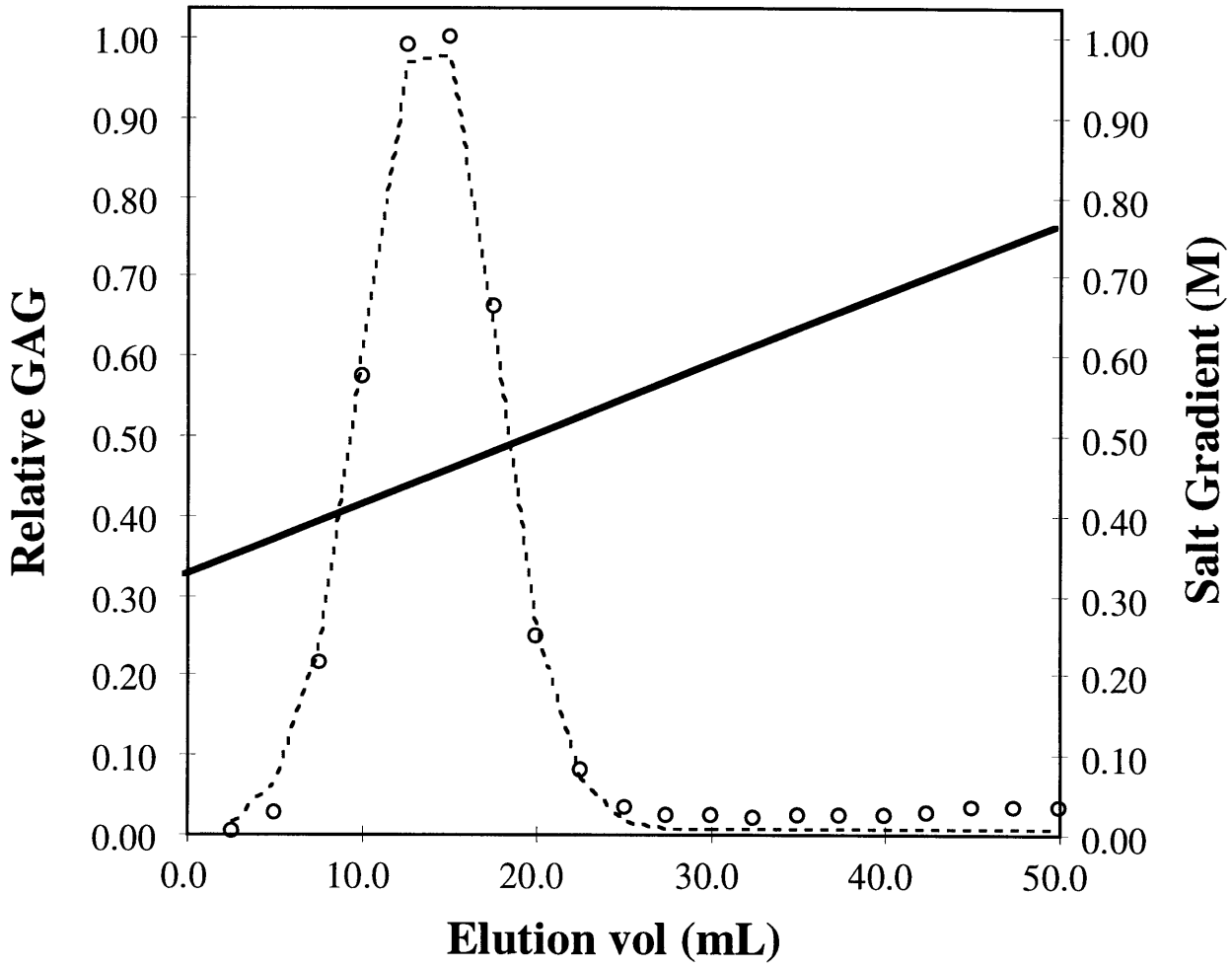

Figure 5.6 Final Q Sepharose Chromatogram: A final Q sepharose anion exchange step removed chondroitinase, keratanase, and GAG fragments. This chromatogram shows the final HS peak that resulted from the purification (o). The solid line represents the salt gradient. The relative amount of GAG was determined by a DMB GAG assay.

5.4 Characterization of Descemet's membrane HS

5.4.1 Molecular Weight of DM Purified HS

The molecular weight distribution of Descemet's membrane HS chains was determined by gel filtration chromatography. The HS had previously been labeled with ^{125}I using the same Bolton-Hunter technique used for bFGF radioiodination. This labeling strategy should randomly attack any available free amines along the HS chains. Analysis of the labeled HS suggested that each radiolabel was associated with a 40 kD region of HS. Figure 5.7 a represents a Sepharose CL6B chromatogram of the purified HS chains. Given the comparatively low labeling efficiency, we treated the amount of radioactivity in each chromatography fraction as a reflection of chain number rather than chain mass. Wasteson [113] correlated chondroitin sulfate MW with Kav data from a CL6B column, and, by applying this conversion, we obtain Figure 5.7 b. Analysis of this data provided a MWn of 42 kD and a MWw of 78 kD for a polydispersity of 1.9. As described earlier, HS chains are heterogeneous in both length and structure, so it was not surprising to see a broad size distribution. Other researchers have measured basement membrane HS chains of similar size [123, 124]. For our studies the heparan sulfate molecular weight was used primarily to convert mass concentrations into molar concentrations. We used the 42 kD MWn to determine molar concentrations. Using the number averaged molecular weight of heparan sulfate of 42 kD, and the membrane mass concentration of heparan sulfate of 1.1 mg/mL gave a HS concentration of 26 μM.

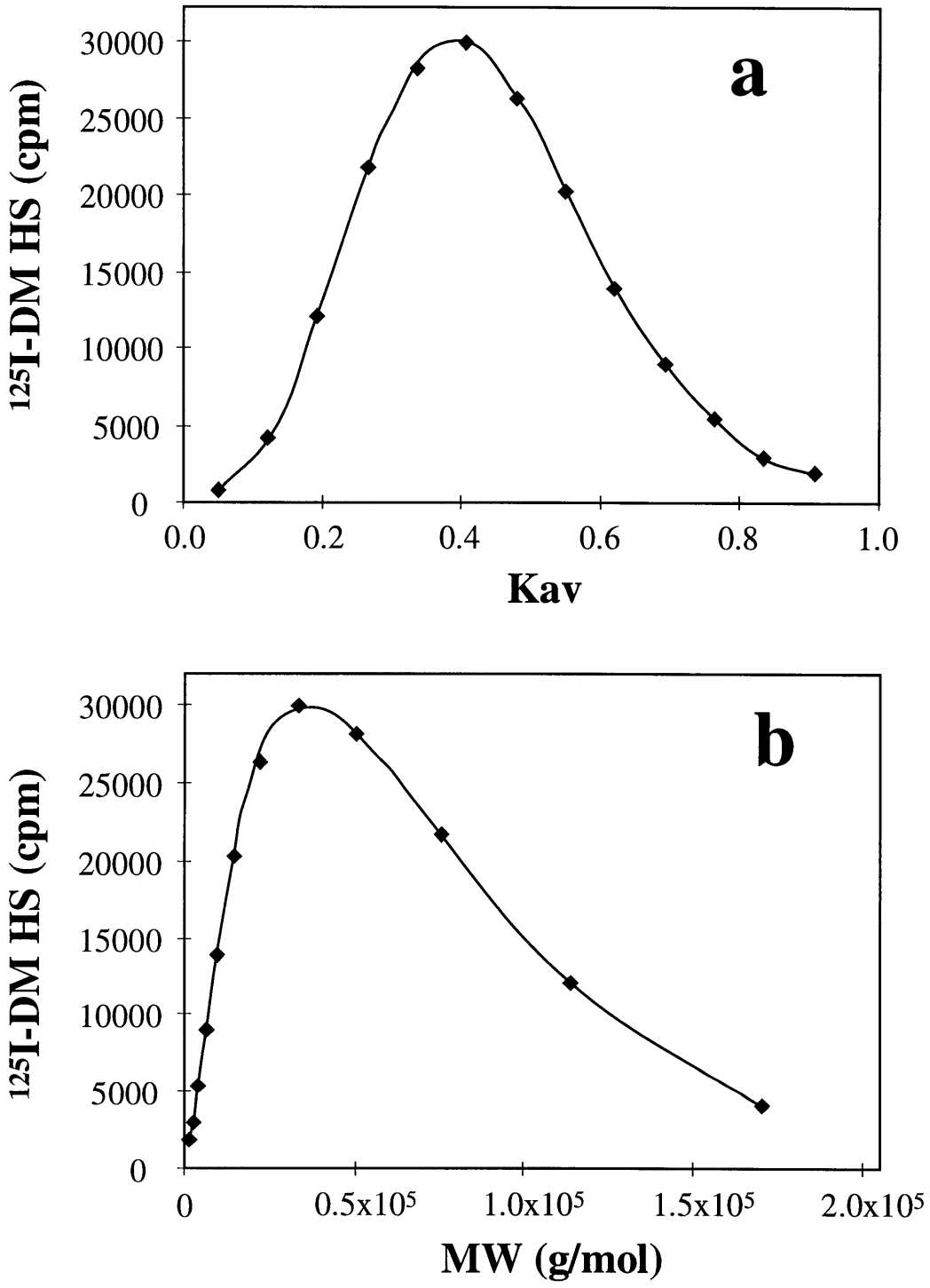

Figure 5.7 DM HS for Molecular Weight Distribution: (a) ^{125}I-DM HS was resolved on a CL6B gel filtration column. The total column volume (V_t) was determined with free [^{35}S] and the void volume (V_v) was determined with 2 million MW FITC Dextran. Kav was then calculated for each eluted volume fraction (V_e): $Kav=(V_e-V_v)/(V_t-V_v)$. (b) Kav data was converted to GAG molecular weight based on published results for chondroitin sulfate standards with CL6B chromatography media.

5.4.2 Equilibrium Binding Constant for bFGF and Descemet's Membrane HS

The binding of bFGF to heparan sulfate is proposed to be a critical step in the diffusion process through the basement membrane. Furthermore, differences have been noted in the binding constant for bFGF and HS from various sources as can be seen in the table below.

Source	Kd (nM)	technique	Reference
BALB3T3 Surface Syndecan	29	ACE	[125]
EHS tumor HSPG	31	Solid Phase	[84]
Bov. Corneal EC ECM	610	Solid Phase	[82]
Bov. Capillary EC Surface	280	Cell Surface Binding	[126]
BALB3T3 Cell Surface	0.76	Cell Surface Binding	[71]
Rat Growth Plate ECM Extract	14	Solid Phase	[127]

Table 5.3: Literature values for HS equilibrium binding constant to bFGF

Consequently, characterizing the interaction between bFGF and DM heparan sulfate was an important step in understanding and modeling the larger system. The interaction of bFGF with heparin and heparan sulfate was discussed in section 1.4.1. The approach described here is based on the fact that gel filtration chromatography can be used to rapidly separate free bFGF from the much larger bFGF/HS complex.

Radiolabeled ^{125}I-bFGF (2 nM) was incubated with varying concentrations of DM HS (10 pM - 150 nM) for a minimum of 2 hours at 4°C. The binding reaction took place in PBS-BSA buffer in Corning NBS coated vials to minimize adsorption losses of

bFGF. The incubation solution was passed over a 5 mL Sephadex G-75 column under gravity flow with a PBS-BSA. buffer, and the elution profile of the labeled bFGF was determined. Most of the DM HS eluted in the void volume in a column poured with Sephadex G-100, a gel filtration media with a larger pores size that G-75. We chose G-75 media to ensure that the bFGF/HS complex would remain exclusively in the column void volume. Figure 5.8 presents the chromatogram for the runs with no heparan sulfate, 10 nM, and with a saturating amount of 100 nM. A small peak of high molecular weight material was evident even with no heparan sulfate present. This peak probably represented aggregated bFGF. The free bFGF eluted as a broad peak due to nonspecific adsorption to the Sephadex media. Preincubation of bFGF with heparan sulfate resulted in a clear complex peak resolved in the void volume which corresponded to large bFGF/heparin complexes. The magnitude of the complex peak was sensitive to HS concentration up to a saturating value. A binding isotherm was generated by repeating these experiments with varying heparan sulfate concentrations.

To analyze the data, the background bFGF aggregate peak was subtracted from all the peaks with bFGF and HS. Furthermore, denaturation during the freeze-thaw process inactivates a certain percentage of the bFGF. The percent active bFGF was determined from the ratio of the saturated peak area to the total load. This number was used in conjunction with the specific radioactivity of the bFGF to calculate the complex concentration from the peak areas. The free bFGF-HS binding site concentration was calculated by assuming a 1:1 association of bFGF with heparan sulfate.

Figure 5.9 is the binding isotherm generated by these calculations along with a fit of the data based on a single site reversible binding model. The dissociation constant determined from this experiment was 3.9 ± 0.4 nM. As seen in the table above, this value fell in the midst of other measured values for the dissociation constant. While some of the variability in the values tabulated here can be attributed to differences in technique, the known heterogeneity of the HS must also be a major factor.

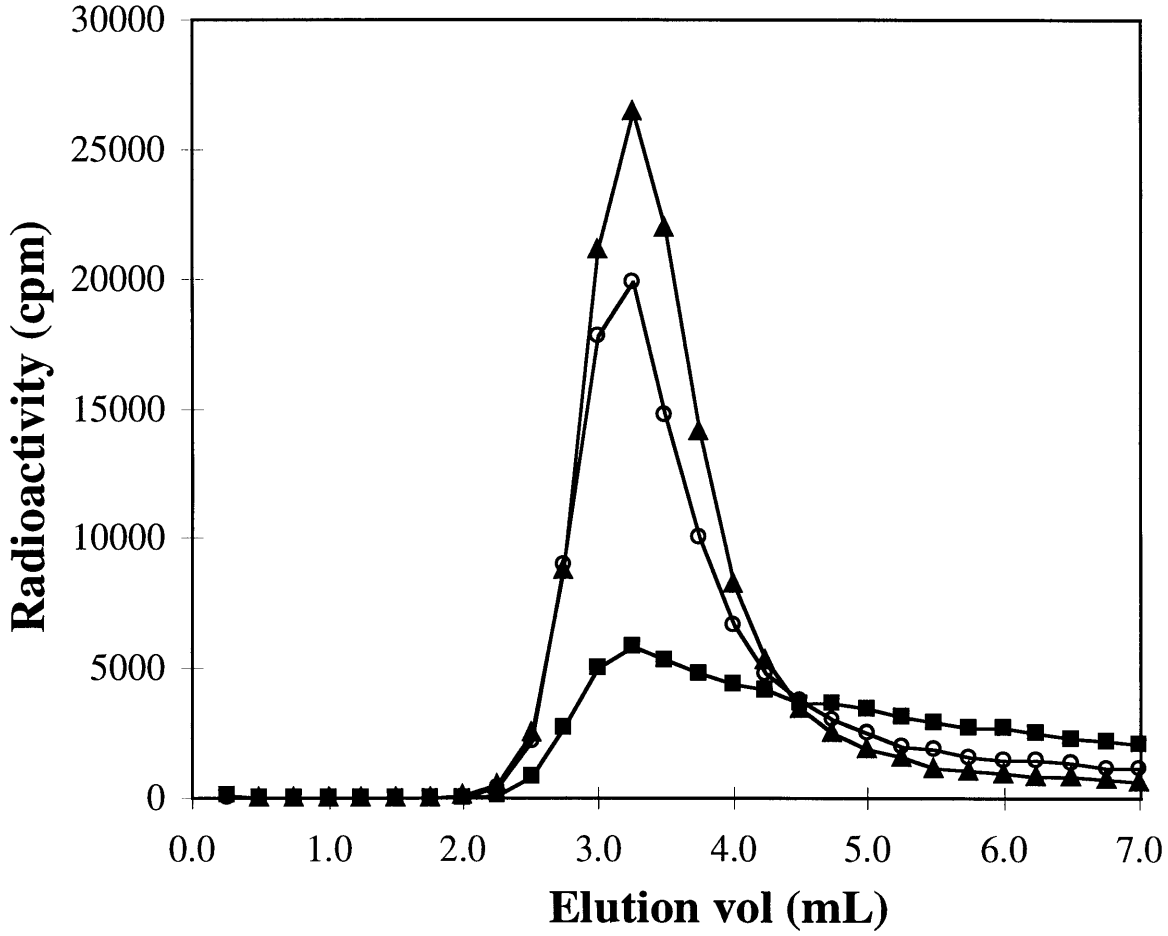

Figure 5.8 Raw Binding Constant Data for bFGF and DM HS: ^{125}I-bFGF/DM HS complexes were resolved using a Sephadex G75 column. Chromatograms of ^{125}I-bFGF incubated with 100 nM (▲), 10 nM (o), and 0 nM (■) DM HS are shown here.

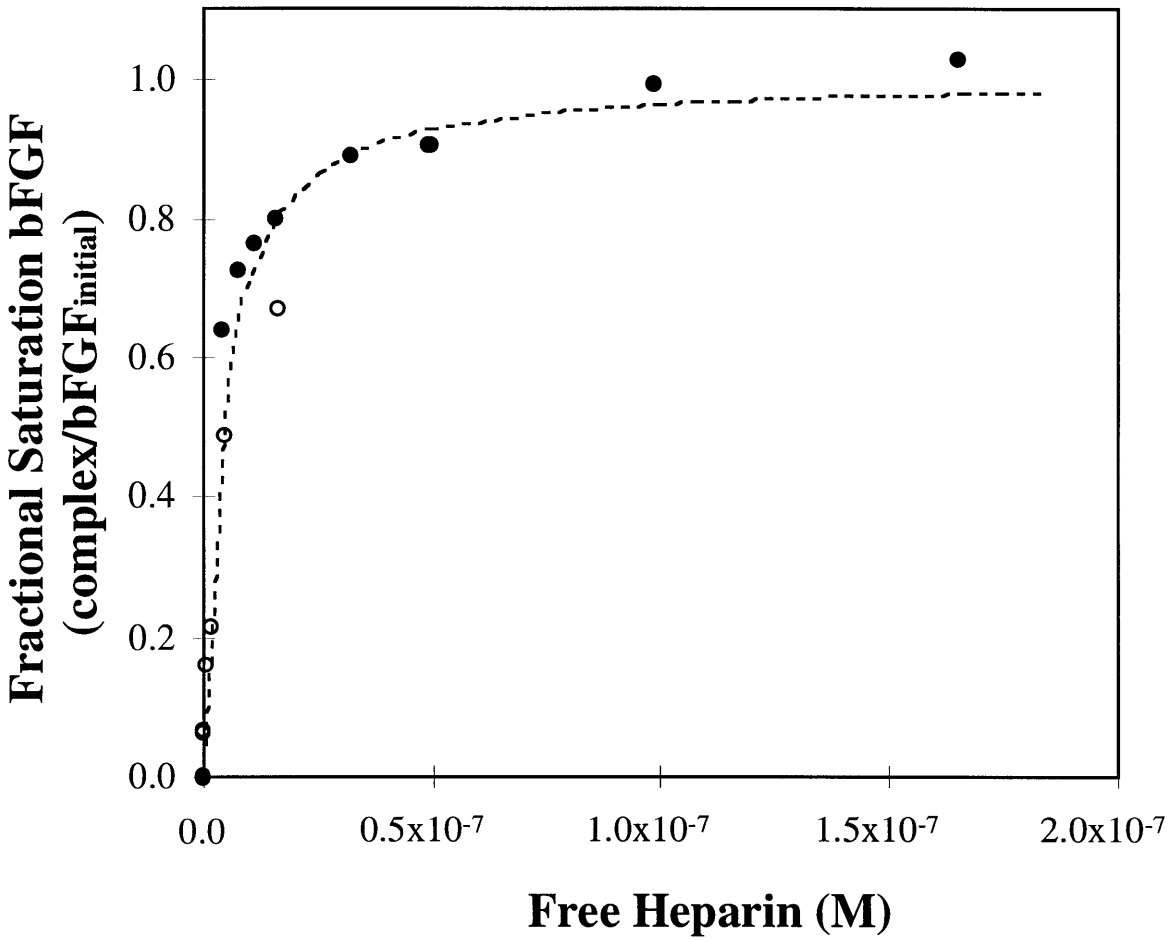

Figure 5.9 Binding Isotherm for bFGF and DM HS: The bFGF/DM HS binding isotherm was fit to the equation C/b° = Kd / (H+ Kd), where C/b° is the fractional saturation of bFGF (ratio of bFGF/HS complex to the initial bFGF concentration), H is the concentration of free heparin, and Kd is the equilibrium binding constant. Two independent data sets (○●) were fit to this equation yielding a Kd of 3.9 ± 0.4 nM with an R^2 of 0.98.

5.4.3 Kinetics of bFGF and DM HS Interaction

A dynamic model of bFGF diffusion through Descemet's membrane must include the kinetics of the bFGF association with heparan sulfate. We assumed simple reversible association of bFGF to HS was valid for this system [71], consequently our goal was to measure on and off rate constants.

Experiments to determine the on rate constant were based on the same principle as the equilibrium binding constant studies, except the incubation time was varied. Even at the shortest incubation time, the association reaction was complete. Our assay system requires a minimum of approximately 1.5 min to load and resolve the aggregate peak. As a result, shorter time constants cannot be measured with this approach.

Given the high affinity of bFGF for HS, it seemed reasonable that the off rate might still be measured with our assay system. In these experiments, the bFGF/HS complex was allowed to equilibrate, the system was perturbed with a 800 fold molar excess of unlabeled bFGF, and the incubation time with unlabeled growth factor was varied. A large excess of unlabeled bFGF was essential to the success of the experiment since it ensured that virtually no ^{125}I-bFGF would bind the heparan sulfate. Here, too, the kinetics of the reaction proved to be too rapid for analysis. While accurate values for the on and off rate constants could not be determined, these results did permit us to place an lower limit on the value of koff at 0.01 sec^{-1}. Using the measured Kd of 3.9 nM, we arrive at a minimum kon of $2.6x10^6$ / M s. Nugent [71]and Moscateli [126] reported koff measurements of $1.1x10^{-3}$/sec and $2x10^{-3}$/sec. These values are somewhat lower than the minimums reported here. However, they were both based on cell surface assays. The difference could be attributed to cell surface versus basement membrane HSPG, or it could be a reflection of the difference between measured kinetics on a two dimensional surface versus free solution. Effective diffusivity measurements of bFGF through Descemet's membrane (Chapter 7) demonstrated that the binding reactions occurred much faster than

diffusion. Hence, the equilibrium binding constant and these minimum values for the kinetic constants were sufficient to describe the system.

5.5 Water Content of Descemet's Membrane

An accurate measurement of the water content of the DM can be used to convert concentrations initially based on dry mass of membrane into a per volume basis. On a more fundamental level, the water content is a key parameter in understanding how dense the membrane is and how great its inherent resistance to diffusion of macromolecules might be.

Descemet's membrane is a very thin hydrogel, thus accurate measurements of it's water content were difficult to make. Taking a wet weight of the membrane requires removal of surface water without allowing the membrane itself to lose water to evaporation. After dicing the membranes with a razor they were placed in a microcentrifuge tube with a perforated bottom. Centrifugation at 50x g was found to remove the surface solution without drying the membranes themselves. The membranes then could be weighed "wet". Lyophilization of the membranes removed the hydrating water and permitted a "dry" measurement to be made. Some question remained as to the effectiveness of this approach, so we pursued a complementary, independent approach.

This strategy measures the volume of membranes in solution by comparing the changes in concentration between 2 million molecular weight dextran and [^{14}C]urea incubated with the membrane. Previous experiments had established that 2 million MW Dextran did not penetrate the membrane. We assumed that the urea had free access to all aqueous regions of the membrane and that, as a small uncharged molecule, it did not interact with any membrane components. Again, diced membranes were added to a PBS buffer, and known concentrations and volumes of [^{14}C]urea and 2 million MW FITC Dextran were added to the membrane preparation and allowed to equilibrate. Samples were taken and analyzed for fluorescence and radioactivity. Since the urea moved freely

through the membrane and the free solution, it provided a measure of the total volume of the solution. The FITC Dextran, in turn, provided a measure of the volume of the solution excluding the membrane. The difference between these two numbers was used to calculate the membrane volume.

Both of these techniques were applied to the same membrane preparations. The first approach provided dry weight as a fraction of total weight. While the second approach provided a ratio of dry weight to aqueous membrane volume. This approach neglects the volume occupied by the solids in the membrane. Since most of the membrane's volume is attributable to water, we equated the membrane weight to a membrane volume for comparative purposes. Both approaches produced very similar estimates of 85% water content that deviated by less than 1%. Dohlman and Balaz [9] report a water content of 79% for Descemet's membrane, while Krause[128] reported a water content of 83%.

5.6 Concentration of bFGF binding sites in Descemet's membrane

The number of bFGF binding sites can be determined from the experiments presented above. The concentration of HS on a mass basis, 1.1 mg/mL, was determined following the extraction process. The average molecular weight of the purified HS chains, 42 kD, was measured with size exclusion chromatography. Equilibrium binding constant measurements gave one bFGF binding site per chain. Lastly, the amount of water in a given mass of membrane was measured at 85%. Together this data provides a total concentration of bFGF binding sites in the membrane of 26 $\mu M \pm 13\ \mu M$.

5.7 Summary

Researchers have characterized Descemet's membrane with regard to its overall composition and its ultrastructure. No studies have focused on the heparan sulfate of

Descemet's membrane as we have done. The cornea is one of the few avascular extracellular matrices in the body. However, Descemet's membrane has a comparatively high concentration of bFGF, and angiogenic factor that stimulates new blood vessel growth. Despite the intimate connections between Descemet's membrane and the stroma, the bFGF from the DM does not stimulate new blood vessel growth in the stroma under normal conditions. The HS in the DM is probably responsible for sequestering the growth factor in the DM. Consequently, the DM heparan sulfate must be studies to understand this aspect of cornea physiology.

Immunostaining confirmed the presence of perlecan, the major basement membrane heparan sulfate proteoglycan. Our initial observations showed preferential staining of the endothelial DM face, as reported by Ljubimov [14] for human DMs. However, a more in depth study with the confocal microscope suggested that some of this apparent perlecan anisotropy could be attributed to the inability of the immunoglobulin to penetrate the dense DM matrix. The result was preferential staining of the DM edges. Confocal microscope views of the upper and lower cut planes revealed a more uniform staining profile. The perlecan on the endothelial face of the DM might also have been associated with the endothelial cells that were likely destroyed by the freeze thaw that he corneal sections underwent.

The isolation of heparan sulfate required a novel approach. Typical extracellular matrices can be extracted using high salt and denaturants. However, Descemet's membrane proved to be resistant to these approaches, confirming its overall insolubility reported by other researchers [9]. Ultimately, the beta elimination method was used to free GAG from the membrane. Pure HS was obtained through a combination of ion exchange chromatography and specific enzymatic degradation of keratan sulfate and chondroitin sulfate chains. To the best or our knowledge, no one has obtained purified heparan sulfate from Descemet's membrane before.

Our analysis of purified heparan sulfate provided data on the GAG's molecular weight distribution, equilibrium binding constant for bFGF, and placed limits on the on and off rate constants for the bFGF/HS interaction. These results fell within the range of values determined by other researchers for HS derived from different sources. The high content of keratan sulfate in the DM is not typical of most basement membranes. These keratan sulfates eluted at higher salt concentrations than heparan sulfates. High charge density keratan sulfates are characteristic of the corneal stroma. [129, 130]. These results support the contention that the DM may be a product of both the corneal stroma and the endothelium, as suggested by Ljubimov [14].

This study reports an overall water content of 85% for the DM. This measurement was in agreement with the literature. The water content of the membrane was used to obtain aqueous concentrations in the membrane. However, it is an important parameter for understanding the potential diffusion resistance the membrane can present to macromolecules. In every instance, the water content must be used with the knowledge that some fraction of the water in the membrane is probably closely associated with the GAG and protein constituents of the membrane.

5.8 Conclusions

Descemet's membrane is composed of a dense protein glycosaminoglycan meshwork. The large HSPG of the DM is held in this network through physical entrapment and through a variety of specific associations with other DM components. The comparatively high percentage of keratan sulfate (50%) in the DM reflects it dual stromal and endothelial cell origins. The heparan sulfate of Descemet's membrane has many overall similarities to heparan sulfate from other basement membranes including having comparatively large molecular weights (40 kD) and a high affinity for bFGF (Kd=4 nM). The potential of the DM to regulate bFGF activity stems from the fact that its heparan sulfate proteoglycans are firmly anchored in the matrix, and yet the proteoglycan's large

HS chains remain free to bind and release extracellular bFGF. Descemet's membrane makes up only a portion of the cornea, which is in turn, only a small part of our highly complex visual system. Yet, it is a highly complex tissue in its own right. The data we have obtained for the heparan sulfate of Descemet's membrane is critical to an overall understanding of how bFGF functions in the cornea, and will be used to model the transport of bFGF through Descemet's membrane.

Chapter 6

Limiting bFGF Surface Adsorption

6.1 Introduction

Protein adsorption to surfaces is a complex process that is a function of the protein of interest, the surface, and the solution environment. In aqueous environments the hydrophobicity of the protein and the surface can provide a general guide for predicting the extent of adsorption, with increasing hydrophobicity leading to increasing degrees of adsorption. For example, the adsorption of human serum albumin, IgG, and fibrinogen on a hydrophilic silica surface and a hydrophobic methylated silica surface were measured using elipsometry [131]. The hydrophobic silica adsorbed as much as three times the amount of protein. The surface hydrophobicity may not be as important as the hydrophobicity of the protein core, since adsorption can be accompanied by unfolding of the protein. Latex surfaces bind twice as much BSA denatured in urea than the native form of the protein [132]. This result suggests that the exposure of the internal hydrophobic residues in a protein enhances adsorption.

Approaches to regulating protein adsorption have relied heavily on treatments that increase the hydrophilicity of the surface in question. In particular, polyethylene oxide, PEO, is often an effective surface modification. The ability of PEO coated surfaces to resist protein adsorption is related to the great flexibility of the PEO chains in aqueous solution. In order for a protein to approach close enough to adsorb to the surface, it must

restrict the movement of the PEO chains, and this restriction in mobility is entropically very unfavorable. [133]. Another approach to reducing adsorption relies on saturating available binding sites on a surface using large excesses (1 mg/mL) of a carrier protein such as BSA.

6.2 Surface Modifications

Previous work in this lab with bFGF demonstrated a clear propensity of the protein to adsorb to surfaces. Before any diffusion experiments with the growth factor were begun, several strategies for limiting protein adsorption were evaluated. Our initial goal was to conduct all experiments under carrier free conditions.

Unless otherwise stated, all of the surface adsorption experiments described below were conducted in 4 mL glass vials containing 2 mL of phosphate buffered saline (PBS). Adsorption was carried out at 4°C with ^{125}I-bFGF for 24 hours. Solution concentrations for bFGF were between 2 and 7 ng/mL for all experiments. At the completion of the experiment, the contents of the vial were removed, the vial was washed two times with PBS, and the contents, washes, and vial were counted. The experiments were conducted in duplicate with a control of untreated glass.

Glass surfaces were initially treated with dimethydichlorosilane (DDCS). This reagent leaves exposed hydrophobic methyl groups on the surface of the glass, and it is a typical siliconizing reagent. This approach was chosen out of the belief that the positively charged bFGF would be largely hydrophilic and would not interact with the hydrophobic surface. The result of this experiments was that 40% of the bFGF bound untreated glass, whereas, close to 70% bound to the treated surface. This outcome suggested that bFGF has some hydrophobic nature. It is not clear whether surface hydrophobic groups were responsible for the adsorption, or perhaps partial unfolding of the protein during the adsorption process exposed internal hydrophobic residues. Regardless, it was clear from this data that hydrophilic coatings would be required to inhibit bFGF adsorption.

Amiji and Park developed a process for applying a PEO coating to glass surfaces [134]. It relied on polyethylene oxide -polypropylene oxide triblock copolymers known as pluronics (BASF). Glass surfaces were treated with DDCS to make them highly hydrophobic, and they were incubated with F108, a pluronic with two PEO chains containing 129 PEO units bracketing a single PPO chain of 56 residues. The polypropylene oxide chains are very hydrophobic themselves, and they adsorb to the siliconized glass. The hydrophilic PEO chains remain soluble and prevent protein binding. This approach was very effective in limiting bFGF adsorption to glass as indicated by the 2% bFGF that adsorbed to the treated surface vs. almost 40% bound to untreated glass. Since the pluronic's association with the glass surface was based on hydrophobic interactions, it was destabilized by exposure to air. The F108 coating of an actual diffusion chamber is not nearly as effective as the glass vial coatings. It was not technically feasible to rinse out the F108 without exposing the surfaces briefly to air, and with each air exposure, some of the pluronic appeared to partition to the air water interface. The ambiguous results with pluronics suggested that covalent modification of the glass surface might be more effective at preventing protein adsorption.

PEO chains can be covalently linked to a glass surface in a procedure developed by Sofia and Merrill [135] that involves tresyl chloride activation of the PEO hydroxyl groups. The PEO chains are linked to aminated glass. An experiment with this surface yielded 33% bFGF bound to the treated vials, and 96% bound to untreated glass. The PEO coated glass outperformed the untreated glass. We attributed the high percentage of bFGF adsorption to the control glass to a higher amount of denatured bFGF in that particular preparation of ^{125}I-bFGF. PEO star molecules have multiple PEO arms, and they are often more effective in these coating processes [136], but their expense made them impractical for the repeated coatings that would be required of the diffusion chamber.

Regnier et al. [137] developed another covalent coating approach for glass based chromatography media. This strategy bonded a layer of carbohydrate to the glass

surface. Using this approach, almost 70% of the bFGF bound to untreated glass, but the glycophase G glass adsorbed only 30% of the growth factor. The ratio of bound bFGF for control vs. treated surface is similar for both PEO coated and glycophase G coated. However, the glycophase G coating was simpler and cheaper.

Coating the glass surface of the membrane mounts and the diffusion cells only addressed one of the sources of adsorption. The chambers were stirred with Teflon microstir bars. As a highly hydrophobic surface, the Teflon had a pronounced avidity for bFGF. Glass coated stir bars were manufactured in the lab to circumvent the use of Teflon stir bars. Unfortunately, magnetized glass stir bars could not by created without specialized equipment, and the non-magnetic bars were not effective at mixing the chambers. Corning developed a commercial process for coating plastics to minimize protein adsorption. They generously agreed to coat our Teflon stir bars. In parallel experiments with stir bars in Glycophase G coated glass vials, coated Teflon bars were responsible for binding 18% of the bFGF, while the uncoated Teflon accounted for 38% of the bFGF lost.

6.3 Carrier Protein

Ultimately, none of these coating approaches were as effective as was initially hoped. As a final option, a solution of 0.22 μm filtered 1 mg/mL BSA was screened for its ability to prevent bFGF adsorption at 4°C. A bFGF binding study was conducted in glycocoated glass vials with Corning coated Teflon stir bars and these results are shown in Table 6.1.

	+ BSA	- BSA
vials	0.9% ± 0.04%	13.5% ± 0.5%
stir bars	8% ± 2%	30 ± 1%

Table 6.1 The percentage of total bFGF bound to the glass vials or stir bars with or without 1 mg/mL BSA in solution with ^{125}I-bFGF is represent as the average of duplicate samples half the total range.

The solution BSA greatly diminishes protein adsorption to even the coated surfaces and has some effect on the stir bar adsorption as well.

We confirmed that the ability of solution BSA to reduce bFGF adsorption was the result of a BSA/surface interaction rather than an interaction of bFGF with the BSA itself. Figure 6.1 shows the results of size exclusion chromatography of ^{125}I-bFGF with a running buffer containing 2 mg/mL BSA and in buffer containing no BSA. The bFGF chromatographed with BSA was also preincubated with the protein for 4 hours prior to gel filtration. The plots show that BSA clearly reduced the amount of bFGF lost to the column itself. The aggregate peak for bFGF without BSA represented 3% of the monomer peak area, whereas the inclusion of BSA brought the aggregate up to 11% of the total monomer amount. Other experiments suggested that the amount of aggregate was approximately linearly proportional to the BSA concentration. Our diffusion experiments were conducted with 1 mg/mL BSA, and we estimated the amount of aggregate to be 5-7% of the total monomer amount.

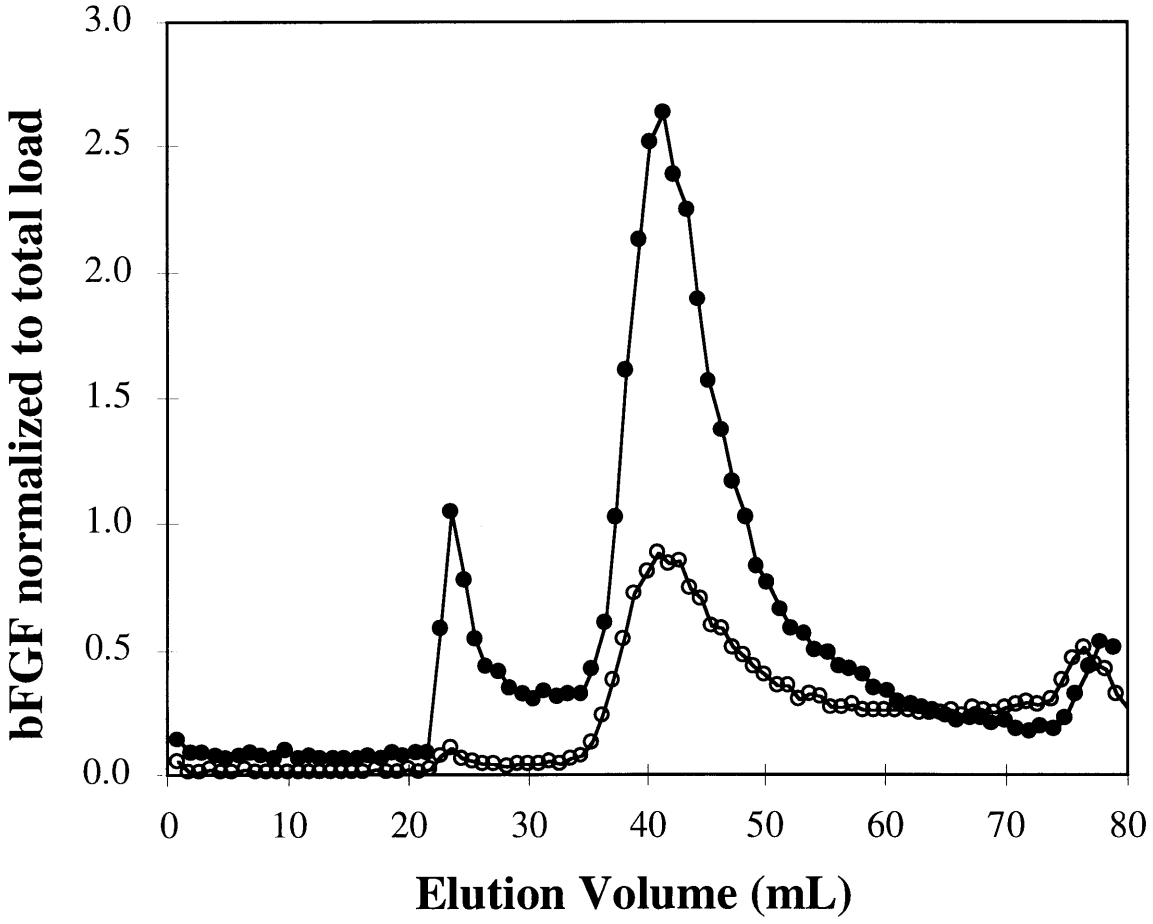

Figure 6.1 bFGF/BSA Interaction in Aggregate Formation: ^{125}I-bFGF aggregate formation with BSA was explored with a 60 mL Sephacryl HR 100 column run with 2 mg/mL BSA in PBS (●) and run with PBS alone as the running buffer (o). The y-axis represents eluted radioactivity normalized to the total amount of ^{125}I-bFGF loaded onto the column.

6.4 Conclusions

Based on these studies, 1 mg/mL BSA was included in all subsequent buffers that contained bFGF. However, the Corning treatment of stir bars was continued, and all glass surfaces in the diffusion apparatus were coated with glycophase G. The BSA greatly increased the range of possible experiments with bFGF. Coating of all the surfaces that contacted bFGF was never feasible. However, adding BSA to the buffer in all experiments was practical, and it decreased non-specific loss of bFGF in general.

Chapter 7

Diffusion Studies with Descemet's Membrane

7.1 Introduction

We have characterized the interaction of bFGF with purified Descemet's membrane heparan sulfate. The diffusion/binding model of bFGF transport through Descemet's membrane requires values of the effective diffusivity of bFGF in the DM independent of binding to the DM HS. Since the binding interaction is bimolecular, it was disrupted, in experiments, through changes to the binding site on the protein and the binding site on the HS. The first portion of this chapter covers the characterization of the diffusion apparatus and presents results of control experiments for DM diffusion. The second portion of the chapter covers the actual diffusion experiments used to determine the effective diffusivity of bFGF in Descemet's membrane.

7.2 System characterization

Diffusion studies with bFGF were carried out with a diffusion chamber apparatus. A variety of control studies were conducted to ensure the proper functioning of the apparatus and the suitability of this approach to measuring bFGF diffusion through the DM. Experiments with [^{14}C]urea established that the diffusion chambers were well mixed. The integrity of the DM and its size selectivity were evaluated using FITC

dextrans with a broad molecular weight distribution. A protocol was developed to separate non-heparin-binding bFGF from the native form of the protein, and the impact of this step on the diffusion studies was assessed. Finally, the bFGF detected in the sink chamber was shown to be active and intact.

7.2.1 Experimental System Design

Figure 7.1 is a schematic of the apparatus used in all the diffusion experiments. The two diffusion half cells each have a volume of 3 mL, a sample port, and stir bar wells. The chambers are stirred with NBS coated Teflon micro stir bars (3mm x 10 mm). The diameter of each diffusion cell at it's mouth was 1 cm. This diameter proved to be too large for the sections of DM that were available from dissections. Consequently, an alternative mounting system was designed for the chambers.

Membrane mounts were made from 2 large glass slides (3 x 1.5 inches) as depicted in Figure 7.1. The mounts have a diffusion hole of 0.5 cm in diameter, and two bolt holes of 0.65 cm diameter each. This arrangement had several advantages. As mentioned above, smaller membrane portions could be successfully mounted. The mounts secured the membrane in place with an even pressure distribution. Finally, the membranes could be observed for damage before they were placed between the diffusion half cells. The possibility that the membrane mounts might adversely affect mixing in the region of the membrane hole cut-out was investigated by varying the stirring rate in the chambers.

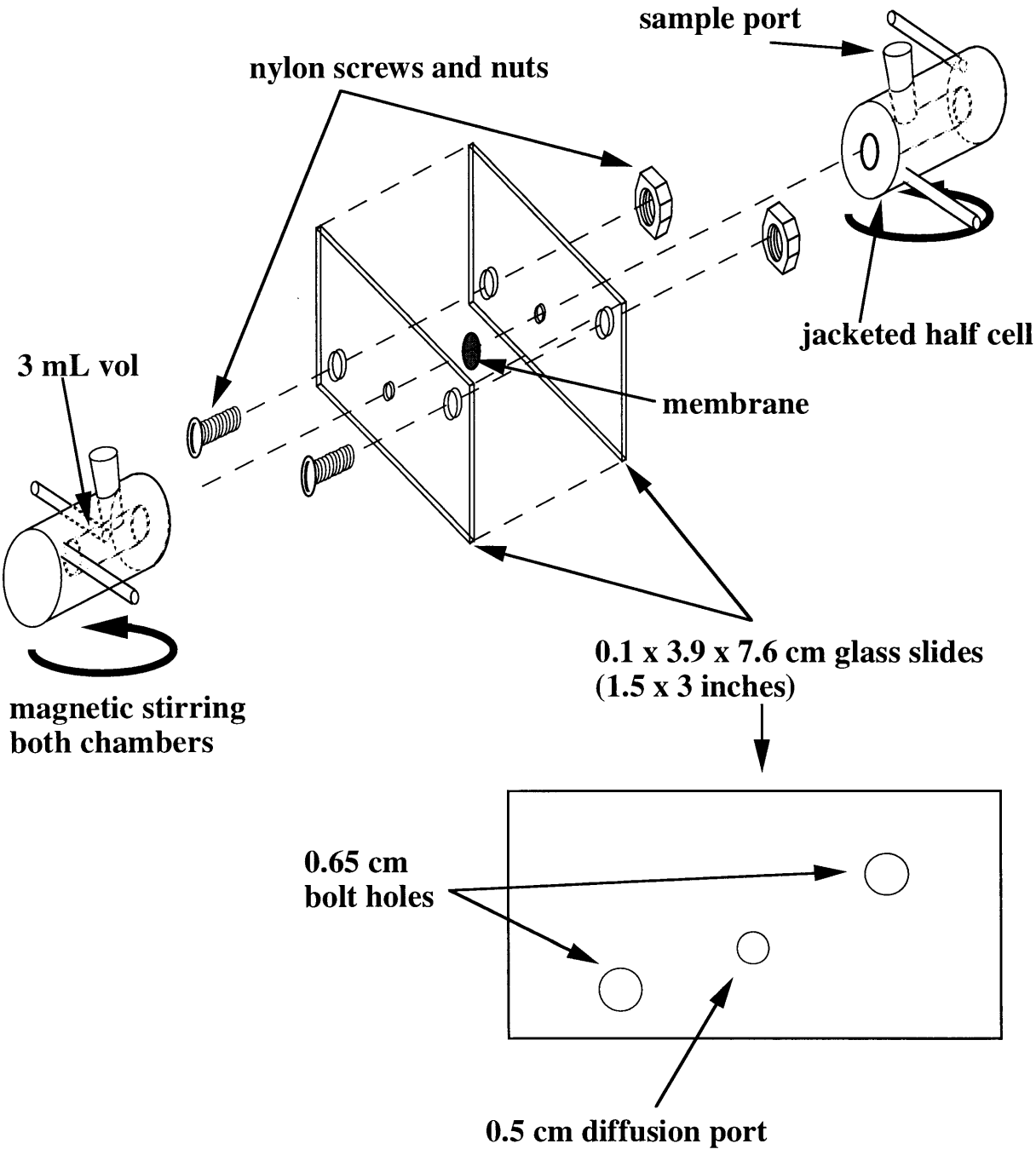

Figure 7.1: Schematic of diffusion chamber apparatus including membrane slide mounts

7.2.2 Affect of Stir-rate and Slide Mounts on Diffusion

A large stagnant boundary layer along the membrane surface would complicate the diffusion results if it presented a greater diffusion resistance to bFGF than the membrane itself. Inadequate stirring in the chambers and the presence of the membrane mounts could both contribute to this problem. Figure 7.2 presents data for two experiments conducted with [^{14}C]urea as the diffusing substance and using Millipore Durex DV membranes (0.65 μm pore size). At stirring speeds of 260 and 1180 rpm, the flux through the membrane was the same after it was normalized for variations in the source chamber concentration. These results suggested that the chambers were well mixed at the 500 rpm stirring rate used in the diffusion studies with Descemet's membrane, and this stirring experiment also implied that the membrane hole cut-outs were not creating a significant stagnant layer on the membrane's surface. This latter contention was confirmed by a study conducted with no slide mounts present at a stir rate of approximately 600 rpm. The results of this experiment were normalized for the increased area available for diffusion and are plotted with the slide mount data in Figure 7.2. The normalized flux of [^{14}C]urea across the Durex DV membranes is the same with or without the membrane mounts in place.

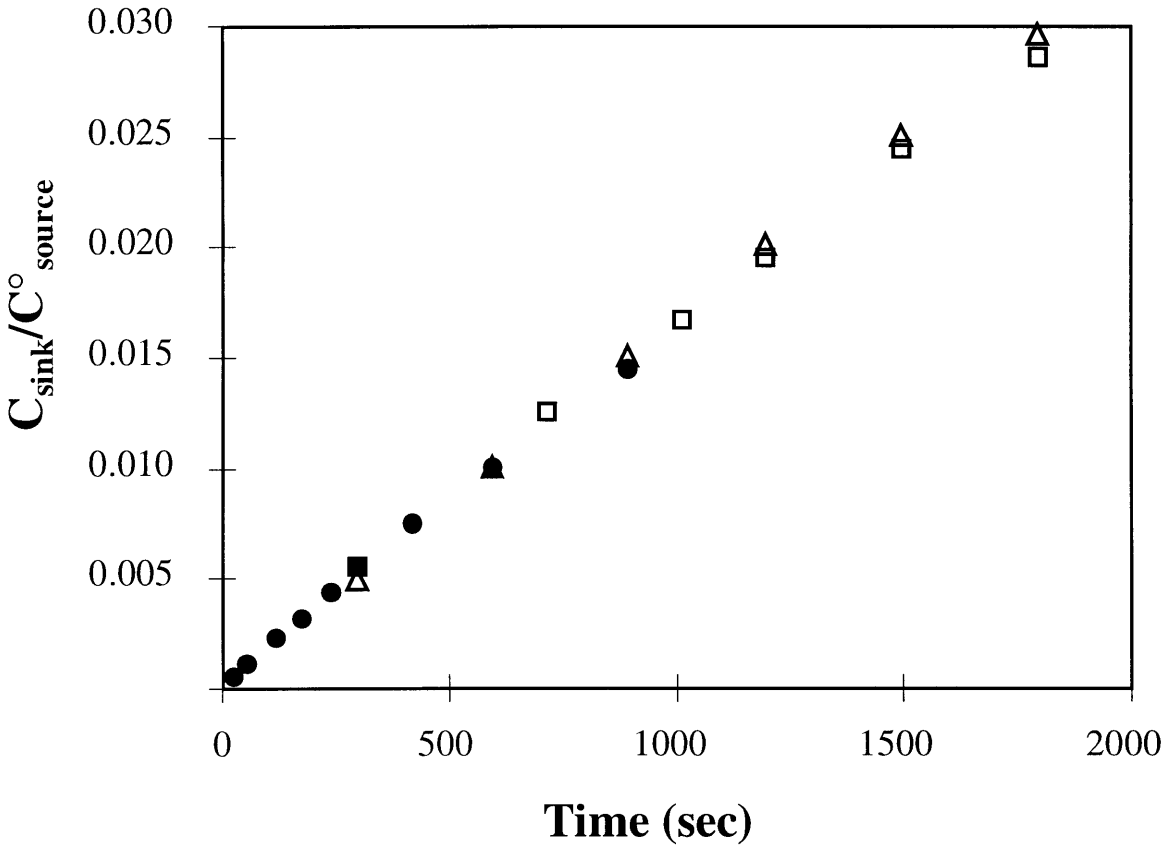

Figure 7.2 Chamber Mixing: [^{14}C]urea flux under different stir rates and chamber configurations. The concentration in the sink chamber has been normalized for variations in the initial source chamber concentration. Experiments were conducted without membrane slide mounts at stir rates of 500 rpm (●), with slide mounts at 260 rpm (□), and with slide mounts at 1180 rpm (△).

7.2.3 Descemet's Membrane Integrity and Size Selectivity

Examination of Descemet's membrane under the light and the confocal microscope revealed no obvious pores or defects in its structure. However, before conducting diffusion studies with bFGF we wanted to confirm that submicroscopic pores or "pin holes" did not extend through the DM matrix. If they existed, such structures could provide a path of low diffusion resistance for bFGF to rapidly cross the DM without interacting with the DM HSPGs. A series of experiments with FITC dextrans having a wide range of molecular size were conducted to determine if these types of pores did penetrate the membrane, and, if no pores existed, to estimate a molecular size cut off for the DM.

Membranes from three different mature cow eyes were mounted in diffusion cells. The source chamber of each apparatus was charged with a mixture of FITC Dextrans of 150 kD and 40 kD. At time points of 24, 52, and 94 hours, 0.5 mL samples were drawn from the sink chambers and replaced with PBS. Ten microliters were removed from the source chamber at these times. Both the source and sink samples were run over a CL6B gel filtration column to determine the molecular weight distribution of these dextrans. The amount of FITC dextran in each collected fraction was determined using a fluorescent spectrometer. The sink chromatograms were resolved into 2 gaussian peaks through a least squares fit of the data, and the chromatograms from the source chamber were fit to a single gaussian peak. The CL6B column was calibrated with a series of FITC Dextrans of known molecular weight. Using data from Poitevin and Whal [138], the dextran molecular weights were converted, in turn, to stokes radii for the dextrans.

Figure 7.3 shows the changing molecular weight distribution of the dextran over time in one of the sink chambers and is representative of all 3 sink chambers. For reference, the same plot is included for the source chamber. For the FITC dextrans used in this study, FITC was randomly conjugate to the glucose hydroxyl groups of the dextran. Consequently, the fluorescence of a sample of FITC dextran reflects the total mass of dextran in the sample and the molecular weight distributions shown here should be viewed accordingly.

The broad distribution of dextran in the source chamber is overlayed on the sink chamber distribution in Figure 7.3a. The source chamber peak had an average molecular weight (MW_w) of 125 kD, and the total amount of FITC dextran in the source chamber changed little over the course of the experiment because only a small fraction of the dextran crossed the membrane during the course of the experiment. At the 92 hour point the total fluorescence in the sink was 0.5% of the source fluorescence.

The lower molecular weight peak in Figure 7.3a represents trace amounts of free fluorescein that eluted in the included volume of the column. The other peak represents small molecular weight dextrans with an average molecular weight of (MW_w) 17 kD. This low molecular weight stands in sharp contrast to the 125 kD dextran in the source chamber. Correlation of dextran molecular weights with stokes radii provided by Poitevin and Whal [138] gave a radius of 30 Å for a 17 kD dextran and 80 Å for a 125 kD dextran. The total free fluorescein increased by 16% from 24 to 92 hours as determined by the area of its deconvoluted peak. This result suggested that the free fluorescein had nearly equilibrated across the DM after 24 hours. However, the amount of low molecular weight dextran increased linearly throughout the course of the experiment as seen in Figure 7.3b. The amount of dextran at the 92 hour time point was 3.2 fold greater than at the 24 hour time point. The increase in dextran in the sink chamber did not coincide with any shift in the average molecular weight of the dextran.

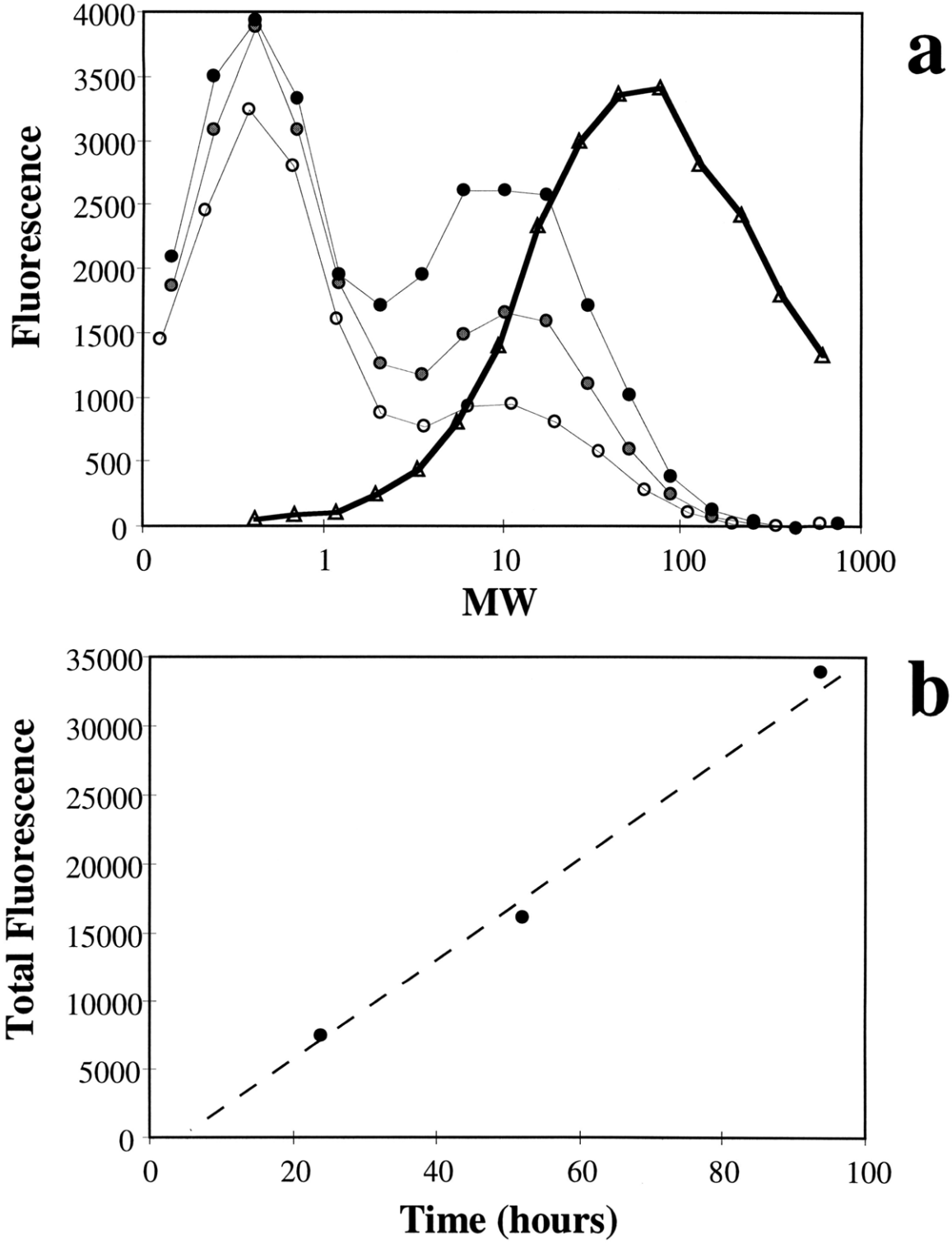

Figure 7.3 Membrane Integrity from FITC Dextran Diffusion: (a) The molecular weight distribution in the sink chamber at time points of 24 (○), 52 (◍), and 94 (●) hours is compared to the unchanging distribution in the source chamber (△). (b) The low molecular weight dextran peak area increases linearly with time in the sink chamber.

The steady-state flux of a particular molecular weight dextran through an aqueous channel across the membrane would be proportional to the aqueous diffusivity of the dextran and the concentration of that particular species in the source chamber. The linear increase in 17 kD dextran plotted in Figure 17.3 b supports the supposition that a steady state has been reached. If we take the 17 kD dextran as our base case, we can compare its flux through hypothetical aqueous channels to the expected flux of a larger 50 kD species. The aqueous diffusivity of this larger dextran would be approximately 70% of the 17 kD form. Based on the molecular weight distribution in the source chamber, the fluorescence of the 50 kD species is approximately 50% greater that of the 17 kD form. However, the fluorescence correlates with overall mass of dextran, and if we use the molecular weights to convert to a molar basis, then the source concentration of 50 kD dextran is almost 50% the source concentration of the 17 kD dextran. If the 17 kD dextran has reached the sink chamber by passing through aqueous channels in the membrane, then a 50 kD form of dextran should have a flux of approximately 35% of the 17 kD form. Over time, the accumulation of these increasingly higher molecular weight dextrans in the sink should result in a gradual increase in the average molecular weight of the dextran in the sink chamber. Our study showed no evidence whatsoever of any change in the average molecular weight of the dextran in the sink chamber over the course of this study.

We conclude that the DM does not have pores or pin holes that are large compared to the largest dextrans in the source (100 Å). Furthermore, the DM demonstrates size selectivity for dextrans, preferentially retarding the passage of molecules with a Stokes radius greater than 30 Å. Although electron microscopy studies have confirmed that the DM does have a defined molecular architecture based on a hexagonal lattice (see Figure 1.2), it would not be expected to have an exact molecular weight cut-off given the flexible nature of the DM's collagen scaffolding. The 30 Å limit should be regarded accordingly. Furthermore, the lower molecular weight dextrans in the sink chamber eluted toward the end of the gel filtration column where the resolution of the

CL6B gel filtration media was poor. The measured molecular weights in the sink chamber probably reflect an underestimation of the actual molecular weight. These results suggest that the DM is comprised of a tight protein meshwork, and helps to explain the difficulty of extracting the large molecular weight HSPG even under very harsh denaturing conditions. Lastly, these results confirmed that the membrane integrity will not change during the course of our 24 hour diffusion studies with bFGF.

7.2.4 Radio-iodinated Protein Purification

The free radioactive label is much smaller than both bFGF and IL1β, and, consequently, it crossed the membrane much faster than either protein in the diffusion experiments. During these experiments all the samples from the source and the sink chambers were precipitated with trichloroacetic acid (TCA). This step selectively precipitated protein and made it possible to distinguish labeled proteins from free ^{125}I. However, control experiments with TCA and free ^{125}I label revealed that 2% of the free label was trapped in the TCA pellet even when no labeled protein was present. In order to minimize this error, the free label was removed from the radiolabeled protein prior to each experiment.

The IL1β was purified using a Sephadex G-100 PD-10 column and the bFGF was purified with a heparin sepharose column. This step removed free ^{125}I label from the bFGF, and it also separated native bFGF from denatured or damaged bFGF that could no longer bind to heparin. The risk of using heparin sepharose was that small amounts of heparin would leach off the media and interfere with the diffusion experiments by either inhibiting the passage of bFGF by binding it in the reservoir or by facilitating its passage by blocking the sites for bFGF association with matrix HSPG. A control experiment was conducted to determine the amount of heparin that was lost from the sepharose.

A 400 µl Q sepharose anion exchange column was connected in line after a 400 µL heparin sepharose column, and 1200 mL of PBS was run through both columns over a

16 hour period. The Q sepharose column was eluted with 1.5 M NaCl PBS and 86 μg of heparin was recovered. A second, otherwise identical, Q sepharose column was placed in line after the original heparin sepharose column, and 600 mL of PBS were passed over the columns in 9 hours. This second wash recovered 0.09 μg of heparin. A 50% yield was assumed for the column and the molecular weight of heparin was assumed to be 10 kD. These assumptions resulted in an average heparin concentration in the second wash of 30 picomolar. This experiment confirmed that an overnight wash with PBS removed the vast majority of the free heparin (> 95%). In each actual experiment with the heparin sepharose column, the overnight wash was followed by loading the ^{125}I-bFGF, washing off the free label, and then eluting the active ^{125}I-bFGF. Assuming the heparin leached from the column at the same rate that it did during the second wash of the column in the control study, then there would be 30 picomolar of heparin coeluted with the bFGF. The 30 picomolar heparin would be in solution with at least 1.5 nanomolar bFGF, and, consequently, would not influence the bFGF experiments.

As mentioned earlier, the heparin sepharose also was used to separate non-heparin-binding bFGF from the native form of the growth factor. The significance of this separation was evaluated in a control study in which bFGF was incubated with heparin sepharose and the unbound growth factor was washed off with 0.5 M NaCl PBS. The non-heparin-binding bFGF was passed over a PD-10 gel filtration column to remove the free label and this bFGF was used in a diffusion studies in parallel with the purified native bFGF. Both preparations of ^{125}I-bFGF had approximately 1% free radioactive label. These experiments employed two separate diffusion cells, however, each contained a portion of DM from the same bovine eye. The results are depicted in Figure 7.4 as dimensionless sink concentration as a function of time. The sink concentration has been normalized for differences in source concentration and membrane thickness. The two curves are dramatically different. The non-heparin-binding bFGF rapidly diffused across

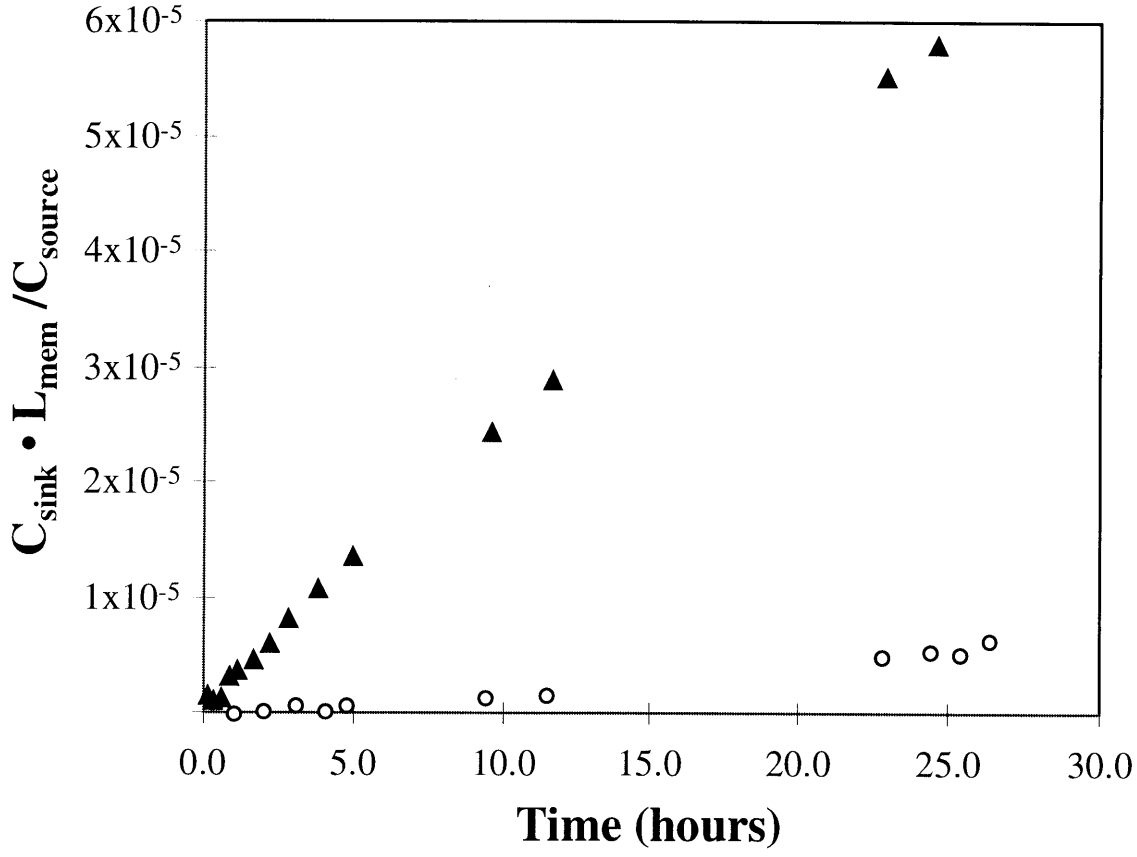

Figure 7.4 DM Diffusion of Binding and Non-Heparin Binding bFGF : Comparison of native bFGF (o) and non-heparin binding bFGF (▲) diffusion across DM. The sink chamber concentration has been normalized for experimental variations in membrane thickness and source chamber concentration.

the membrane, and it reached a pseudo-steady state with a constant flux in a matter of minutes. The native bFGF demonstrated a significantly lower flux over the course of the entire experiment. These results suggested that bFGF's interaction with HS retarded bFGF passage through Descemet's membrane.

Presumably, the non-heparin-binding bFGF was formed by either denaturation of the bFGF as a result of repeated freezing and thawing or as a result of damage to its heparin binding site during the Bolton Hunter labeling process. This experiment highlighted the importance of removing the non-heparin-binding bFGF prior to conducting any diffusion experiment. More importantly, it revealed the importance of heparin binding to the transport of bFGF across Descemet's membrane and provided a starting point for comparing diffusion of bFGF across the DM under different diffusion conditions.

7.2.5 Characterization of Sink Chamber bFGF

As was discussed in section 6, every effort was made to ensure that bFGF remained active and in solution during the course of our experiments. After several experiments the capacity of the bFGF in the source and sink chamber to bind heparin was evaluated using heparin sepharose chromatography. In a typical experiment, after 24 hours 60% of the bFGF bound and could be eluted from a heparin sepharose column. In the same study 40% of the bFGF in the sink chamber bound heparin sepharose. The low fluxes measured in the studies with native bFGF diffusing through the DM verified that over 24 hours, the denatured bFGF in the source chamber did not rapidly cross the membrane as was the case for the non-heparin-binding bFGF. Apparently, the bFGF denatured during the course of an experiment is different than the non-binding bFGF isolated from heparin sepharose flow through. Gel filtration chromatography of the source and sink chamber suggested that the denatured bFGF formed during an experiment was present as very large aggregates (> 200 kD) that could not cross the membrane.

In the diffusion experiments, bFGF was detected in the sink chamber by radioactive counting. Detailed analysis of the sink contents were performed after some experiments to ensure that the radioactive protein accurately reflects the presence of intact bFGF. Western blot analysis using anti-bFGF antibodies identified a protein band at 18 kD, identical to that of the native bFGF starting material. Further, autoradiographic analysis revealed that the band is the only protein containing ^{125}I-bFGF. Figure 7.5 illustrates these results.

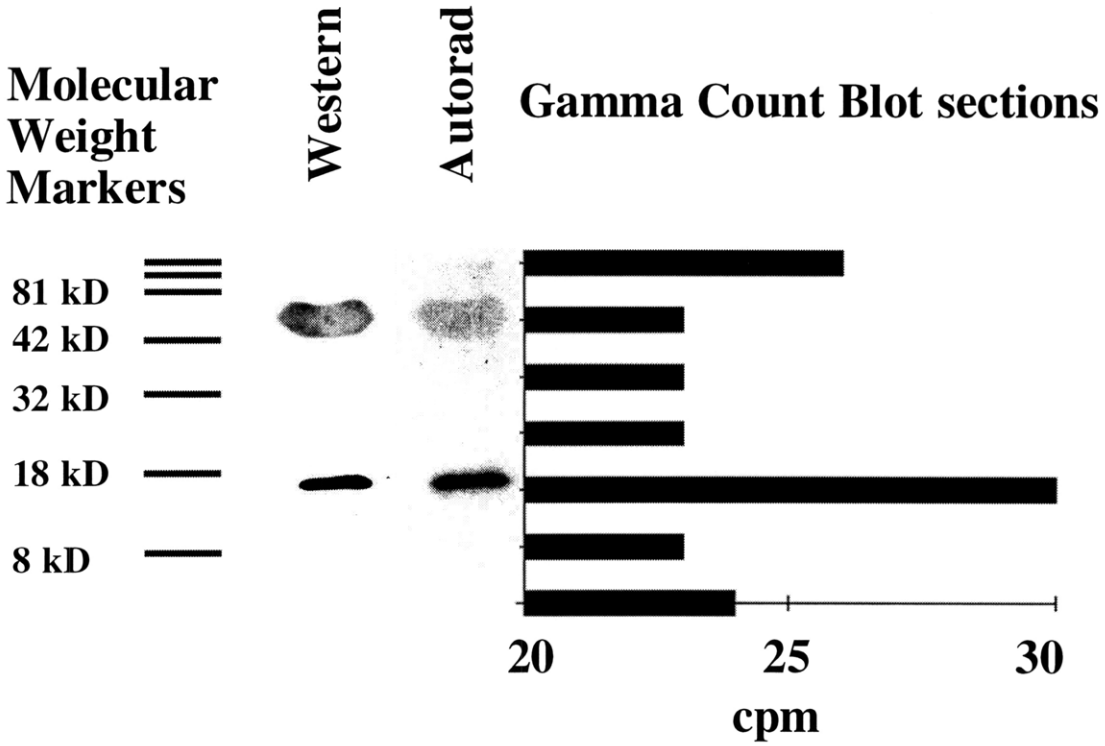

Figure 7.5 Western Blot and Autoradiography of Sink bFGF: bFGF in the sink chamber at 18 kD was identified with a specific monoclonal antibody on a Western blot. The larger molecular weight band corresponded to BSA in the buffer that nonspecifically bound to the secondary antibody. The 18 kD bFGF band also appeared in an autoradiograph of the Western blot. Again, a trace of the high molecular weight band was visible due to residual chemiluminescense activity on the Western blot when it was exposed for autoradiography. Subsequent sectioning of the Western blot itself, followed by gamma counting of the sections, showed that the only radioactivity above the 26 cpm background was associated with the 18 kD bFGF.

7.3 The Steady-State Approach for Diffusivity Measurement

The steady state approach to measuring effective diffusivities was discussed in Section 2.4.1. In these studies, the source chamber volume was large enough that the concentration in that chamber remained relatively constant over the course of the experiment. No bFGF was present initially in the sink chamber, and during the experiment the concentration of bFGF in the sink chamber remained less than 1% of the source chamber concentration. Under these conditions the driving force for bFGF diffusion is constant and equal to the source concentration, and once a linear concentration gradient has been established in the membrane, the following equation describes the rate of accumulation of bFGF (b_{sink}) in the sink chamber:

$$\frac{db_{sink}}{dt} = \frac{AD_{eff}Kb^{\circ}}{lV_{sink}} \qquad 7.1$$

The rate of accumulation of bFGF in the sink chamber was measured in each diffusion experiment by sampling the sink chamber at multiple time points. The effective diffusivity was determined by independent measurement of the sink volume (Vsink), the membrane thickness (l), the diffusion area (A), the source concentration (b°), and the partition coefficient (K). The volume of the sink chamber was 3 mL. The source concentration was determined by sampling the source chamber throughout the experiment. The diffusion area was determined by the 0.5 cm diameter hole in the slide mount (0.2 cm^2). This entire area was not available for diffusion because 15% of the membrane is solids. An 85% correction factor was used, therefore, to estimate the reduced area for diffusion. The partition coefficient for bFGF in the DM was measured independently, and DM thicknesses were measured for each membrane used in an experiment.

7.3.1 Partition Coefficients in the DM

The partition coefficient of a protein in the DM should be influenced by its size, charge, the ultrastructure of the DM, and the charge density of the DM. The partition coefficients for ^{125}I-bFGF and ^{125}I-IL1β were measured in equilibrium partitioning experiments. The non-heparin-binding form of bFGF and IL1β were equilibrated with diced DM's for a 5 hour period in 1 mL microcolumns, the incubation solution was removed, and the soluble radioactivity in the membranes was eluted by flowing buffer over the membranes. This approach made it possible to distinguish soluble radiolabeled bFGF or IL1β from bFGF or IL1β that had become irreversibly adsorbed to the membranes or the microcolumns. The partition coefficient for bFGF in the DM was 1.48±0.03 and for IL1β was 1.49±0.05. The reported errors represent half the total range for duplicate experiments. The similarity of partition coefficients for the uncharged IL1β (pI 7.0) and the positively charged bFGF (pI 9.6) suggested that the overall charge density of the DM is not high enough to significantly influence the partition coefficient. The fact that both numbers are slightly greater than 1.0 implies that each protein has some non-specific interaction with the membrane.

7.3.2 DM Thickness

All experiments were conducted at physiological saline ionic strengths (150 mM NaCl) to minimize alterations in membrane thickness once the DM was removed from the eye, except for those studies conducted in 3.0 M NaCl PBS-BSA. Measurements of DM thickness made from fixed, sectioned, and stained whole corneas did not deviate significantly from thickness measurements made of dissected DMs. Furthermore, after mounting the DMs in the diffusion chamber apparatus, they were allowed to equilibrate in the particular buffer system overnight to avoid potential changes in membrane thickness or structure during the course of the experiments. This precaution was particularly important in studies where high concentrations of salt were used in the buffer.

The thickness of the DM varies from one animal to another, so thickness measurements were made after all experiments. The DM curls over on itself if it is allowed to sit free in aqueous solution. Figure 7.6 illustrates how we took advantage of this DM property to obtain multiple thickness measurements from a single micrograph of the 200x magnified membrane cross-section. This figure also shows the variation in membrane thickness. It was observed that the membrane thickened toward the periphery of the cornea, so photographs were taken at multiple points along the length of the rolled-up membrane. The average membrane thickness for all our experiments was 40±8 μm and the average difference between the maximum and minimum thicknesses was 14 μm. An average thickness for use in determining the effective diffusivity was determined for a given membrane based on the multiple thickness measurements made along its length.

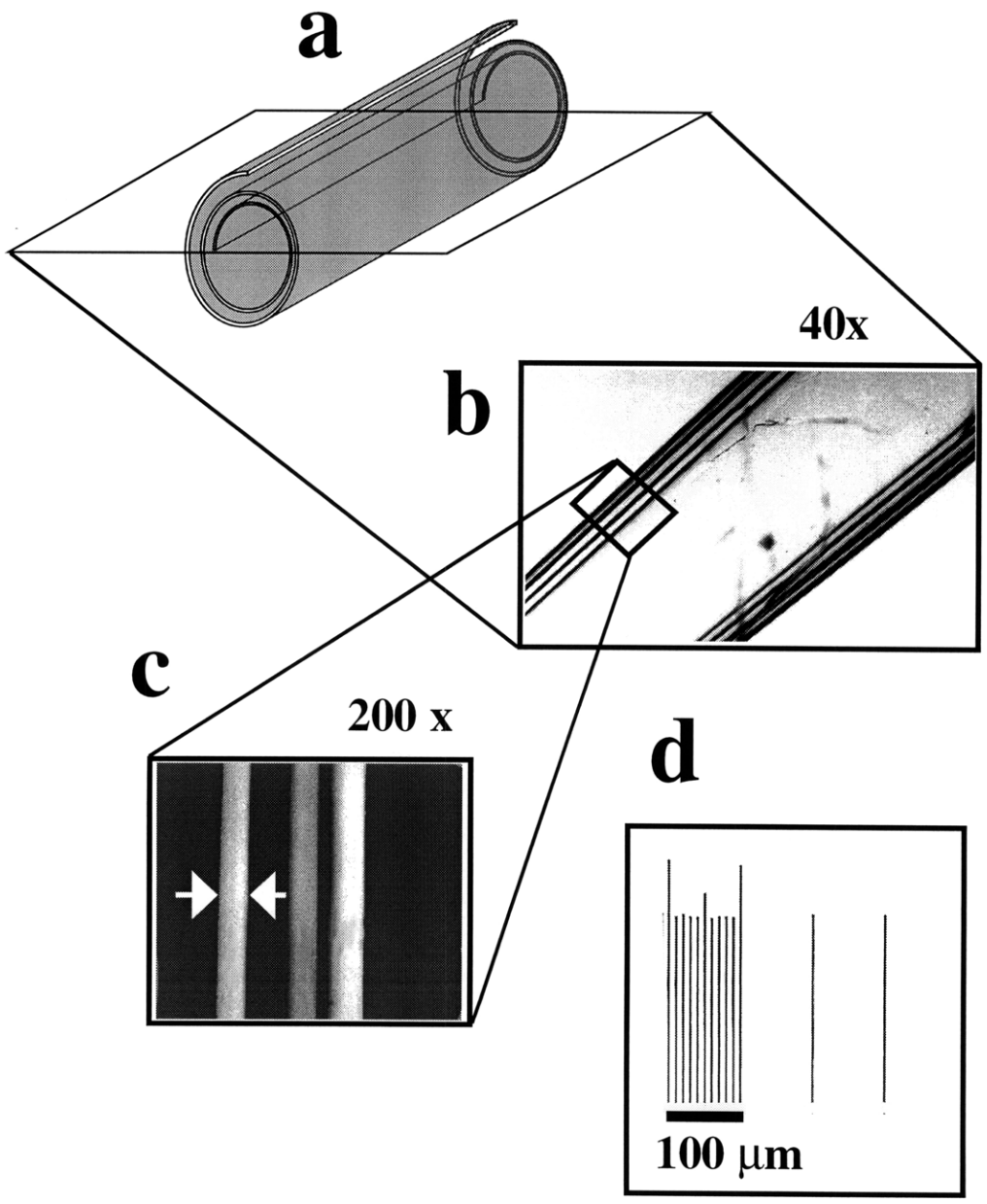

Figure 7.6 DM Thickness Measurement: Descemet's membrane roles over on itself (a), and the focal plane of a microscope can be adjusted to view the membrane in cross-section seen at 40x here (b). At 200 x the thickness of the membrane is resolved(c), and a calibrated micrometer can be used to measure its thickness.

7.4 bFGF Diffusion without binding

The goal of these studies was to determine an effective diffusivity of bFGF through Descemet's membrane without the association of bFGF with DM HS. As discussed above, binding can be disrupted through both changes to the growth factor and changes to the HS. The diffusion of the non-heparin-binding bFGF is representative of the first approach, but the latter strategies also were employed in this study.

7.4.1 A non-heparin binding bFGF analog: IL1β

Interleukin 1β (IL1β) is an important element in the immune response. *In vivo* studies have suggested it has a role in hypotension, fever, inflammation, and resistance to bacterial infection, among others [139]. IL1β was used as a bFGF analog in these studies. It has a molecular weight of 17.3 kD, as compared to 18 kD for bFGF. Although bFGF and IL1β have only a 12% sequence homology, 50 of bFGF's 146 α carbons can be superimposed in a spatial mapping onto α carbons of IL1β [52]. This comparison suggests overall structural similarities between the two proteins as can be seen in Figure 7.7. IL1β lacks a heparin binding region and has an isoelectric point of 7.0. Consequently, it provides a neutral analog of bFGF for diffusion experiments. Structures from both solution NMR and x-ray crystallography show that the two molecules have very similar molecular volumes [140, 141]. Although bFGF has a larger molecular weight, it's average molecular diameter from NMR and x-ray crystallography molecular models is 29 Å, while IL1β has a molecular diameter of 32 Å. Hence, they should have similar aqueous diffusivities. Consequently, IL1β can be used as a bFGF "analog" that cannot bind heparin.

Figure 7.8 is a comparison of non-heparin-binding bFGF and IL1β transport through Descemet's membrane. The y-axis is the molar concentration of ^{125}I-protein in the sink chamber normalized for differences in source concentration and membrane thickness. Both non-heparin-binding proteins demonstrated very similar transport

properties. Both molecules reached a steady-state constant flux across the membrane in under 15 minutes. The effective diffusivities for non-heparin-binding bFGF and for IL1β were $8x10^{-9}$ and $7x10^{-9}$ cm^2/sec respectively. These are the results that would be expected for two molecules of very similar size passing through the DM without interacting with the DM HS chains.

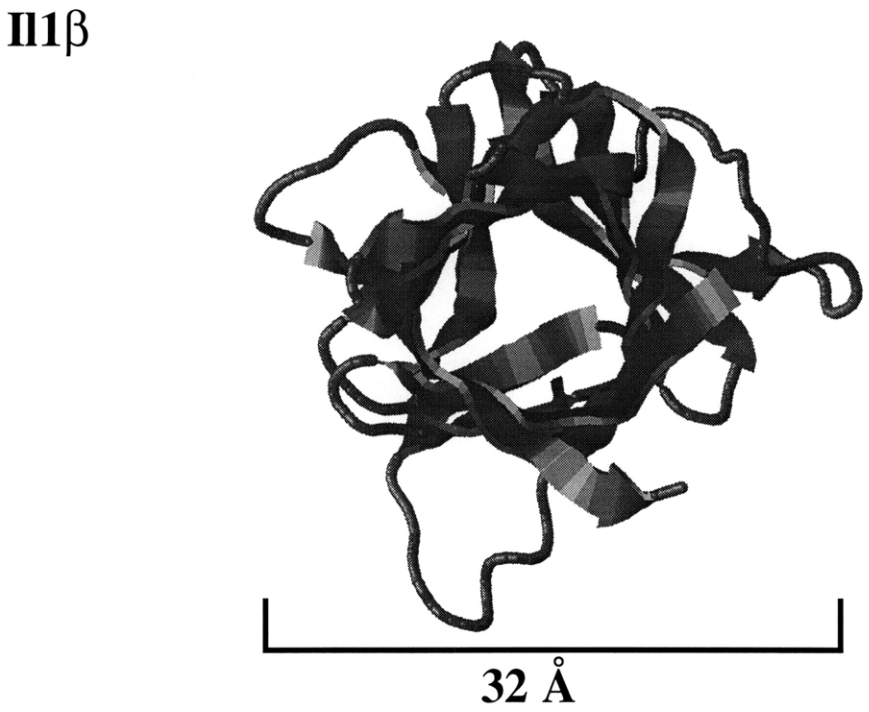

Figure 7.7 Structures of IL1b and bFGF : The molecular weight, overall structure, and molecular size of bFGF and IL1β are very similar, as can be seen from these representations of the crystal structures of the two proteins. X-ray crystal structure data was obtained from the Brookhaven National Lab Crystal Structure Data Base (Abola et al., 1987), (Bernstein et al., 1977). The visualizations were generated using RasMol v2.6 (Sayle, 1995).

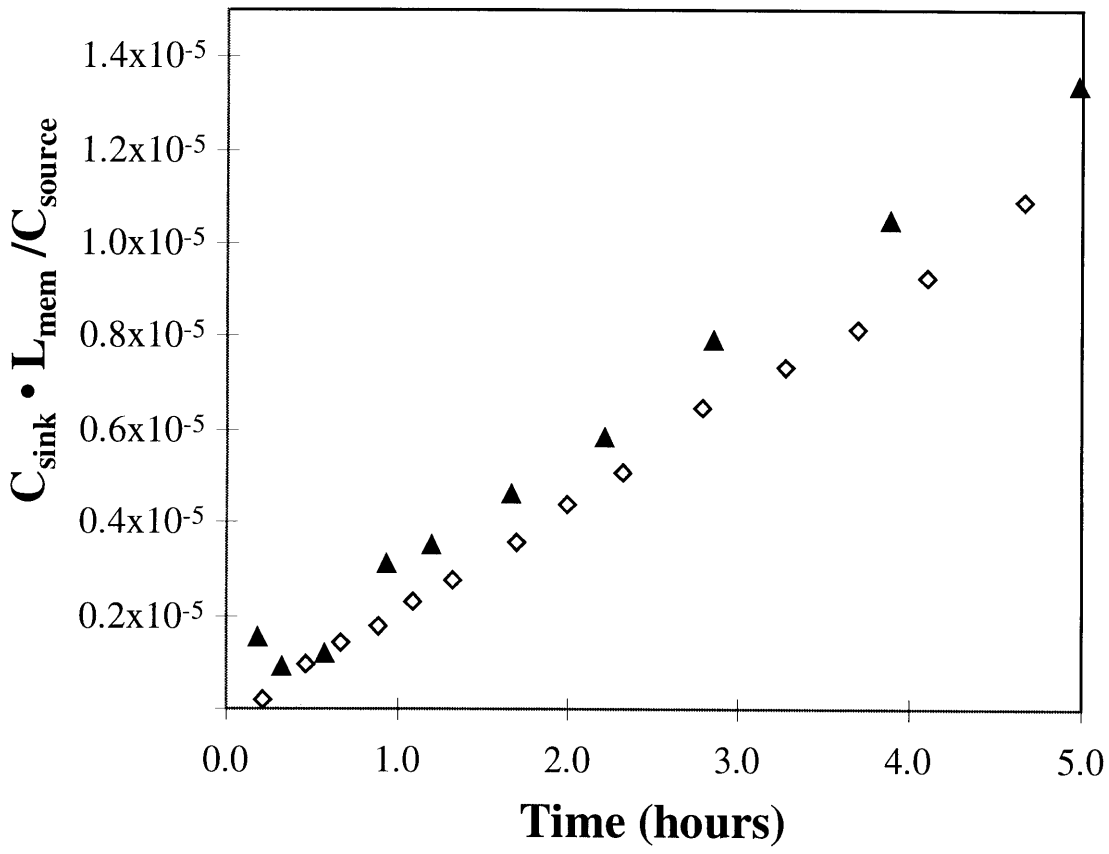

Figure 7.8 IL1β DM Diffusion: IL1β (◇) and non-heparin binding bFGF (▲) diffuse through the DM with similar normalized fluxes. The sink chamber concentration has been normalized for experimental variations in membrane thickness and source chamber concentration.

7.4.2 High Ionic Strength Disrupts bFGF association with HS sites

High ionic strength buffers will disrupt general electrostatic interactions in the membrane and will prevent bFGF binding to HS. The diffusion of ^{125}I-bFGF and ^{125}I-IL1β through Descemet's membrane in a PBS-BSA buffer with 3.0 M NaCl is shown in Figure 7.9. Normalized sink concentrations are plotted as a function of time. The data for IL1β diffusion through the DM under physiological saline conditions is shown for comparison. As expected, the high salt dramatically increased the flux of the bFGF through the membrane by preventing it from associating with the HS in the DM. The normalized flux of bFGF and IL1β in 3.0 M NaCl are almost identical. However, the normalized fluxes for both proteins in a 3.0 M NaCl PBS-BSA buffer are approximately 60% of the normalized flux of IL1β in physiological saline buffer. In an independent experiment, the DM was seen to reduce in thickness approximately 10% in 3.0 M NaCl. The high salt probably shielded the charge groups on the GAG chains in the membrane and reduced their mutual repulsion. As the GAG began to collapse, the membrane shrank. This change in thickness translated into a reduced effective pore size, and reduced fluxes. The possibility that the high salt extracted the HS chains from the matrix during the experiment also was explored. No HS loss was detected in high salt extracts of DM.

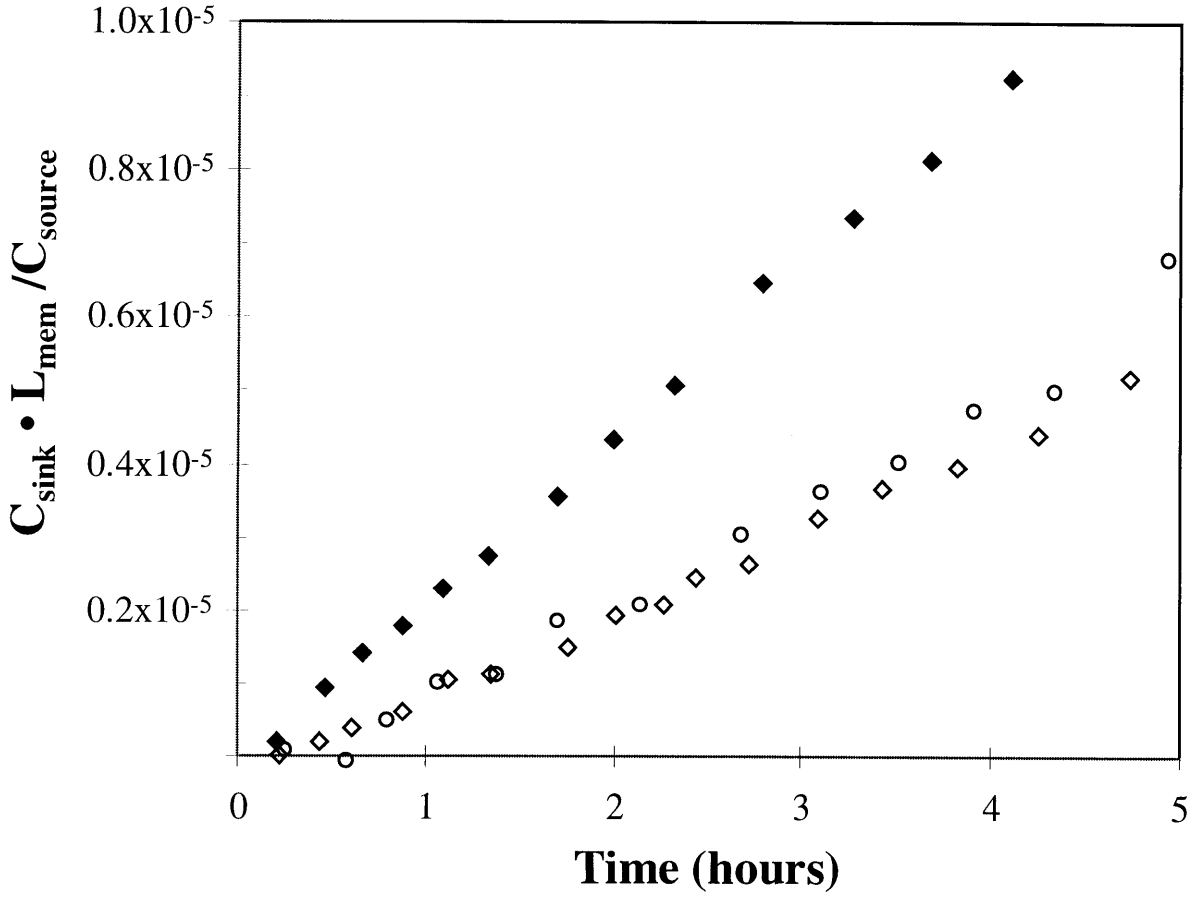

Figure 7.9 bFGF and IL1b DM Diffusion in 3.0 M NaCl: The flux of bFGF (o) and IL1β (◇) through DM in 3.0 M NaCL PBS-BSA buffer is lower than the flux of IL1β in 150 mM NaCl (physiological saline) (◆), but fluxes in all three studies were much higher than for heparin binding bFGF in 150 mM NaCl buffer. The sink chamber concentration has been normalized for experimental variations in membrane thickness and source chamber concentration.

7.4.3 Blocking the bFGF sites on Heparan Sulfates with Protamine Sulfate

Protamine sulfate, a family of highly positively charged proteins, binds heparan sulfate, thereby preventing the association of bFGF with the HS chains [142]. In this study, membranes were pre-incubated in a 10 mg/mL protamine sulfate buffer with PBS-BSA for 48 hours at 4°C to ensure that all the HS sites in the membrane were occupied with protamine sulfate. With an average molecular weight of approximately 6 kD, the protamine sulfate is at a concentration of 1.7 mM. This concentration is over 1 million times the source concentration of bFGF. The diffusion experiment was conducted in the presence of this concentration of protamine sulfate. Consequently, the protamine sulfate should have inhibited any bFGF/HS association. The results shown in Figure 7.10 confirmed these assumptions. Again, the normalized sink concentration is plotted as a function of time, and the data for IL1β without protamine sulfate is included for comparison. The effective diffusivities determined from this data are 6×10^{-9} and 7×10^{-9} cm^2/sec for bFGF in protamine sulfate and IL1β without protamine sulfate, respectively.

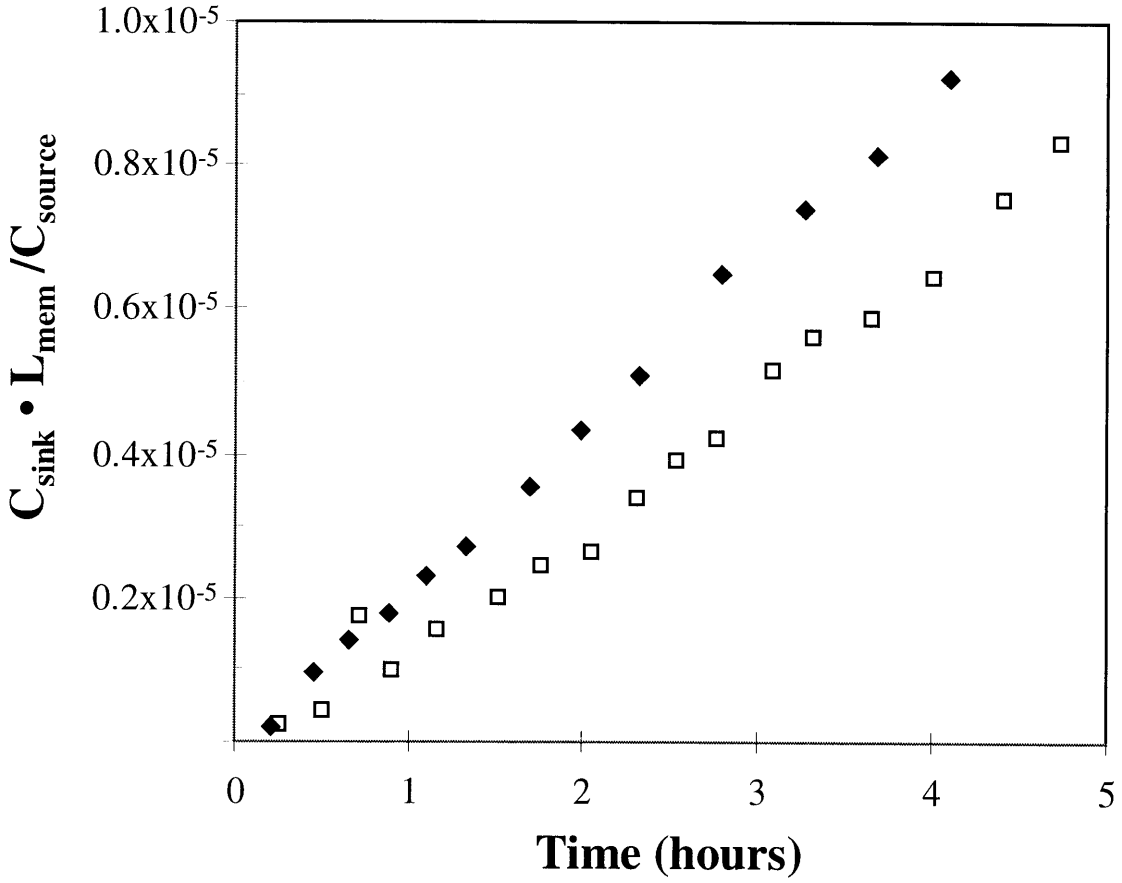

Figure 7.10 bFGF DM Diffusion with Protamine Sulfate: The diffusion of bFGF through DM in the presence of 10 mg/mL protamine sulfate (PS) (□) in a PBS-BSA buffer is very similar to the diffusion of IL1β in PBS-BSA (◆). The sink chamber concentration has been normalized for experimental variations in membrane thickness and source chamber concentration.

7.4.4 Enzymatic Elimination of HS sites in the DM with Heparinase

Heparinases specifically degrade heparan sulfate and heparin. Descemet's membrane was pretreated with heparinase I (10 U/mlL, 20 hours, 37°C, pH 7.2), was washed extensively to remove the enzymes, and was used in a diffusion study with bFGF. Figure 7.11 is a comparison of this experiment and two studies done with bFGF and an untreated membrane with normalized sink concentration versus time. The heparinase treatment increased normalized flux through the membrane. This result further supports the effect of HS in the DM as responsible for modulating bFGF movement. The enzyme reaction was not as effective as protamine sulfate or high salt. These results were not unexpected. The enzymes had to first diffuse into the DM, where the heparan sulfate is part of the tight protein meshwork. Furthermore, the enzymes might have been inhibited by the products of the degradation that could not rapidly diffuse away. These results demonstrated the importance of heparan sulfate in the DM to regulating bFGF transport across the DM.

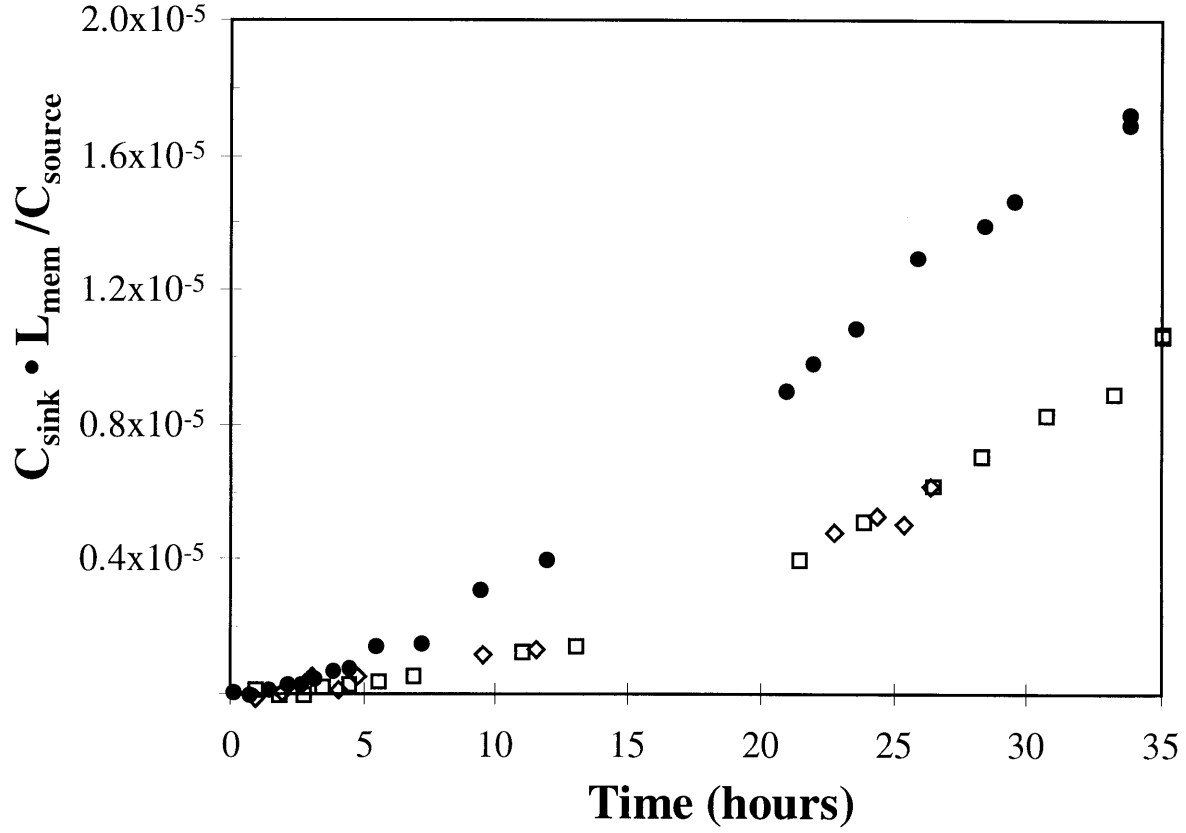

Figure 7.11 bFGF Diffusion through Heparinase Treated DM: The diffusion of bFGF through DM pre-treated with heparinase I (●) is compared to two bFGF diffusion experiments with untreated DM (◇ □). The sink chamber concentration has been normalized for experimental variations in membrane thickness and source chamber concentration.

7.5 bFGF competition for sites

Comparatively low diffusivities were measured for bFGF diffusion without binding compared to the kinetics of bFGF association and dissociation with HS. Furthermore, the affinity of HS for bFGF was high. Given these facts, in a diffusion experiment where bFGF can interact with HS, our model of bFGF transport through the DM suggests that the bFGF should move through the DM with a sharp wave front. Behind the front, virtually all the HS sites are saturated, and in advance of the front, the concentration of soluble and complexed bFGF is very low. The fast kinetics of the bFGF/HS association would ensure that a local equilibrium between soluble and complexed bFGF is always maintained, and, once the wave front had passed through the membrane thickness, the entire membrane would reach a steady state. At this point, a linear concentration gradient of soluble bFGF would have been established in the membrane, and virtually all the HS sites would be saturated with bFGF. After this point in time, the flux of bFGF through the membrane would be constant and equal to the flux measured when no binding was permitted to occur. The rapid kinetics of the bFGF association introduce an important subtlety to this scenario. After a steady state has been achieved in the membrane, bFGF molecules crossing the membrane will still interact with HS chains. However, the association of bFGF molecules with HS will be exactly balanced by dissociation of complexes.

Initial experiments with radiolabeled bFGF and no buffer additives suggested that, for the source concentrations used in those experiments, the time required to observe bFGF saturation of the membrane and it's subsequent breakthrough was not experimentally feasible. Issues of bFGF stability in solution, in particular, ruled out experiments that were significantly longer than 24 hours. However, the approach to

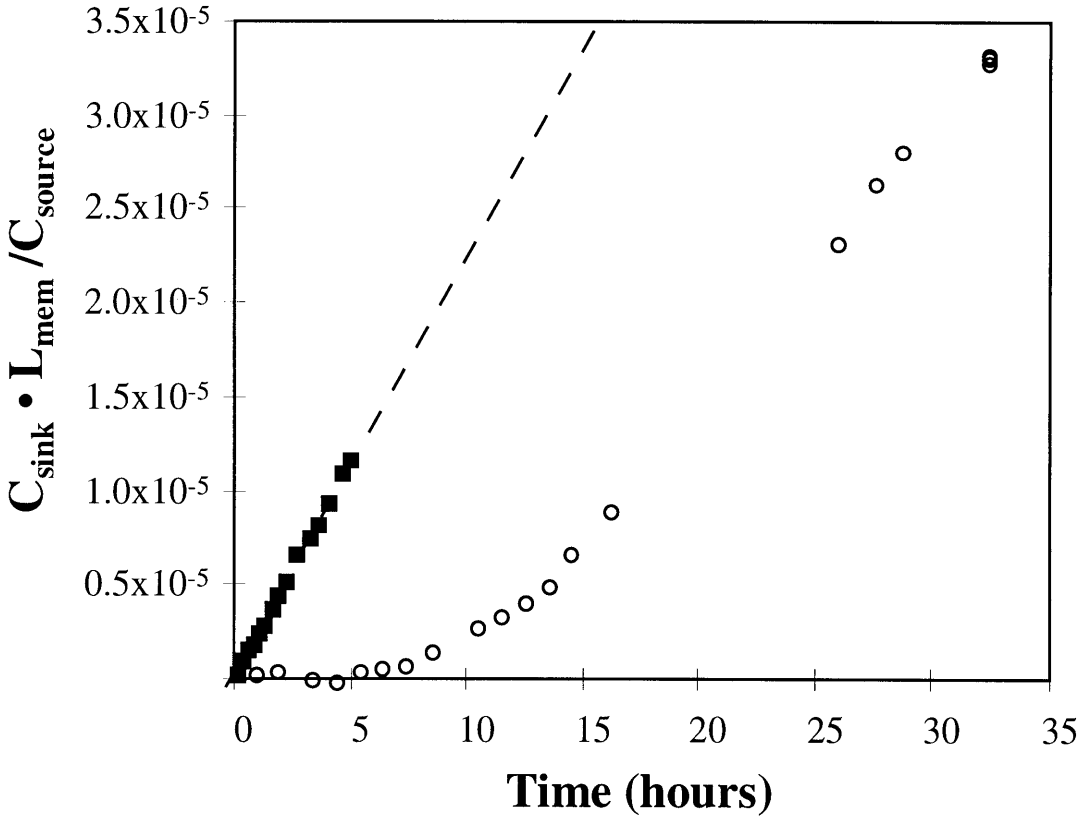

Figure 7.12 Diffusion of ^{125}I-bFGF with Excess Unlabeled bFGF: The diffusion of ^{125}I-bFGF through the DM with a 2000 fold excess of unlabeled bFGF (o) is compared to ^{125}I-IL1β diffusion through the DM (■). While the bFGF takes longer to reach a steady state flux, once it does reach steady state, the normalized fluxes of the two molecules are comparable. The sink chamber concentration has been normalized for experimental variations in membrane thickness and source chamber concentration.

steady state can be greatly accelerated by using higher concentrations of bFGF in the source chamber. To achieve sufficiently high concentrations of bFGF a 2000 fold molar excess of unlabeled bFGF was included with the ^{125}I-bFGF tracer. In Figure 7.12, a 2000 fold higher molar excess of unlabeled bFGF was used. The normalized sink concentration is plotted as a function of time. After a lag period of 11 hours, the normalized flux rose to within 20% of that for IL1β and bFGF with 10 mg/mL protamine sulfate.

7.6 Conclusions

The following table summarizes the results of the diffusion studies.

	$K \bullet D_{eff} \pm$std err ($x10^{-9}$ cm^2/s)	K	steady-state $D_{eff} \pm$std err ($x10^{-9}$ cm^2/s)	lag-time D_{eff} ($x10^{-9}$ cm^2/s)
IL1β	10±1	1.49±0.05	6.6± 0.7	8
IL1β / 3.0 M salt	5.5	1.49±0.05	3.7	
bFGF/ protamine sulfate	9±1	1.48±0.03	5.8 ± 0.8	9
bFGF / 3.0 M salt	5.6±0.2	1.48±0.03	3.8 ± 0.2	2
excess unlabeled bFGF	8±0.5	1.48±0.03	5.3 ± 0.3*	

Table 7.1 Diffusion Experiments Summary

The first column contains the $K \bullet D_{eff}$ data obtained from multiple diffusion studies. Partition coefficients were measured independently. The third column contains calculated effective diffusivities based on diffusion studies and partition coefficient measurements. The standard errors were propagated from the errors in the respective experiments. (* the error in the experiment with excess unlabeled bFGF represents half the total range for duplicate experiments) The final column presents diffusivities estimated from the lag time of the diffusion experiments.

The standard errors reported here were propagated from the estimated error in the partition coefficients and the measured error for the $K \bullet D_{eff}$ obtained from multiple diffusion experiments. The primary source of error in the $K \bullet D_{eff}$ measurements probably arose from the measurement of membrane thickness. We used an average value for the membrane based on multiple measurements of the membrane thickness. Our model of the

diffusion process does not account for variations in membrane thickness. For subsequent modeling purposes we used an effective diffusivity of $6x10^{-9}$ cm^2/sec obtained from the protamine sulfate data. This data set was chosen over those with salt or excess unlabeled bFGF because: 1) the experiments were done with bFGF and not IL1β, 2) the membrane itself appeared to be influenced by the high saline, and 3) the lower effective diffusivities measured in the experiments with high molar excesses of unlabeled bFGF might have been influenced by changes in the bFGF in the source chamber during those much longer experiments.

The diffusivities were all based on the steady state method. However, in chapter 2, the lag-time method was discussed as an alternative approach to determining effective diffusivities. The lag time approach requires that the thickness of the membrane be known and that the lag time required to reach a steady state flux through the membrane be known. The diffusion area, the partition coefficient, and the source concentration are not needed to determine the diffusivity. However, given the variation in membrane thickness for the DM and the difficulties in gaining significant accurate data points at the early times, we elected to use the steady state approach. Nevertheless, effective diffusivities determined using the lag-time method were in good agreement with the values obtained from the steady state approach as can be seen in table 7.1. These results suggested that our estimates of effective area for diffusion and our measurements of partition coefficients were accurate.

The similarity in partition coefficients for bFGF and IL1β was unexpected. Given the positive charge on bFGF and the net negative charge of the DM, we anticipated that bFGF would have a higher partition coefficient than IL1β. However, the results of the diffusion experiments support the results from the equilibrium partitioning experiments. The normalized fluxes for bFGF and IL1β were nearly identical in the 3.0 M NaCl containing buffer which would be expected for two molecules with similar size. Under these high ionic strength conditions electrostatic effects on the partitioning would be

expected to be negligible. The normalized fluxes were also very close for IL1β and bFGF in the presence of protamine sulfate. The concentrations of protamine sulfate were high enough to disrupt bFGF binding to HS, but did not significantly alter the ionic strength of the buffer. If the bFGF partitioned into the DM to a much greater extent than the IL1β, it should have been evident in a much higher normalized flux of bFGF through the DM in the protamine sulfate experiment. Thus, again the partition coefficient measurements are in good agreement with the diffusion data.

The literature contains no direct measurements of diffusivities in Descemet's membrane. The flux of Inulin (5,200 g/mol) through stroma with and without Descemet's membrane has been measured [143], and a permeability for the DM of 1.7x10-6 cm/sec for membranes 70 μm thick was reported. If we use our measured partition coefficient of 1.5, this permeability corresponds to a Deff of $8x10^{-9}$ cm^2/sec. Given the indirect nature of this measurement and the smaller size of the inulin molecule, this value is in good agreement with the diffusivities measured here.

Diffusivities for a globular protein of bFGF dimensions in free aqueous solution (D_o) would be expected to be approximately $1.5x10^{-6}$ cm^2/sec using the Stokes-Einstein equation based on a bFGF radius of 14.5 Å. Hence the ratio D_{eff}/D_o is 0.004. Several factors can contribute to reduce measured diffusivities in hydrogels. If the hydrodynamic radius of the protein approaches that of the spaces through which it must pass, drag forces can retard its progress. Fatt [144] reported a hydraulic conductivity (k) for Descemet's membrane of between $1x10^{-15}$ to $3x10^{-15}$ cm^2. These values do not represent direct measurements of the hydraulic permeability of the membrane as they were based on a mathematical model of corneal swelling applied to swelling data for corneas with and without Descemet's membrane attached. Using a hyraulic permeability of $2x10^{-15}$ cm^2 in conjunction with the molecular radius of bFGF (r_s), the effective diffusivity of bFGF in the DM can be estimated based on the work of Phillips et al. with the following equation:

$$D_{eff} = D_o \left[\frac{1}{1 + (r_s^2 / k)^{1/2} + \frac{1}{3}(r_s^2 / k)} \right] \qquad 7.2$$

This equation predicts D_{eff}/D_o of 0.13 compared to the measured value of 0.004. One potential source of error in the theoretical estimate of the effective diffusivity is in Fatt's determination of the hydraulic permeability of the DM. It was not a direct measurement and was subject to errors in both the experimental swelling data and in the theoretical model of corneal swelling. Secondly, the effective medium model was based on diffusion of a solute through fibrous matrices. The heavily hydrated GAG chains in the DM could introduce another layer of complexity that the model does not account for.

The effective diffusivity of bFGF in Descemet's membrane was a critical variable in our model of bFGF transport through the DM. Consequently, several different approaches were employed to obtain a reliable value for this parameter. The effective diffusivity of IL1β, a similarly sized non-heparin binding bFGF analog, was measured. The effective diffusivity of bFGF was determined in a high salt environment in which bFGF could not associate with DM HS. High concentrations of protamine sulfate were used to specifically block the association of bFGF and HS. Lastly, bFGF sites in the membrane were saturated with high concentrations of unlabeled bFGF, and effective diffusivity of bFGF was measured based on the steady state flux. All of these techniques yielded relatively similar diffusivities, and ultimately a value of 6×10^{-9} cm^2/sec was chosen for use in subsequent experiments.

Chapter 8

Synthetic Membranes

8.1 Introduction

Descemet's membrane represents a complex biological system subject to a certain amount of variability in composition and structure. A secondary objective of this work was to develop synthetic GAG hydrogels to further explore how heparan sulfate imbedded in a hydrogel can regulate the passage of bFGF through the gel. Our goal was to create a model Descemet's membrane in which heparan sulfate extracted from the tissue was incorporated into an inert hydrogel. The importance of variables such as heparan sulfate concentration and molecular weight distribution to the transport of bFGF could be explored with this model. Ultimately, other components of the matrix might be introduced to the gel, as well.

8.2 Choice of Hydrogel

Although it was not our goal to duplicate the elaborate ultrastructure of actual Descemet's membrane, the hydrogel should have a similar effective pore size and water content as Descemet's membrane to ensure that the diffusion is much slower than the binding interaction. The gels should also have enough mechanical strength to withstand the rigors of the diffusion experiments when cast as thin membranes. We wanted to avoid introducing a mesh support into the gel and the added complications to data analysis that

would result. The gels should have low protein adsorption characteristics. Lastly, a body of characterization literature should support it. Given these restrictions, we chose polyacrylamide.

Polyacrylamide has been used as a matrix for zone electrophoresis for over 40 years [145], and it has become a key tool for research in the biological sciences. Using high grade acrylamide monomer and bis-acrylamide crosslinker, and standardized polymerization procedures, uniform gels can be produced. By adjusting the polymer content of the gel, the effective pore size of the gel can be controlled. Adjustment of the bis-acrylamide cross-linker offers control over the mechanical strength of the gel as well.

8.3 Linking GAG to the Gel

Our requirements for linking glycosaminoglycan to the polyacrylamide were: the attachment must be covalent, the GAG must not be significantly altered by the procedure, and the GAG must be accessible to bFGF diffusing through the hydrogel. Several procedures exist in the literature for attaching heparin or chondroitin sulfate to polyacrylamide.

Amine functional groups were introduced to the polyacrylamide gel by copolymerizing acrylamide with allylamine [146]. Heparin was then covalently attached to these amine groups via its own carboxyl groups using the carbdiimide reaction. Yields for this approach were less than 1%.

A second strategy [147] involved derivatizing chondroitin sulfate such that its reducing terminus contained the allyl group. This GAG was then copolymerized with the acrylamide and bis-acrylamide, and the authors reported that the technique worked with heparin, as well. Yields were not available for this approach.

Sofia et al [136] used electron beam radiation to form PEO gels and to graft PEO onto surfaces. In the case of PEO, the following reaction describes the formation of free radicals on the main chain PEO carbons.

$$2\,HOH \xrightarrow{e^-} 2\,^{\bullet}OH + H_{2(g)}$$
$$^{\bullet}OH + \text{-}(CH_2 - CH_2 - O\text{-})_n \rightarrow HOH + \text{-}(CH_2 - ^{\bullet}CH - O\text{-})_n \qquad 8.1$$

It is likely that similar reactions could be used to covalently incorporate heparin into a polyacrylamide gel with electron beam irradiation. Although the mechanism for polyacrylamide cross-linking and covalent attachment of heparin has not been formally identified, the hydroxyl radical would presumably be responsible for mediating similar reactions as described above.

Copolymerization of a derivitized heparin with acrylamide could significantly alter the structure of the gel. Polymerization of modified acrylamide containing a reactive group for subsequent heparin attachment would require that heparin diffuse into the gel prior to the ligation reaction. While this approach should not unduly influence the polymerization reaction, it would be susceptible to low ligation yields and heparin gradients in the gel. However, the electron beam should crosslink the heparin into the polyacrylamide network *in situ*; no prior derivatization of the heparin would be required. E-beam dosages must be optimized for maximal incorporation with minimal alteration to the gel and heparin structure.

8.4 Incorporation of Heparin into Gels

The efficiency of E-beam mediated covalent attachment of GAG to polyacrylamide was assessed with heparin. The extent of heparin incorporation into polyacrylamide gels was assayed for two different initial heparin concentrations and four different E-beam dosages. Polyacrylamide gels were cast with 10% polymer and heparin in the polymerization buffer. Following electron beam exposure, the gels were washed extensively in buffer to remove unbound heparin. The wash steps consisted of incubating the gels in PBS for a minimum of 24 hours, transferring them to fresh buffer, and determining the heparin content of the incubation buffer using the dimethylmethylene blue assay. The washing was considered complete when heparin was no longer detectable in the gel (< 400 ng/mL). The heparin remaining in the gels was determined with a uronic acid assay. The results of these experiments are shown in Figure 8.1. These results demonstrated that the heparin was incorporated in the gel, and that the yields for incorporation were a function of the E beam dosage, ranging from 10% to 20%. The different concentrations of heparin did not appear to significantly influence the overall yield. Staining these gel with dimethylmethylene blue and observing the gels under a microscope confirmed uniform incorporation of heparin into the gels.

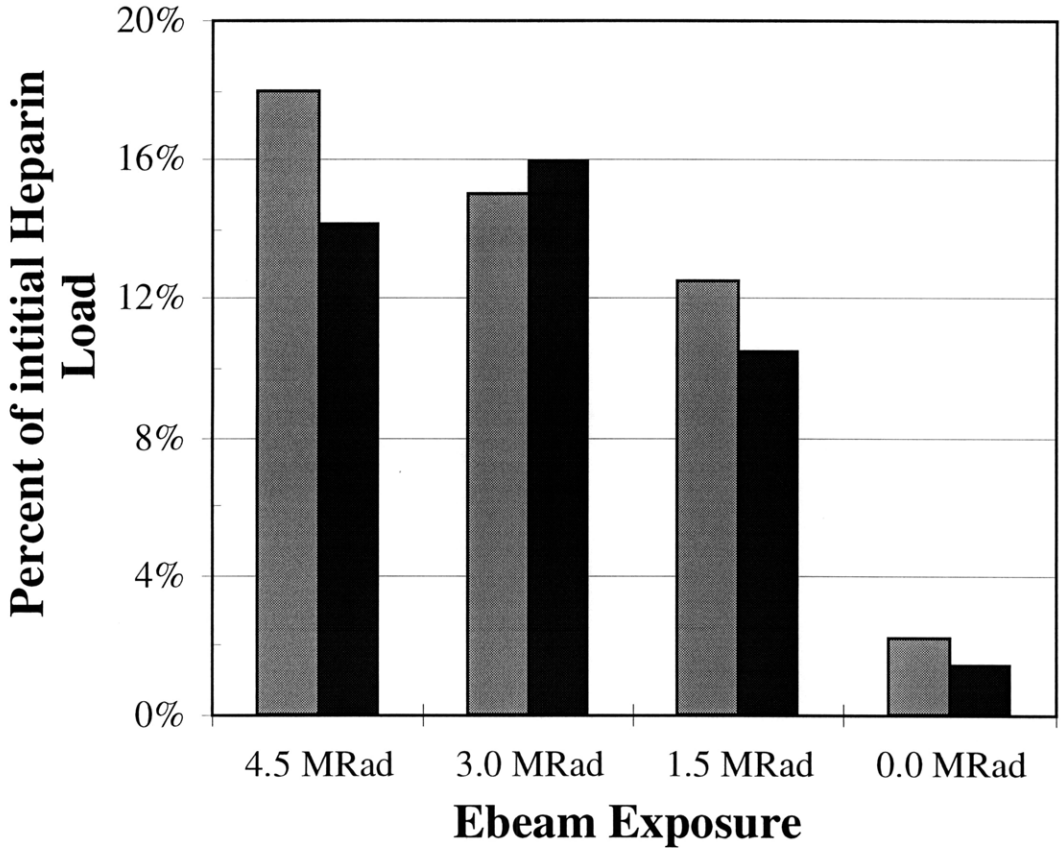

Figure 8.1 Heparin Incorporation in Polyacrylamide Gels: The yield of heparin incorporation in polyacrylamide gels exposed to electron beam radiation is presented for initial heparin concentrations in the gel of 0.4 mg/mL (■) and 2.0 mg/mL (▩).

The capacity of GAG gels to bind bFGF is depicted in Figure 8.2. In this experiment, gels with no GAG, with chondroitin sulfate, and with heparin were synthesized and incubated with bFGF in a PBS-BSA. The gels were washed with PBS-BSA containing, 0.5 M NaCl, 1.0 M NaCl, 3.0 M NaCl, and a final wash with 4 M guanidine hydrochloride with 3.0 M NaCl. The figure shows the total bFGF released from each gel as a percentage of the total amount in the initial incubation solution for the 1.0 M NaCl, 3.0 M NaCl and the guanidine hydrochloride washes. The data represent the average of duplicate gels with pairs of measurements differing by at most 15%. The results show very little non-specific bFGF adsorption to the polyacrylamide itself. The chondroitin sulfate did bind some bFGF that was release with the high molar salt washes. Uronic acid assays confirmed similar initial concentrations for the chondroitin sulfate and heparin in the gels. Some binding of bFGF is expected to chondroitin sulfate based solely on electrostatic interaction of the positively charged growth factor with the negatively charged glycosaminoglycan chain. The heparin containing gels bound the most bFGF. Interestingly, the guanidine hydrochloride data suggests that a significant proportion of the bFGF bound to heparin gels (5% total bFGF) involved a hydrophobic interaction between bFGF and heparin. While the chondroitin sulfate containing gels showed evidence of this hydrophobic interaction, it was much more pronounced for the heparin containing gels. Heparin does have small hydrophobic regions associated with the N-acetylated glucosamine units. The electron beam might also have altered the structure of the heparin and introduced more hydrophobic regions.

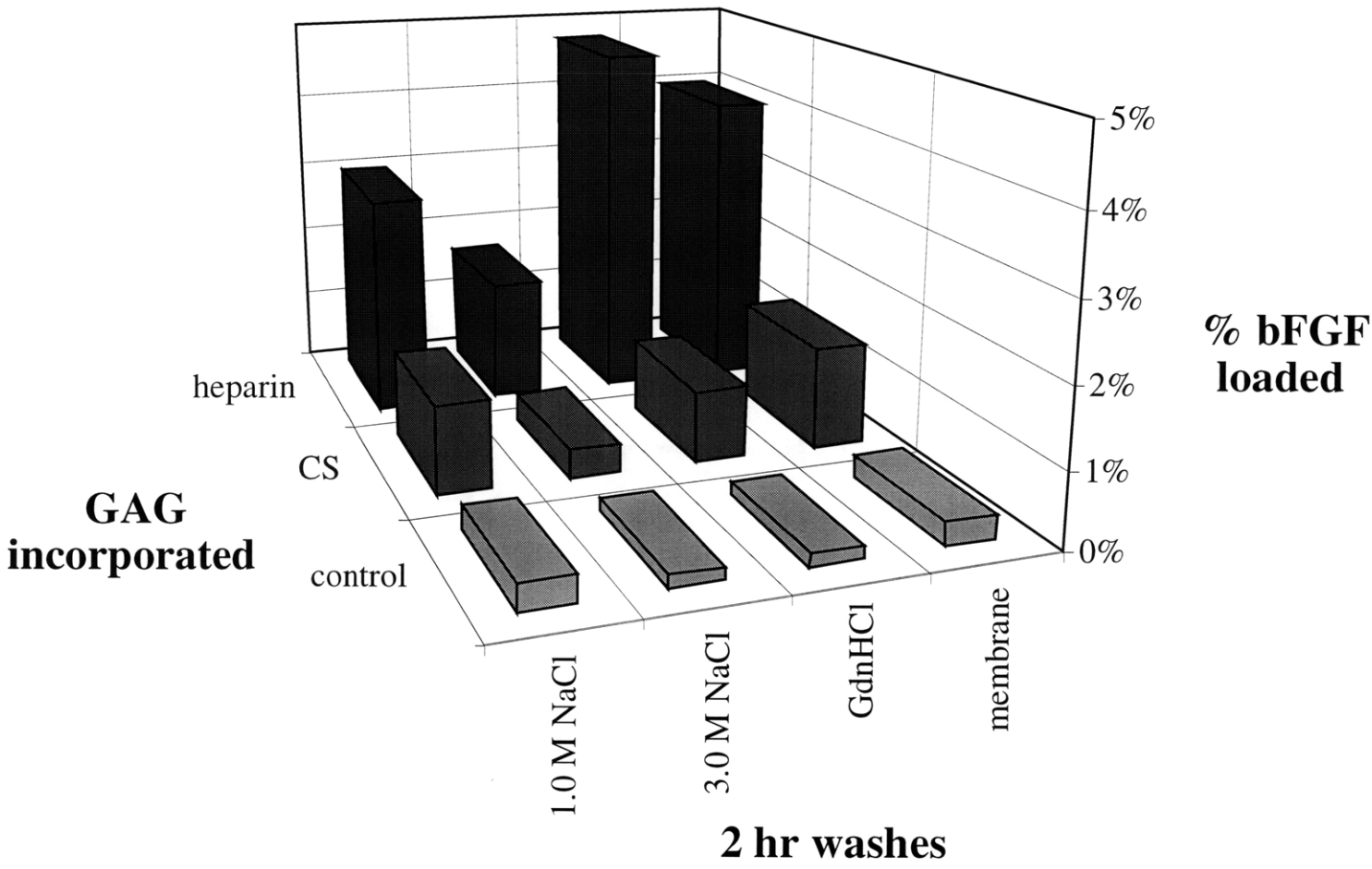

ure 8.2 bFGF Binding to GAG-Polyacrylamide Gels: bFGF bound to gels with heparin, chondroitin sulfate, no GAG can be desorbed with different salt washes and guanidine hydrochloride. Desorbed bFGF percentages are ed on the total amount of bFGF initially incubated with the gels.

8.5 Effect of E-beam radiation on the heparin bFGF interaction

Basic FGF bound to the heparin gels, but given the high affinity of the bFGF/heparin interaction, we expected greater amounts of bFGF retention. Using the method developed for determining the dissociation constant for bFGF and heparan sulfate, we compared the amount of complex formed between bFGF and heparin that had received varying dosages of E-beam radiation. Identical bFGF and heparin concentrations were used in each experiment. Figure 8.3 shows the elution profiles of the bFGF-heparin peak from the sephadex G-75 gel filtration column. The results indicate that with increasing E-beam dosage, the amount of complex formed decreased, and this suggests that the electron beam is damaging the bFGF binding sites on the heparin. Dimethylmethylene blue interacts with heparin on a charge basis. When these heparin samples were assayed with DMB, the decrease in bFGF complex was mirrored by decreased binding to the DMB. This results suggests that some of the alteration in the heparin structure involves loss of negatively charged sulfate groups from the carbohydrate backbone.

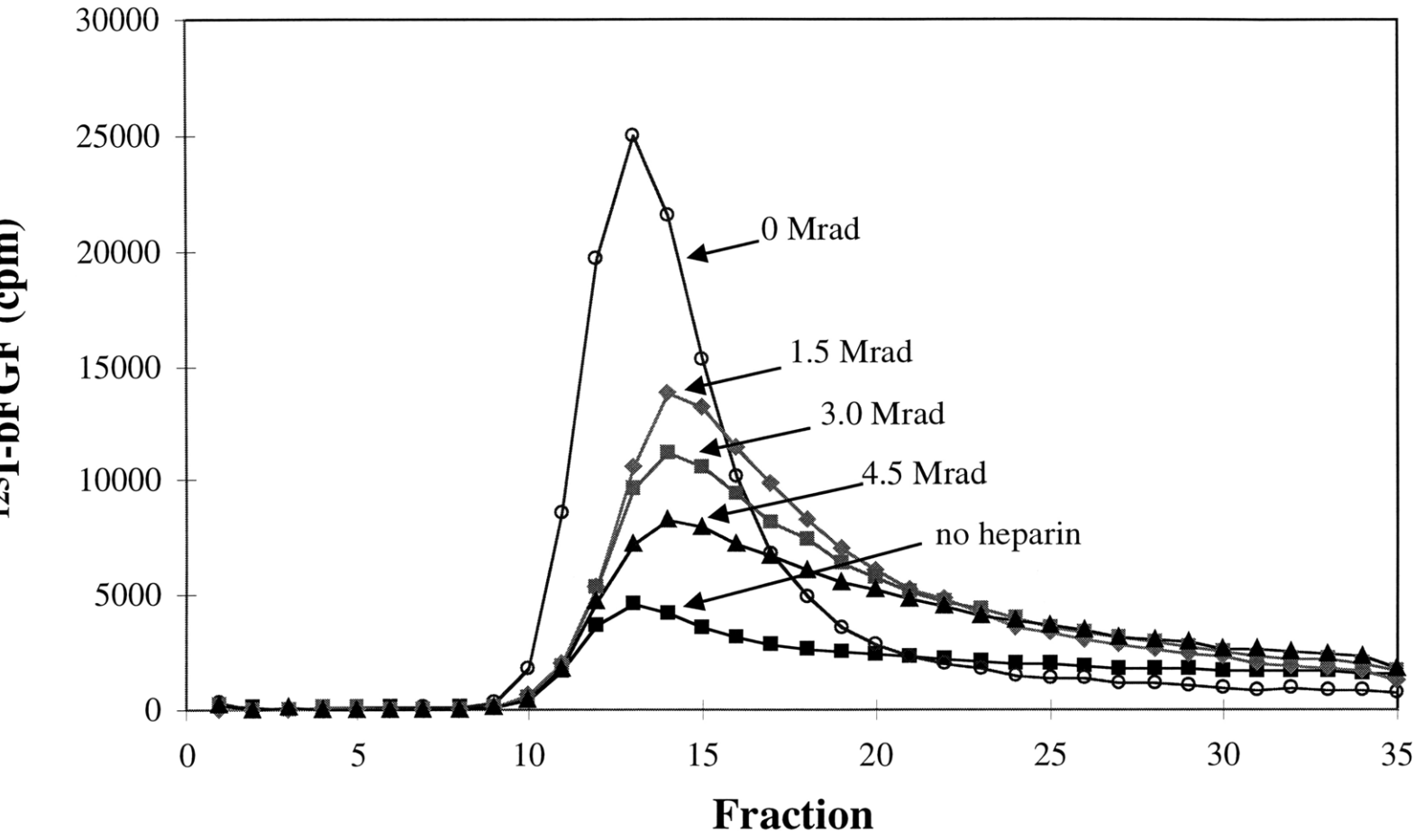

gure 8.3 E-beam Damage to Heparin: A Sephadex G-75 chromatogram of ^{125}I-bFGF complexes with heparin xposed to differing amounts of electron beam radiation shows decreasing complex formation with increasing heparin oncentration.

8.6 Diffusion of bFGF through polyacrylamide gels with/without heparin

Despite the apparent reduction in heparin's affinity for bFGF, the heparin gels would still be useful as an experimental model if they could be shown to decrease bFGF flux in a predictable manner. Figure 8.4 shows diffusion experiments conducted with polyacrylamide gels with and without heparin. The large gel to gel variability in flux when no heparin was present made it impossible to judge the affect of heparin on diffusion through the gels. This result highlights the difficulty in obtaining reproducible results with this system. The results from Figure 8.3 indicated that the electron beam altered the structure of soluble heparin and reduced its affinity for bFGF. Although Figure 8.2 revealed that bFGF did bind preferentially to heparin gels, much of the bFGF was washed off the gels with 0.5 M NaCl. A comparatively low amount of the bFGF bound with high affinity to the heparin in the gels. If the electron beam has altered the heparin to the extent that rates of binding and release are significantly slower than diffusion then the impact of heparin in the diffusion experiments would be imperceptible.

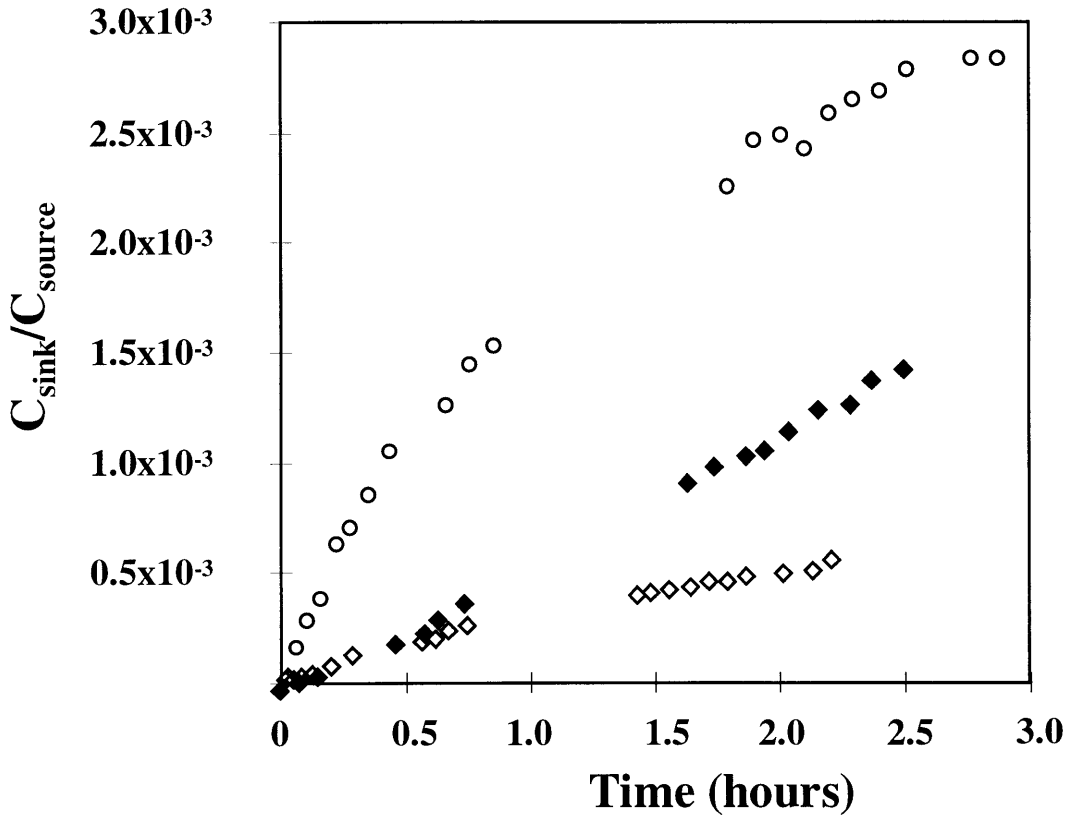

Figure 8.4 bFGF Diffusion through Gels with and without Heparin: bFGF diffusion through polyacrylamide gels with covalently incorporated heparin in a single experiment (◆) is compared with two diffusion experiments with gels lacking heparin (◇ ○). The gels were of the same thickness, and the sink concentration has been normalized to differences in source concentration

8.7 Conclusions

The results with electron beam treated heparin gels should be viewed in perspective. The approach was successful in binding heparin to the polyacrylamide, and the bound heparin retained specificity for binding bFGF. Several avenues remain to be explored before this approach is abandoned. The electron beam dosage could probably be reduced considerably before heparin incorporation yields reached unacceptable levels. The lower dosages should do less damage to the heparin. Much of the variability in bFGF diffusion through electron beam treated polyacrylamide without heparin might be associated with the initial polymerization step itself. The extremely thin gels (250 μm) might have been more susceptible to polymerization inhomogeneities at the interfaces with the glass plates and the gel spacers. Thicker gels with lower polymer percentages could circumvent this problem. Other hydrogel systems such as agarose or PEO might also be considered. Descemet's membrane is a powerful tool for analyzing real bFGF ECM interactions, but a deeper understanding of the mechanisms involved must come from more defined systems.

Chapter 9

Numerical Solutions to the Diffusion/Binding Problem

9.1 Introduction

We have postulated that bFGF transport through Descemet's membrane is dependent on the hindered diffusion of bFGF through the DM matrix coupled with reversible association to the resident HS chains. This hypothesis was the basis of the diffusion/binding model that guided the design of our experiments. In order to test the validity of the model and to determine its implications for *in vivo* systems, the coupled diffusion and reaction equations must be solved with the parameter values obtained from our independent experiments. However, the general problem of diffusion of a solute through a membrane with reversible binding to sites in the membrane has no analytical solution (see section 2.4.2). The relevant equations are presented here for reference:

$$\frac{\partial b}{\partial t} = D_{eff}\frac{\partial^2 b}{\partial x^2} - \frac{\partial c}{\partial t} \qquad 9.1$$

$$\frac{\partial c}{\partial t} = k_{on} h b - k_{off} c \qquad 9.2$$

$$h_{tot} = h + c \qquad 9.3$$

Numerical methods must be employed to solve this equation set. The experiments described in the previous sections were geared toward obtaining values for the unknown variables in these equations. In this section, these values will be incorporated into the numerical model for diffusion with binding, and the simulation results will be compared to an independent set of experiments. The numerical model will then be used to extend our findings to *in vivo* scenarios.

9.2 Solution Method

Equations 9.1 - 9.5 were solved with a semi-implicit finite difference method. The FORTRAN code may be found in Appendix A. This approach was more efficient than a fully implicit strategy. With a semi-implicit formulation, the equation matrix that had to be inverted had a single diagonal band 3 columns thick. The simple structure of this matrix was exploited by using a band solver rather than the more computationally expensive, and less efficient, full L-U decomposition with back-substitution. The time scale for diffusion in the DM experiments was on the order of 1 hour, while the association of bFGF with heparan sulfate occurred on the order of 0.1 seconds. This wide disparity of time scales in the problem placed constraints on the solution method. The equations were non-dimensionalized with respect to time using an l^2/D term. Consequently, the dimensionless time steps were on the order of $1x10^{-6}$ to capture the kinetics of the association reaction. This time step approached single precision limits ($1x10^{-8}$) in some of the calculations. The code was run at double precision to avoid round-off errors.

Equations 9.1-9.2 were non dimensionalized with the following parameters, and are presented in dimensionless form below:

$$\alpha = \frac{c}{h_{tot}} \text{ (a)} \qquad \beta = \frac{b}{b^{\circ}} \text{ (b)} \qquad \chi = \frac{x}{l} \text{ (c)} \qquad \tau = \frac{t}{l^2 / D_{eff}} \text{ (d)} \qquad 9.4$$

$$\frac{\partial \alpha}{\partial \tau} = Da^{\alpha}_{on}\beta - Da^{\alpha}_{on}\alpha\beta - Da^{\alpha}_{off}\alpha \qquad 9.5$$

$$\frac{\partial \beta}{\partial \tau} = \frac{\partial^2 \beta}{\partial \chi^2} - Da^{\beta}_{on}\beta + Da^{\beta}_{on}\alpha\beta + Da^{\beta}_{off}\alpha \qquad 9.6$$

9.3 Test Case

While no analytical solution exists for the general diffusion/binding problem, a solution does exist for the special case of fast reversible binding to unsaturable sites in the membrane. This case was discussed in section 2.4.3, and was used to test the accuracy of the code. Table 9.1 shows the parameter values used in the test run. These values were not chosen for any practical problem, but, rather, to satisfy the constraints of the special case.

kon	1 / mM s	koff	100 / s
partition coefficient (K)	1	effective diffusivity (D_{eff})	0.5 cm^2/s
chamber volumes (V_{chamb})	500 mL	diffusion area (A)	0.2 cm^2
membrane thickness (l)	5 cm	spatial increments	300
total time (t)	100 sec	temporal increments	$1x10^6$
solute source (b°)	1 mM	total binding sites (h_{tot})	100 mM

Table 9.1 Parameters For Numerical Solution Test Case

The values for the on and off rate constants (k_{on} and k_{off}) yield an equilibrium dissociation constant (K_d) of 100 mM. The binding constant is 100 fold higher than the maximum concentration of free solute in the membrane. Consequently, the maximum occupancy of the membrane binding sites will be 1%. The Dahmkholer number for the slower association rate ($l^2 \bullet k_{on} \bullet b° / D_{eff}$) is 50 for these parameters, so reaction takes place much faster than diffusion. Figure 9.1 shows the results of the test run. Equations 9.1 and 9.2 were discussed in section 2.4.3, and will be used to analyze the results of the run.

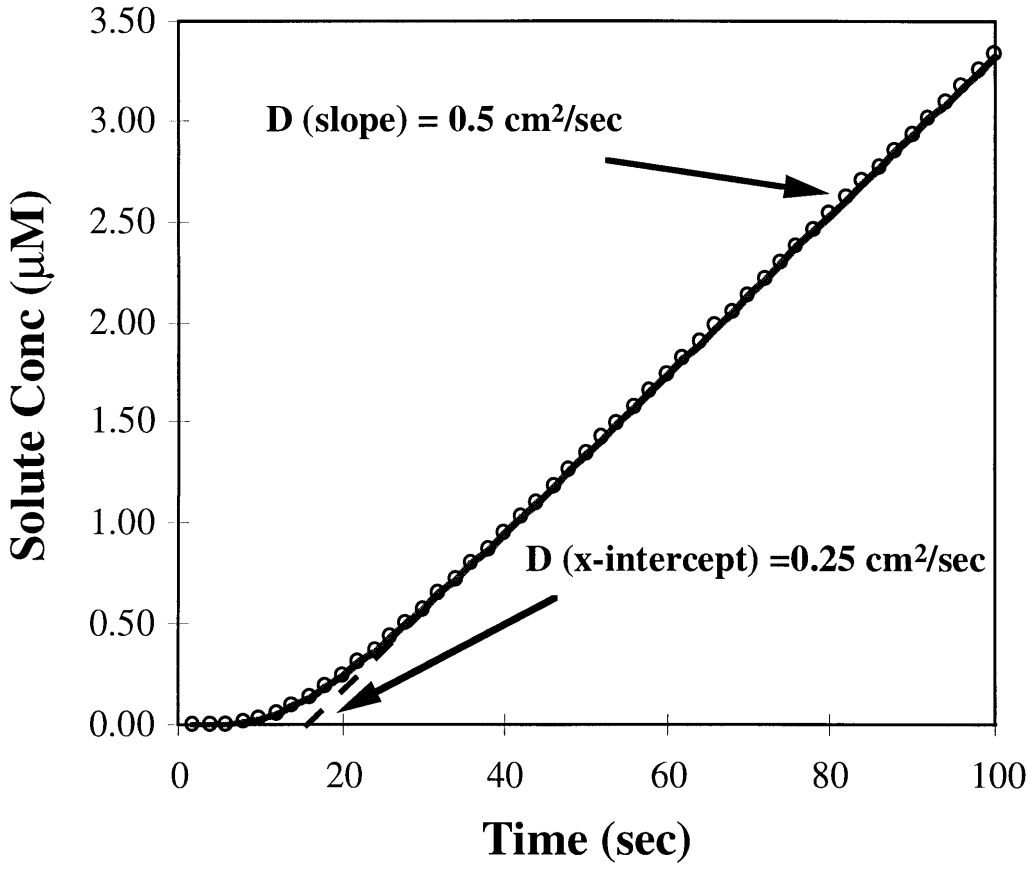

Figure 9.1 Numerical Solution Test Case: The numerical solution for diffusion with fast, reversible, unsaturable binding(o) is compared to the analytical solution for the same problem (——). The diffusivity (D) determined from the slope reflects a steady state solution that is independent of the binding interaction, while the diffusivity determined by the lag time is apparently reduced by a factor of 2 by the binding interaction.

$$b_{\sin k} = \frac{AD_{eff}b^{\circ}}{lV_{\sin k}}\left(t - \frac{l^2}{6D_{rxn}}\right) \qquad 9.7$$

$$D_{rxn} = \frac{D_{eff}}{\left(1 + \frac{h_{tot}}{K_d}\right)} \qquad 9.8$$

If the simulation operated properly, then the slope in equation 9.4 should yield the effective diffusivity unaffected by the reaction. However, the lag time should correspond to a diffusivity reduced by a factor of 2 by the interaction of solutes with binding sites. Both of these predictions were born out by the, suggesting that the numerical method was suitable for use with the more general diffusion/binding problem in the DM.

9.4 Descemet's Membrane Simulations

The following table summarizes the results obtained from the characterization of Descemet's membrane and its HS components, and the results from the bFGF diffusion studies with the DM.

k_{on}	2.6×10^6 / M s	koff	0.01 / s
partition coeff.	1.5	D_{eff}	6×10^{-9} cm^2/s
chamber volume	3 mL	effective area	0.17 cm^2
membrane thickness	40 μm	HS sites	26 μM

9.2 Parameters for bFGF DM diffusion simulation

Table 9.3 summarizes the values of the Damkholer numbers for the parameters used in the model.

Da^{α}_{on}	$k_{on}\, l^2\, b^{\circ} / D_{eff}$	10
Da^{α}_{off}	$k_{off}\, l^2 / D_{eff}$	30
Da^{β}_{on}	$k_{on}\, l^2\, h_{tot} / D_{eff}$	$2x10^5$
Da^{β}_{off}	$k_{off}\, l^2\, h_{tot} / D_{eff}\, b^{\circ}$	$7x10^5$

Table 9.3: Damkholer Number Values

These parameters were used in conjunction with the diffusion/binding model to simulate the diffusion study described in section 7.5. In this diffusion experiment, an excess of unlabeled bFGF was introduced to the source chamber with the ^{125}I-bFGF for a total concentration of bFGF of 1 μM. The high concentration of unlabeled bFGF accelerated the saturation of HS sites in the membrane. Prior to the saturation of sites, the flux of bFGF through the membrane was low, but once the HS sites were saturated, the flux of bFGF in the sink chamber rose to the level observed in experiments where binding had been blocked.

9.4.1 Model Simulation

Figure 9.2 represents the results of a diffusion/binding simulation with 1 μM bFGF. The simulation results were based on independently measured parameter values incorporated into the diffusion/binding model. The model predicted a lag time of several hours, followed by a constant steady state flux that was within 10% of the experimental flux. These results suggested that the transport of bFGF across a complex tissue can be represented with a comparatively simple diffusion/binding model. The model produced a reduced lag time compared to those observed in the actual experiments. The experimental results yielded lag times of 10 and 14 hours as contrasted with a model lag time of 6 hours.

The model predicted a very abrupt breakthrough to steady state flux, while the experiments showed a smoother transition. This abrupt breakthrough is characteristic of a very steep concentration gradient of bFGF moving through the membrane. This phenomenon was discussed in section 7.6. The fast association/dissociation rates, the high affinity bFGF/HS interaction, and the comparatively low diffusivity of bFGF in the membrane combined to create a moving wave front of bFGF in the membrane. Figure 9.3 shows the evolving concentration profile of free and bound bFGF in the membrane during the first 6 hours of the simulation. The absence of this abrupt breakthrough in the experimental data was likely attributed to the fact that, while the model assumes the membrane is a constant thickness, the actual membranes demonstrated some thickness variation. This issue will be explored more thoroughly in the following section. These results suggest that the diffusion/binding model can be a useful tool for exploring the role of ECMs in controlling the bioavailability of bFGF in various tissue environments.

The Damkholer numbers for the system suggest that the binding reaction takes place much faster than diffusion, and that local equilibrium exists at all points in the membrane between bound and free solute. Consequently, simulations were also performed for the more specific case of diffusion with local equilibrium. As expected, these results were identical to those for the solutions for the more general case.

Additional simulations were conducted to assess the significance of the errors in individual parameters to the results (Figures 9.4-9.7). The largest errors were associated with the thickness of the membrane (36 μm - 46 μm), measurement of the concentration of HS binding sites for bFGF in the membrane(13 μM - 39 μM), and the effective diffusivity of bFGF through the DM ($5x10^{-9}$ cm^2/s - $7x10^{-9}$ cm^2/s). While the other parameters in the model had error associated with them, their deviations had insignificant effects on the model results.

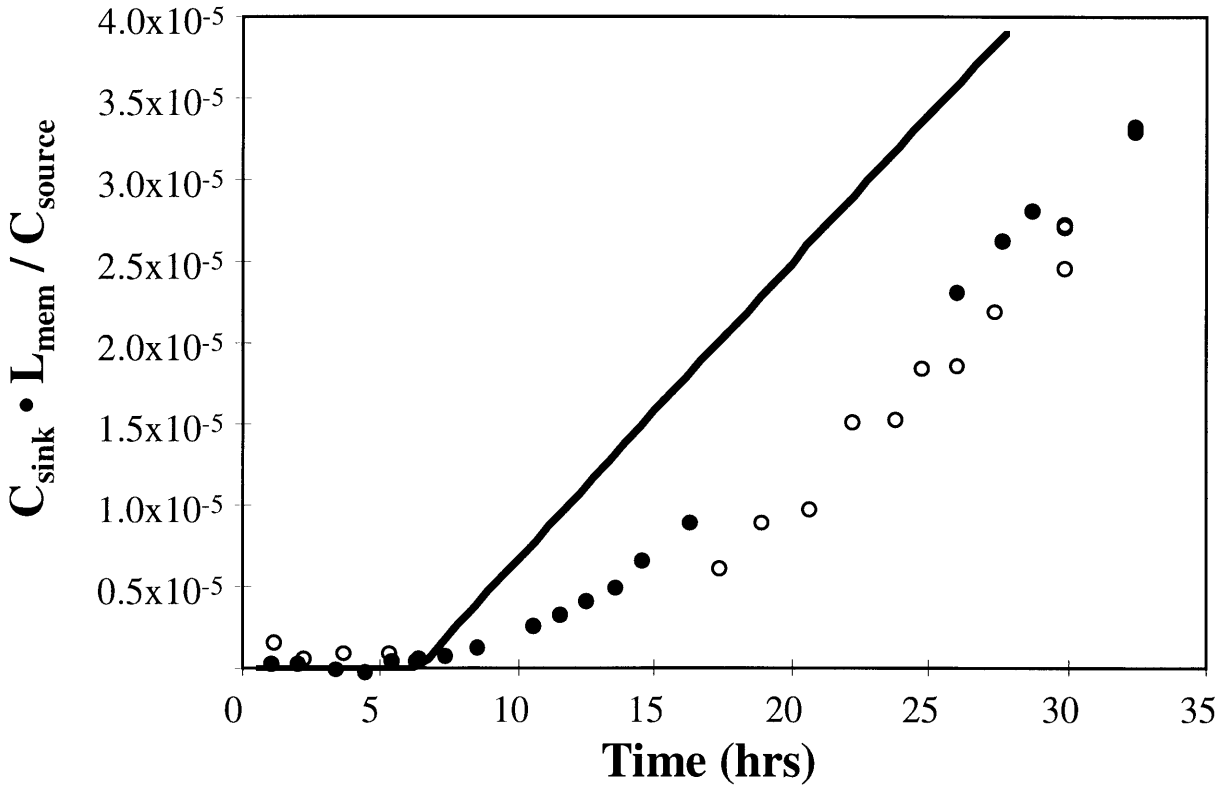

Figure 9.2 Base Case Simulation for bFGF Transport through DM: The simulation of the diffusion/binding probem using experimentally determined parameters (—) is compared to 2 sets of experimental data for diffusion of ^{125}I-bFGF with an excess of unlabeled bFGF (o ●). The concentration in the sink chamber was normalized for experimental variations in membrane thickness and source concentration.

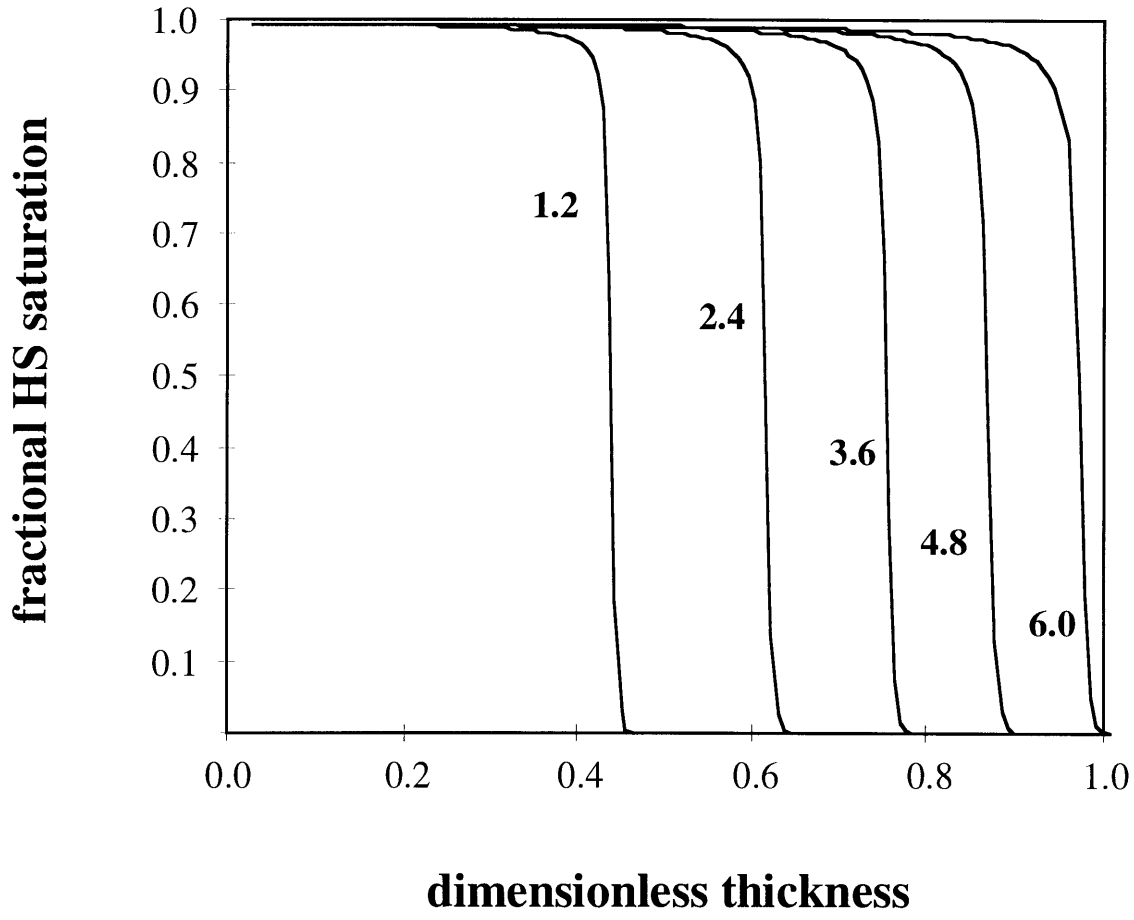

Figure 9.3 bFGF Concentration Profiles in the DM: The moving wave front of bFGF passing through the membrane is visualized at 5 timepoints of 1.2, 2.4, 3.6, 4.8, and 6.0 hours. A comparison with the simulation data in Figure 9.2 shows that after the 6 hour time point, a steady state flux of solute is established in the sink chamber coinciding with saturation of HS sites in the membrane.

9.4.2 Variation in Membrane thickness

The Descemet's membranes used in the diffusion experiments discussed in Chapter 7 had an average thickness of 40 μm. However, the thickness was noted to vary for a given membrane. The average difference between maximum and minimum measurements for a given membrane was 14 μm. The two membranes used in the diffusion study simulated here had a total thickness range of 36 to 46 μm, with an average of 40 μm. Simulations were conducted with these thickness extremes with all other parameters held constant at their baseline values. Figure 9.4 presents the results of this simulation. As expected, increases in the membrane thickness corresponded to increases in lag time. We attributed the smooth transition to steady state flux in the experiments to the variation in membrane thickness in a given membrane. The flux should start to rise in the sink chamber when the moving concentration front of bFGF reaches the edge of the membrane at its thinnest point; however, the true steady-state won't be reached until the entire membrane is saturated. Only one of the experimental data sets in Figure 9.4 has data in the transition region. This particular membrane ranged in thickness from 36 to 46 μm, the range explored in the simulations. The time interval in which the flux rose from zero to its steady state value was approximately 3 hours. Interestingly, the difference in lag times between the two thickness extremes is also approximately 3 hours. Thus the simulations would predict a approximately 3 hour transition period where the flux would smoothly rise to the constant steady state flux. This result is consistent with our hypothesis regarding the effect of variation in membrane thickness on the flux of bFGF through the membrane.

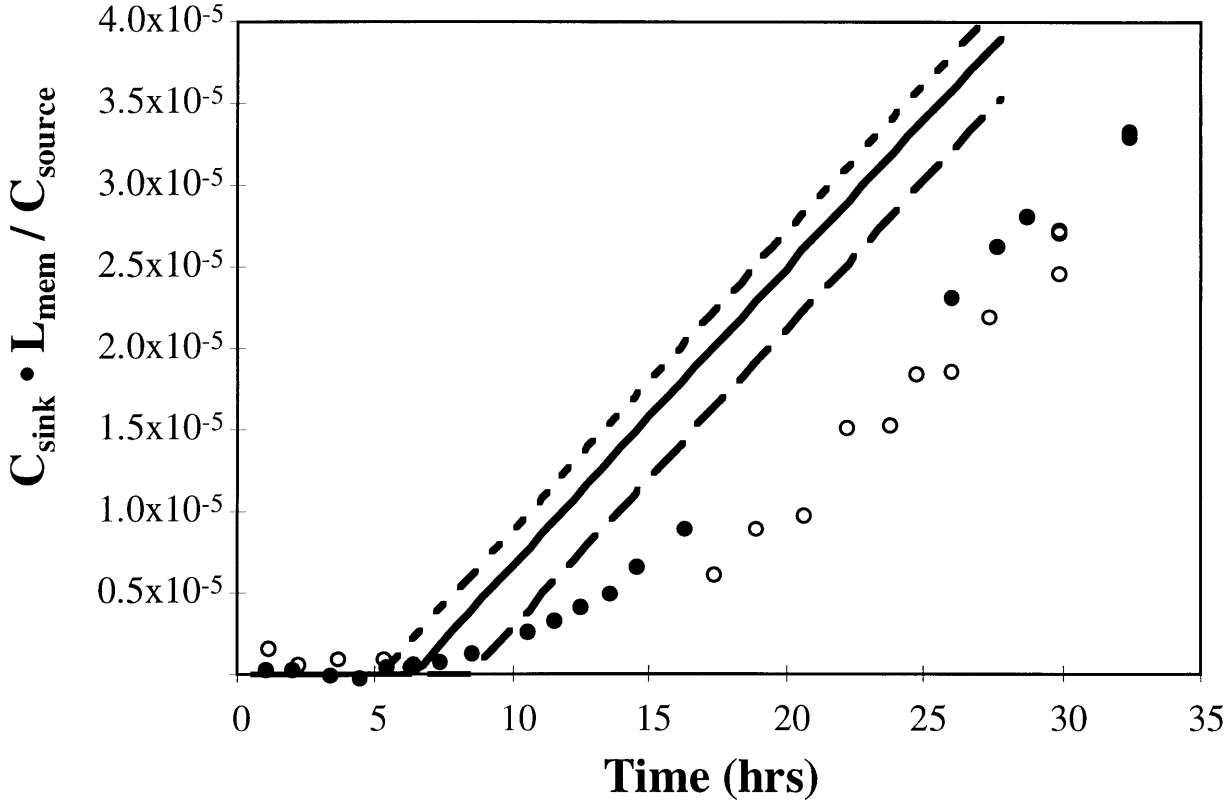

Figure 9.4 Simulation of Effect of DM Thickness Variation: The diffusion/binding model was used to simulate the variations in membrane thickness. The base case of 40 μm (——) is compared to a minimum thickness of 36 μm (- - -), a maximum thickness of 46 μm (— —), and experimental data from a codiffusion experiment with ^{125}I-bFGF and excess unlabeled bFGF (o ●). The sink concentration of bFGF was normalized for experimental variations in membrane thickness and source concentration.

9.4.3 Error in HS sites and Effective Diffusivity

Based on the extraction of heparan sulfate from Descemet's membrane, the concentration of HS binding sites in the membrane was estimated at 26 μM ± 13 μM. The impact of this error on the simulation results is represented in Figure 9.5. Increases in the concentration of sites resulted in an increased lag time, but the steady state flux was not affected. The lag time increased linearly with increasing HS concentration. Therefore, an underestimation of the total HS concentration would lead to an underestimation of the lag time by the model.

The effective diffusivity of bFGF in Descemet's membrane was measured to be 6 ± 1 $x10^{-9}$ cm^2/sec. The effect of this error on the simulations is demonstrated in Figure 9.6. The steady state flux increased linearly with increased effective diffusivity in accordance with Fick's law. The lag time decreased linearly with increasing effective diffusivity.

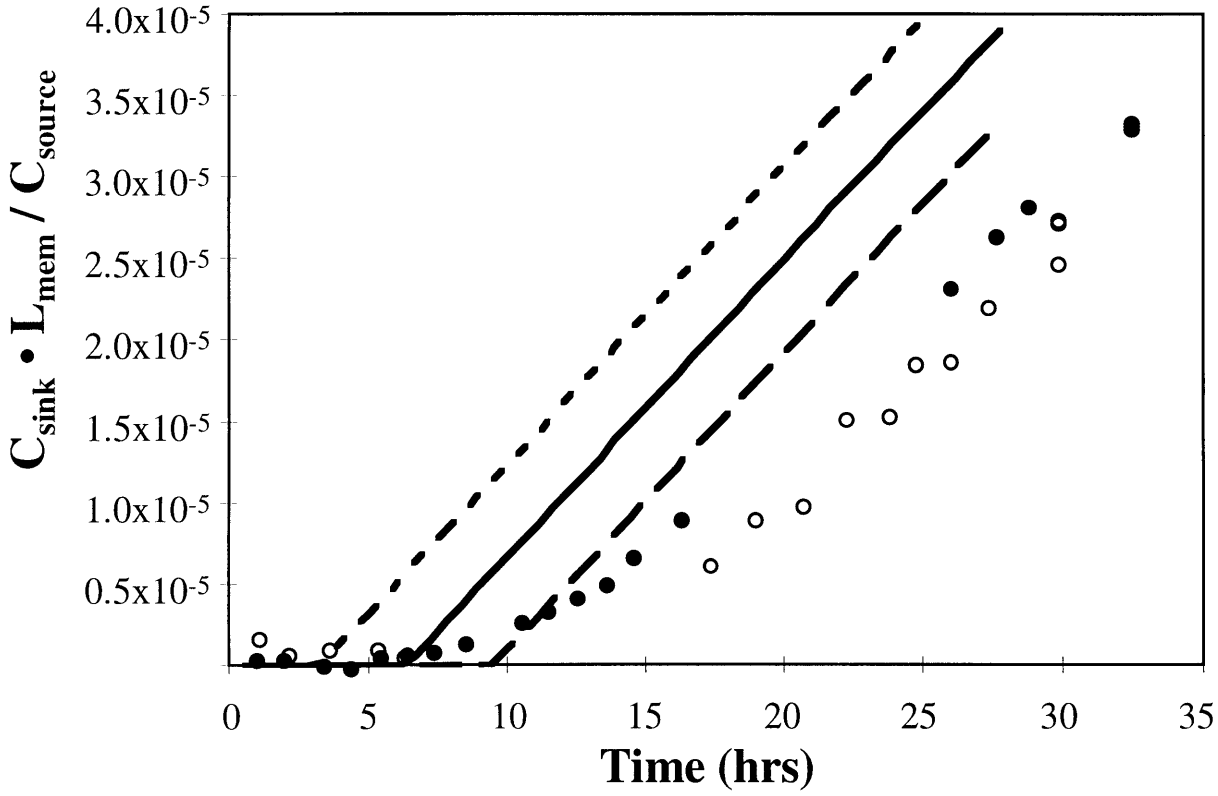

Figure 9.5 Simulation of Effect of DM HS Concentration Variation: The diffusion/binding model was used to simulate the error range for HS binding sites in the membrane. The base case of 26 μM (——) is compared to a minimum concentration of 13 μM (- - -), a maximum concentration of 39 μM (— —), and experimental data from a codiffusion experiment with ^{125}I-bFGF and excess unlabeled bFGF (o●). The sink concentration of bFGF was normalized for experimental variations in membrane thickness and source concentration.

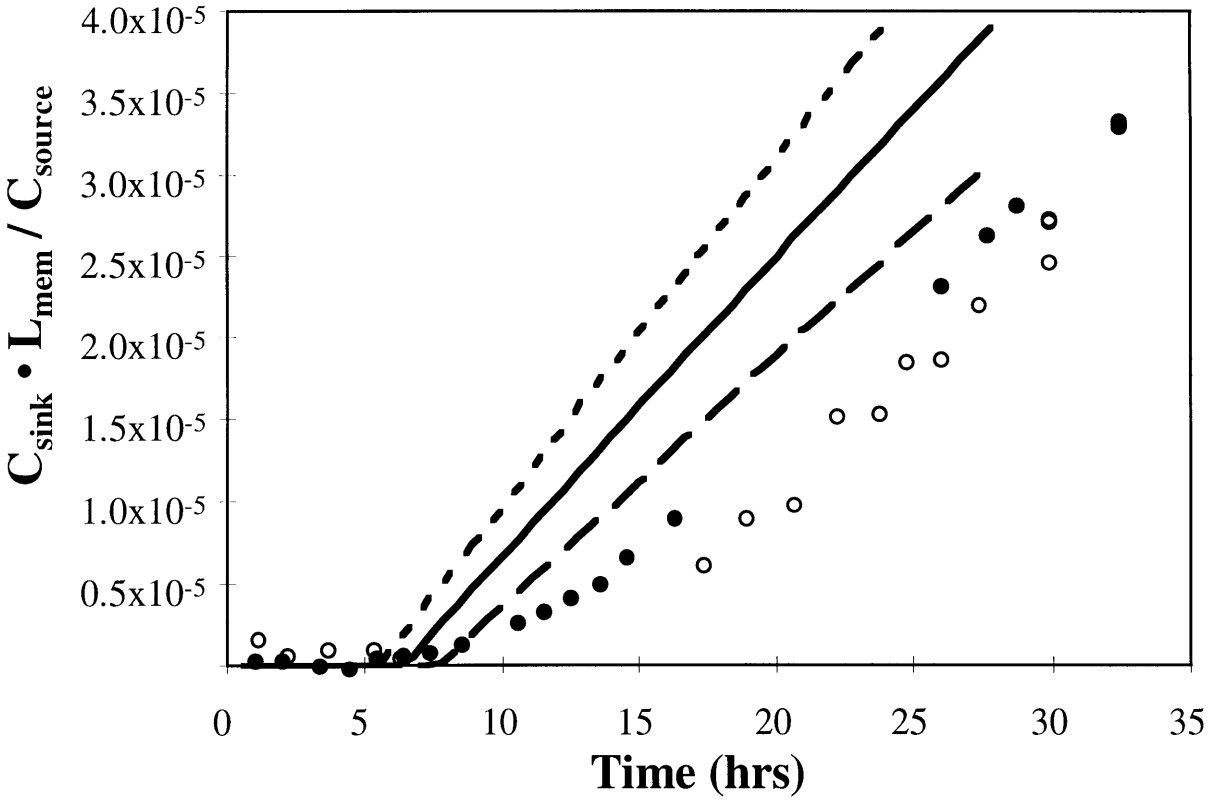

Figure 9.6 Simulation of Effect of Effective Diffusivity Variation: The diffusion/binding model was used to simulate the error range for the effective diffusivity of bFGF in the membrane. The base case of $6x10^{-9}$ cm^2/s (——) is compared to a minimum diffusivity of $5x10^{-9}$ cm^2/s (- - -), a maximum diffusivity of $7x10^{-9}$ cm^2/s (— —), and experimental data from a codiffusion experiment with ^{125}I-bFGF and excess unlabeled bFGF (o●). The sink concentration of bFGF was normalized for experimental variations in membrane thickness and source concentration.

9.4.4 Cumulative Effect of Error

Up to this point, the model has been used to assess the impact of the error associated with individual parameters on the overall results. In order to determine the maximum range of possible simulation results, multiple model parameters were adjusted simultaneously. Since variations in the three parameters described above (length, HS sites, and effective diffusivity) appeared to have the greatest impact on the lag time, parameter sets were selected to generate the maximum and minimum lag times possible. The results of these simulations are presented in Figure 9.7 along with the base case and the actual data. The total error in the lag time ranged from 3 to 16 hours. The experimental data fell within this error range toward the extreme of longer lag times. These results suggest that the concentration of HS sites in the membrane may be closer to the upper estimate of 39 μM, and that the effective diffusivity may be closer to the lower estimate of 5×10^{-9} cm^2/s. We conclude that the model can accurately represent the processes governing bFGF transport through the DM, and, with slightly more precise parameters, could match the experimental data very closely. The model can now be used to gain valuable insight into the movement and distribution of growth factors in complex *in vivo* situations.

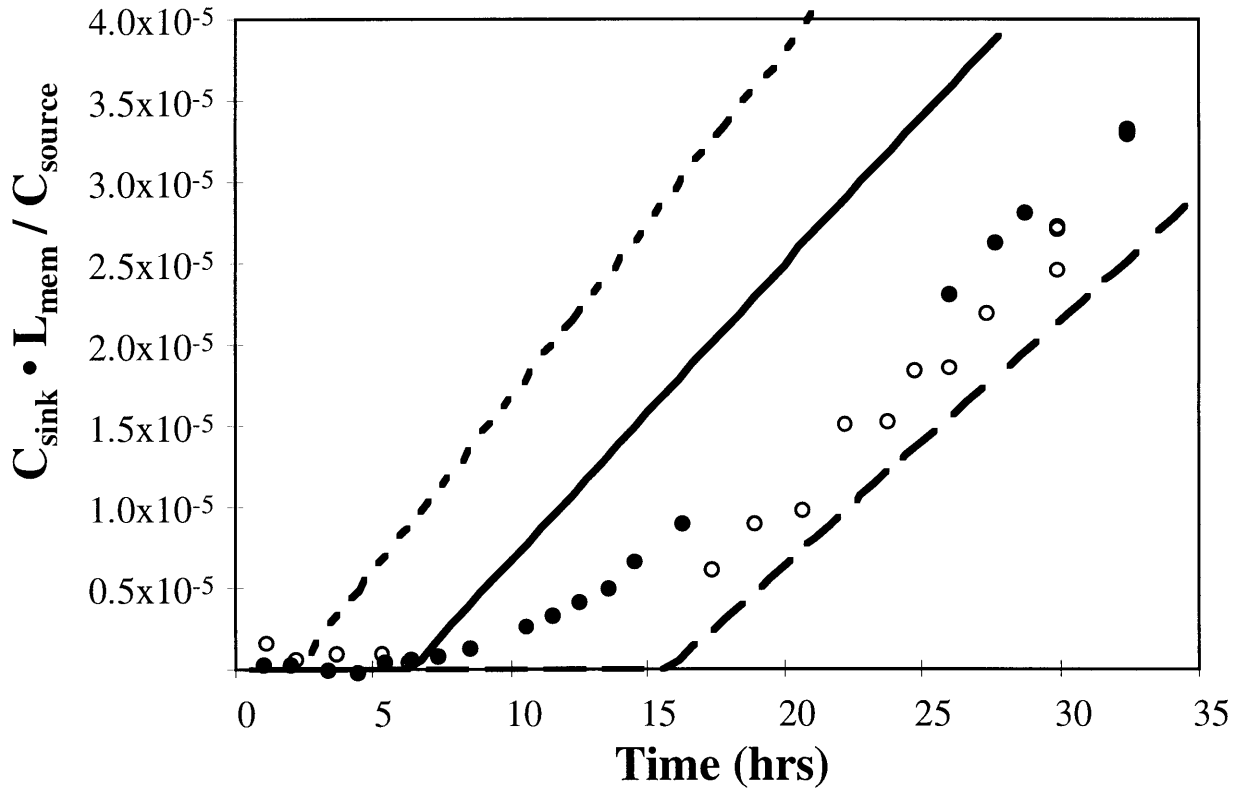

Figure 9.7 Simulation of Cumulative Effect of Experimental Error: The diffusion/binding model was used to simulate the cumulative error range for variations in membrane thickness, HS binding istes, and effective diffusivity. The base case (——) is compared to a lower bound (– – –), an upper bound (— —), and experimental data from a codiffusion experiment with ^{125}I-bFGF and excess unlabled bFGF (o ●). The sink concentration of bFGF was normalized for experimental variations in membrane thickness and source concentration.

9.5 Potential *in vivo* Implications

Most basement membranes are much thinner than Descemet's membrane and are typically 50 to 100 μm thick. On this length scale, diffusion and binding events will occur on similar time scales. Consequently, a 100 nm thick basement membrane would be expected to behave very differently than a 50 μm thick Descemet's membrane with regard to its ability to act as a bFGF reservoir. In order to determine the implications of our diffusion/binding model for bFGF storage and release from thin basement membranes, several simulations were conducted employing the model parameters determined for Descemet's membrane. However, in this case, a 100 nm thick membrane was initially saturated with bFGF. In the simulation, this membrane is exposed to infinite sinks on both faces, and the loss of bFGF from the membrane was tracked over time. Figure 9.8 presents the results for this study. The concentration of bFGF along the centerline of the membrane is plotted as a function of time. After 10 minutes virtually all the bFGF has been lost from the membrane.

This simulation was an extreme example. In an organism, the basement membrane is likely bound on one surface by a tightly connected cell layer, and on the other face by connective tissue. The connective tissue is another form of ECM and may have lower concentrations of heparan sulfate in its as well. Consequently, bFGF loss from a basement membrane will be, to some extent, determined by the local environment of the membrane. One conclusion that can be drawn from the simulation is that basement membranes provide dynamic reservoirs for bFGF. While in the basement membrane, the bFGF is protected from protease activity and generally stabilized by its interaction with heparan sulfate. However, changes in the environment of the basement membrane, such as physical damage, could result in rapid release of bFGF.

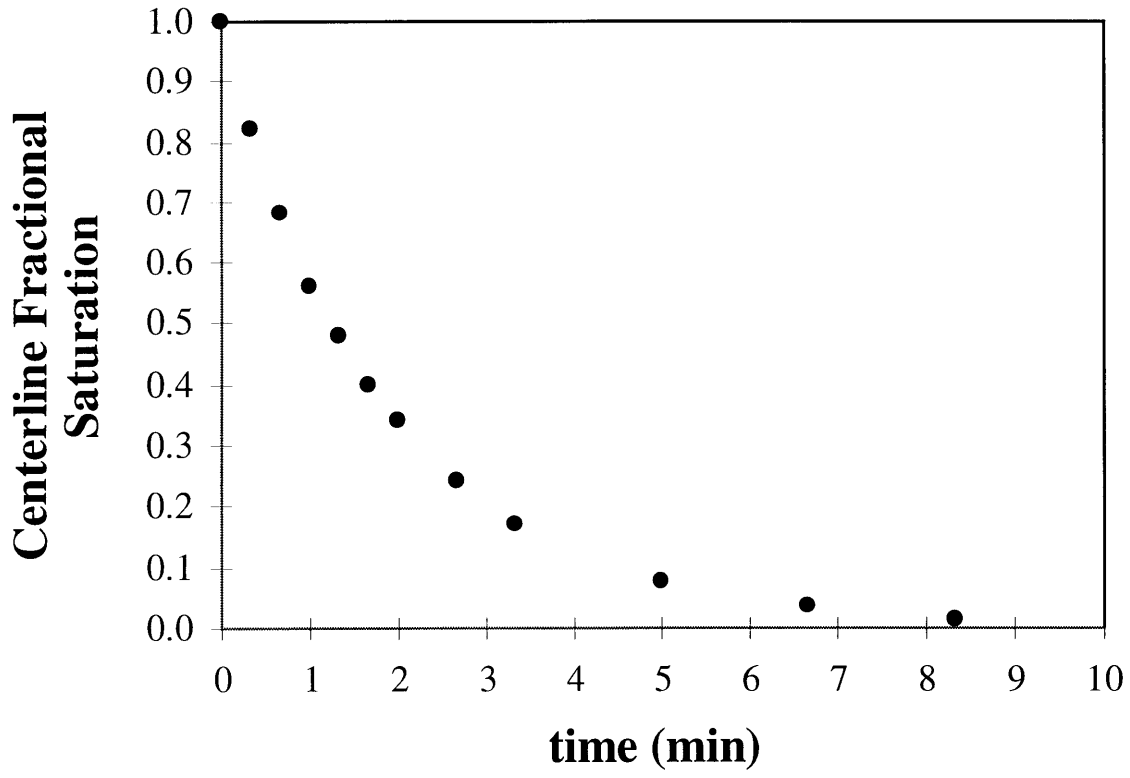

Figure 9.8 bFGF Loss from 100 nm Thick Membrane: The diffusion/binding model was used to simulate the loss of bFGF from a saturated membrane 100 nm thick exposed to infinite sinks on both faces.

HSPGs have been identified in developing embryos, and have been implicated in a variety of developmental processes. Gradients of growth factors have been postulated to have roles in controlling development. However, given the small length scales involved during the early, critical steps in development, gradients of growth factors would be difficult to maintain. HSPGs could potentially facilitate more stable gradients through the interaction of their HS chains with growth factors. To investigate these possibilities, we approached this problem by simulating a 100 μm thick plane of ECM with a pulse of high growth factor concentration introduced along its center line. Again, using the parameters obtained from Descemet's membrane, the dissipation of this pulse of growth factor was compared for matrices with and without binding sites for the growth factor with infinite sinks on both faces of the matrix. Figure 9.9 illustrates the dramatic differences in these two scenarios. The total concentration of growth factor throughout the membrane at 5 different time points is compared for matrices with and without HS. For comparative purposes, similar profiles were selected for each case. However, while the difference between time points in the simulation where HS was present is 24 hours, the difference in the simulation where HS was absent was only 15 seconds. Clearly, HS sites in the matrix could function to sustain a growth factor gradient within a developing embryo for an extended period of time. Furthermore, local variations in HS concentration could act to create a very complex and highly controlled distribution of growth factor concentration throughout developing and adult organisms.

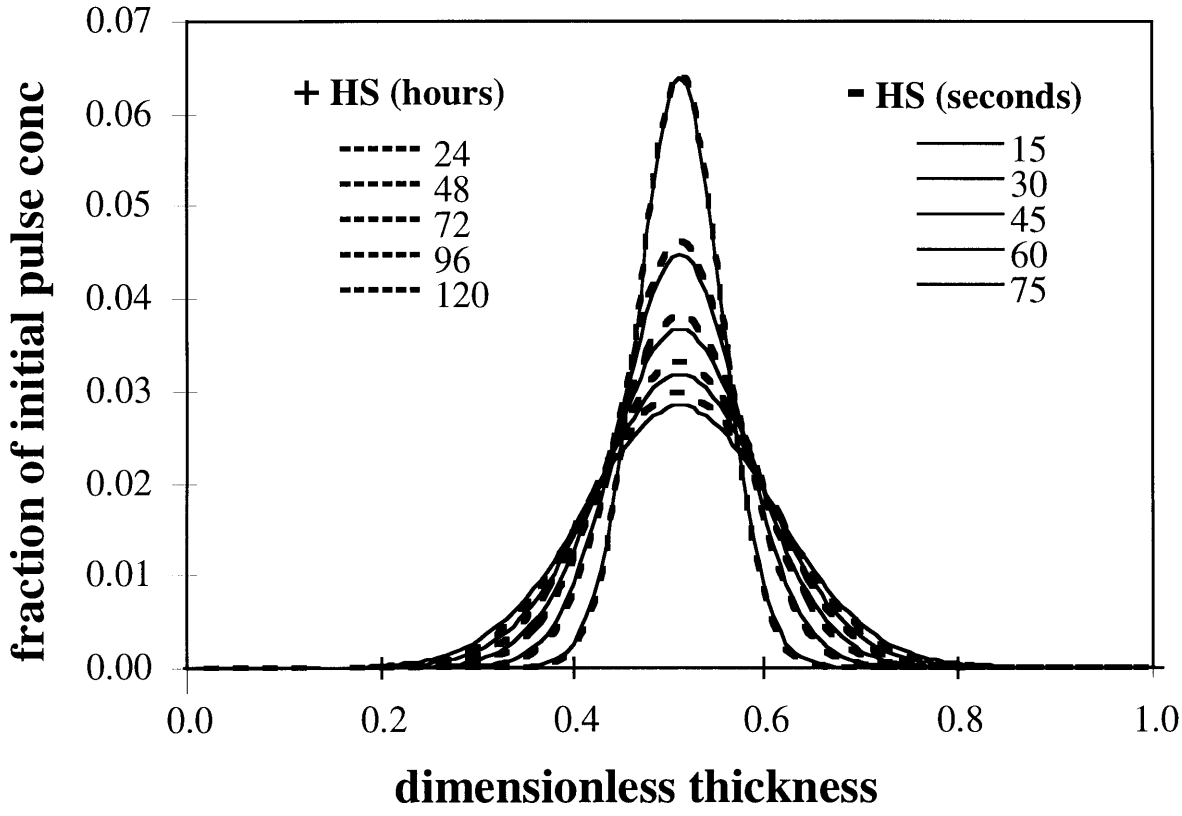

Figure 9.9 bFGF Pulse Decay in Membranes with and without HS: The decay of a thin concentration pulse (26 μM) introduced at the membrane centerline at time 0 is tracked for matrices with and without 26 μM HS sites. The dashed lines represent matrix with HS and each profile is separated from the next by 24 hours. The solid lines represent matrix without HS and each profile is separated by 15 sec.

9.6 Conclusions

The diffusion/binding model for bFGF transport through Descemet's membrane is a simplification of a complex biological process. However, our data suggest that this simplification can fairly and accurately capture the complex process of growth factor movement through a biological tissue. Diffusion of bFGF through the interstices of the composite protein/glycosaminoglycan matrix in the DM was represented by an effective diffusivity term. This approach is an accepted means of describing transport through fibrous matrices, and the results of experiments with IL1β and bFGF were consistent with this formalism. Heparan sulfate is a heterogeneous macromolecule with regard to both its size and the extent to which it's disaccharide units have been modified. bFGF does not bind to an exact sequence in HS, but, rather, to a family of sequences with similar modifications. Consequently, the bFGF/HS interaction should be characterized by a family of similar equilibrium binding constants. However, the association is typically represented with a single binding constant. This strategy provides excellent fits to bFGF/HS binding isotherms, and can be seen with our binding constant analysis (Figure 5.9).

The model was a homogeneous representation of a heterogeneous system. Local variations in bFGF concentrations were averaged out. The concentration of HS throughout the membrane was assumed to be constant. Immunostaining results suggested that a gradient might exist in the membrane, but those results were contradictory [35], [14]. Furthermore, our analysis of HS concentrations in Descemet's membrane was based on a large scale extraction of HS from membranes of 50 different individuals. It is likely that some variation in HS concentration existed from one individual cow to another. All the HS in the membrane was assumed to be accessible to the bFGF. In reality, some of the HS sites are probably occupied through interactions with other matrix components or prevented from interacting with bFGF due to steric considerations. However, the assumption of high accessibility was the logical starting point from a modeling point of view, and the modeling results imply that it was valid. Our objective in modeling this system was to capture the

essential physical and chemical mechanisms of the process. In so doing, a certain amount of error was undoubtedly introduced into the results, yet, in spite of this, we were able to generate a fairly accurate picture of the process.

The largest sources of experimental error in the parameters used in the model were in the measurements of the concentration of HS sites in the membrane, the membrane thickness, and the effective diffusivity of bFGF in the membrane. Actual Descemet's membranes vary in thickness, but the model assumed a membrane of constant thickness. As a result, the model predicted an abrupt transition to steady state flux, while a smoother transition was observed in the experiments. The experimental results were within error bounds predicted by the model. Given the simplicity of the model, the complexity of the system, and the difficulty in obtaining accurate estimates of certain parameters, the model did a good job of predicting the experimental results. Because the model is based on first principles, it can provide insight into the potential role of basement membranes, and other ECMs in general, as regulators of the *in vivo* activity of bFGF and other heparin binding growth factors.

Two sets of simulations were presented for bFGF transport through the extracellular matrix using the binding/diffusion model and parameters obtained from the Descemet's membrane system. Our model of a 100 nm thick basement membrane suggested that bFGF in these thin membranes can be rapidly released without the action of proteases to disrupt the membrane. However, the binding of bFGF to HS sites cannot, by itself, produce a long term storage site for bFGF. While the possibility exists that other components in the matrix can bind bFGF other than heparan sulfate, our results with Descemet's membrane did not support this contention. bFGF cell surface-like receptors have been identified in basement membranes, and it is conceivable that they are absent from the DM but present in other basement membranes. It is clear that the traditional static concept of bFGF storage in basement membranes must be rethought in light of our results.

As the thickness of the modeled ECM was increased, the time scales for diffusion dropped significantly. We found that in a 100 μm thick membrane, a pulse of bFGF introduced along the membranes centerline would take on the order of weeks to dissipate with HS in the matrix. Without the presence of HS, the pulse would dissipate in a matter of hours. Growth factor gradients could be fine tuned in a developing embryo through control over the concentration and fine structure of HS chains in the matrix. Steep gradients of growth factor could be maintained over small distances for long periods of time through the controlled manipulation of growth factor / HS interactions.

Chapter 10

Conclusions

10.1 Summary

The extracellular matrix was long viewed as the inert ground substance that cells in a tissue were imbedded in. Cells are the fundamental building blocks of an organism, and the ECM was thought to be merely the mortar that held them together. This simplistic picture of the ECM/cell relationship has given way to the realization that ECMs are highly complex structures in their own right [15]. Cells can remodel the ECM by selectively degrading and replacing its constituent macromolecules, but the ECM can also dramatically influence cell growth and development The matrix can directly signal the cell through specific cell matrix contacts. Furthermore, all molecular traffic to and from a cell must pass through and be regulated by the ECM. Thus, the focus of this work was the ability of the ECM to modulate or control the access of soluble, growth factor signals that a cell receives through its surface receptors.

Evidence from various aspects of this project suggested that Descemet's membrane is composed of a very tight protein/glycosaminoglycan network. Our initial efforts at extracting the HSPG from Descemet's membrane using harsh denaturing conditions were unsuccessful. The HSPG is a very large macromolecule with a core protein of 400 kD and an average of three highly hydrated 40 kD HS side chains. Our subsequent studies with high molecular weight FITC dextrans further reinforced the picture of the DM as a very

tight matrix. FITC Dextrans with Stokes radii larger than approximately 30 Å were greatly retarded in their ability to cross the isolated DM in diffusion studies.

Hydraulic permeability measurements reflect the effective pore size of a matrix and can be used to estimate effective diffusivities in such a matrix. The diffusivities measured for IL1β and bFGF, independent of HS binding through this DM mesh, were approximately $6x10^{-9}$ cm^2/sec. Using the effective medium approach of Phillips et al. [98] and estimates of hydraulic permeability data from Fatt [144], the D_{eff}/D° ratio was calculated to be approximately 10% as compared to an experimentally determined value of 0.4%. Although Fatt's estimates of DM hydraulic permeability may contain error, the large discrepancy between the model and the data suggests that these types of models may not be suitable for describing diffusion through a multi-component membrane such as DM.

Descemet's membrane's high resistance to larger macromolecules such as proteins and high molecular weight dextrans implies that one of its biological roles may be to control molecular traffic between the endothelium and the corneal stroma. Experimental measurement of the hydraulic permeability of the corneal stroma suggests that it may have a slightly more open structure than Descemet's membrane [148]. While the DM's basic structure is based on the mesh-like basement membrane collagens, the corneal stroma's structure is dominated by highly ordered arrays of fibrillar stroma. Consequently, molecules that pass through the stroma relatively unhindered may not be able to penetrate the DM to reach the endothelium. Furthermore, transport of substances from the aqueous humor posterior to the endothelium into the cornea is accomplished, in part, via vesicular trafficking through the endothelial cells [149] and through gaps in the tight junctions between endothelial cells [150]. The DM may serve as a selective barrier to prevent entrance of large molecular weight molecules into the stroma. In particular, bFGF is found in the aqueous humor at concentrations of approximately 50 pM [151] and is a potent stimulator of blood vessel growth. Corneal transparency is essential to normal vision, and, consequently, the cornea is completely devoid of blood vessels. The DM/bFGF storage

system may be part of the control strategy for maintaining the cornea in an avascular state by preventing aqueous humor bFGF from reaching the corneal stroma under non-pathogenic conditions.

The diffusion binding model for bFGF transport through extracellular matrix captured the essential elements of the experimental process over the timescale of our study. The implications of this model for the storage mechanism of bFGF in basement membranes is very intriguing. Prior to this study, the generally held view was that HS within basement membranes bound bFGF tightly, and that release could only be accomplished through the activity of proteolytic enzymes or GAG lyases. Our results suggest that basement membranes provide a much more dynamic storage mechanism for bFGF. Damage to neighboring basement membranes or removal of bordering transport barriers, could quickly release bFGF to participate in tissue repair processes. Alteration in cell surface receptor concentrations or in the nature of the HSPG expressed on the surface of neighboring cells could act to draw bFGF out of its reservoir in the matrix. Our experimental evidence suggests that bFGF readily denatures and adsorbs to different surfaces. *In vivo*, the HS chains of the basement membrane probably stabilize the bFGF, and protect it from proteolytic attack. Further, the requirement of bFGF to bind HS for stability might provide an additional level of control over the temporal and spatial distribution of active bFGF.

Our results also have implications in the field of developmental biology. During development, cell differentiation must be spatially and temporally regulated. Gradients of soluble morphogens have long been postulated as key determinants of this process [152, 153]. bFGF has been implicated in the development of chick limb bud [106]. More recently, strong evidence has emerged that the Drosophila protein wingless guides differentiation through gradients [154]. Furthermore, wingless binds heparin, and experimental evidence suggests that extracellular matrix HSPG plays a role in the activity of this morphogen [155]. Length scales in the developing Drosophila are on the order of

microns. However, gradients may need to be maintained for many hours to have the desired effect. High concentrations of HS in the matrix could sustain a wingless gradient that would otherwise rapidly dissipate given the small length scales applicable in the developing embryo. By modulating HS concentration and structure, the stability of growth factor morphogen gradients in embryonic extracellular matrix could be finely tuned. The diffusion binding model for growth factor transport through extracellular matrix should have a broad applicability to a large number of soluble proteins that can reversibly associate with specific membrane components. The development of complex organisms consisting of billions of differentiated cells from a single embryonic cell is an enormously complex process, and mathematical models of morphogen/ECM interactions will be valuable tools in understanding how this patterning takes place.

Extracellular matrices are critical components in all multicellular organisms. Understanding the roles of ECMs in controlling extracellular signaling is an essential step toward understanding aspects of development, tissue repair, and tumor pathogenesis. Furthermore, future advances in rational protein design will result in large molecular weight protein based drugs. A quantitative understanding of the role of ECMs in regulating the availability of certain proteins to a target cell population can be used to better design these pharmaceuticals of the future.

10.2 Recommended Future Work

A tremendous amount of work remains to be done in the area of understanding ECM regulation of growth factors. However, this study has laid the groundwork for future work with the DM model system. This experimental system can be used to study bFGF transport processes at a more fundamental and quantitative level than was previously possible, and the mathematical representation of the system can provide a running model that can be used to test possibilities that are not amenable to direct experimental observation.

Future studies should develop alternative approaches to better quantify the HS content of the DM, since this is a significant source of error in our study. Complementary approaches to measuring transport in the membrane would also help provide additional insight into the relevant transport processes. FRAP (fluorescent recovery after photobleaching) might present an interesting approach to studying this system in parallel. Although the potentially very slow diffusion of bFGF could limit the use of this approach. This study does not rule out the possibility that bFGF might associate very tightly or irreversibly to a specific population of sites in the DM. This possibility should be explored in greater depth and its significance to the diffusion/binding model should be evaluated. The role of soluble GAGs as mediators of diffusion of bFGF has not been touched on in this work, but it does present an alternative means for rapid movement of bFGF through a matrix with many potential binding sites. Depending on the sizes, concentrations, and bFGF affinities of these fragments, they could potentially act to hinder or facilitate passage of bFGF across the DM.

Ultimately, the DM is a very complicated model system, subject to variabilities beyond our control. This fact still provides a strong impetus for exploring artificial basement membrane systems as a more controlled environment for transport studies. Our work with the electron beam as a means to crosslink heparin into polyacrylamide can serve as a good starting point for these studies. However, a large number of experimental

parameters must be rigorously optimized to reproducibly synthesize heparin containing gels that are homogeneous and capable of binding bFGF with no loss of affinity. While this work was beyond the scope of the current study, ultimately it holds promise for developing well-defined HS-linked hydrogels.

10.3 Final Conclusions

- Descemet's membrane's structure is based on a tight proteoglycan/protein meshwork that physically entraps its larger macromolecular components, effectively blocks the passage of molecules with stokes radius greater than approximately 30 Å, and significantly reduces the diffusivity of smaller macromolecules like bFGF and IL1β.

- Descemet's membrane presents a powerful experimental tool for studying extracellular matrix transport of heparin binding growth factors in a milieu little altered from the *in vivo* case.

- A model of bFGF diffusion with fast reversible binding to matrix HS chains captures the essential principles of bFGF transport across extracellular matrices.

- Heparan sulfate chains in thin (50 -100 nM) basement membranes provide a dynamic reservoir of bFGF, making this ECM very responsive to changes in the local tissue environment that might demand rapid growth factor release or uptake.

- Heparan sulfate containing matrices, such as those that could be found in a developing embryo, could effectively maintain steep growth factor gradients over relatively long periods of time, and the dissipation rate of such gradients could be finely tuned through modulation of the concentration and structure of the matrix heparan sulfate chains.

Appendix A

Diffusion/Binding FORTRAN Code

```
      PROGRAM DiffRxn
c
c     This is a semi-implicit finite difference code for solving the general
c     diffusion/binding problem.  A band solver is used to take advantage of the
c     sparse nature of the matrix.  Because the equations were nondimensionalized
c          with respect to time using a l^2/D term, the code was run with double precision
c          to avoid round-off errors.

      INTEGER n, np, t, tsteps, tin, din, step
      INTEGER indx(mmax)

      double precision kon, koff, Htot, part, Diff
      double precision vol, area
      double precision Bom, Bo, Bot
      double precision len, dx, dt, tfinal, delt
      double precision amat(mmax,mmax)
      double precision b(mmax), bop(mmax)
      double precision c(mmax)
      double precision space(200)
      double precision carr(10,200),barr(10,200)
      double precision d
      double precision Con, Coff, Bon, Boff, Vnum, dtfin
      double precision cmat(mmax,3),dmat(mmax,3)

      CALL READATA (kon, koff, Htot, part, Diff, vol, area,
     &            Bom, Bo, len, dx, dt, tfinal, n, tsteps,
     &            tin, din, mmax, Con, Coff, Bon, Boff,
     &           Vnum,dtfin, Bot,step,delt)

      CALL MATGEN (cmat, amat, n, dx,dt,mmax,Vnum)
      np=mmax
      call bcinitial (n, b, c,mmax,part)
      open (unit=7, file='difinal')
      call header (kon, koff, Htot, part, Diff, vol, area,
     &          len, n, tfinal, tsteps,Bo)
      do 4 t=2,tsteps
        call newmat (cmat,dmat,mmax,n)
```

```
      call bopvect (n, bop, b, c, dt, t,mmax,Bon, Boff)
      call band (dmat, bop, n, mmax)
      call newc (n, t, b, c, dt, mmax, Con, Coff)
      call newb (n, t, bop, b, Bom,Bo, mmax,dt, Bot,part)
      call store (n,b,c,mmax,t,tin,din,carr,barr,dx,space,
     &            step,delt,Htot,Bo,part)
4     continue
      call output(n,tfinal,barr,carr,len,dx,dt,din,tin,space)
      STOP
      END

      SUBROUTINE readata (kon, koff, Htot, part, Diff, vol, area,
     &     Bom, Bo, len, dx, dt, tfinal, n, tsteps,tin, din, mmax,
     &     Con, Coff, Bon, Boff,Vnum,dtfin, Bot,step,delt)

C     Reads paramater values from "difdat" file
      INTEGER n, tsteps, tin, din,step
      double precision kon, koff, Htot, part, Diff
      double precision vol, area
      double precision Bom, Bo, Bom1, Bot1, Bot
      double precision len, dx, dt, tfinal, dtfin, delt
      double precision Con, Coff, Bon, Boff,Vnum

      OPEN(UNIT=10, FILE='difdat')
      READ(10,*) kon, koff, Htot, part, Diff
      READ(10,*) vol, area
      READ(10,*) Bom1, Bo, Bot1
      READ(10,*) tsteps,tfinal
      READ(10,*) n, len
      dtfin=tfinal*Diff/len**2.0
      tin=int(tsteps/5)
      din=int(n/200)
      step=int(tsteps/50)
      delt=tfinal/tsteps

C     Calculate dimensionless groups

      Con=kon*len**2.0*Bo*part/Diff
      Coff=koff*len**2.0/Diff
      Bon=kon*Htot*len**2.0/Diff
      Boff=len**2.0*koff*Htot/(Diff*Bo*part)
      Vnum=(area*len*part)/(vol)
      dx=1.0/(n-1)
      dt=dtfin/tsteps
      Bom=Bom1/Bo
      Bot=Bot1*Diff/len**2
      RETURN
      END


      SUBROUTINE MATGEN (cmat, amat, n, dx,dt,mmax,Vnum)

C     generates the matrix that will be subsequently inverted
C     (I-dtA)
```

```
      INTEGER i,j,n
      double precision dx,dt,Vnum
      double precision amat(mmax,mmax)
      double precision cmat(mmax,3)


C     Initialize Matrix to 0
      DO 20 i=1,n
        DO 10 j=1,n
          amat(i,j)=0
10      CONTINUE
20    CONTINUE

C     Generate diagaonal band
      DO 30 i=2,(n-1)
        amat(i,i-1)= 1.0/dx**2
        amat(i,i)  = -2.0/dx**2
        amat(i,i+1)= 1.0/dx**2
30    CONTINUE

C     Include flux boundary conditions
      amat(n,n-1)=Vnum/dx
      amat(n,n)=-Vnum/dx

C     subtract (delta t)*A from identity matrix
      DO 50 i=1,n
        DO 40 j=1,n
          IF (i.EQ.j) then
            amat(i,j)=1.0-dt*amat(i,j)
          ELSE
            amat(i,j)=-dt*amat(i,j)
          ENDIF
40      CONTINUE
50    CONTINUE

c     compress A matrix to band C matrix (3 x n)

      cmat(1,1)=0.0
      cmat(1,2)=amat(1,1)
      cmat(1,3)=amat(1,2)
      do 55 i=2,n-1
        cmat(i,1)=amat(i,i-1)
        cmat(i,2)=amat(i,i)
        cmat(i,3)=amat(i,i+1)
 55   continue
      cmat(n,1)=amat(n,n-1)
      cmat(n,2)=amat(n,n)
      cmat(n,3)=0.0
      RETURN
      END

      subroutine header(kon, koff, Htot, part, Diff, vol, area,
     &           len, n, tfinal, tsteps,Bo)
```

```
c         puts the input data at the beginning of the output file
c
      double precision kon, koff, Htot, part, Diff, vol, area
      integer n, tsteps
      double precision Bo, len, tfinal

       write(7,*) 'kon=',kon,' koff=',koff
       write(7,*) 'Kpart=',part,' Diff=',Diff
       write(7,*) 'vol=',vol,' area=',area
       write(7,*) 'length=',len,' xstep=',n
       write(7,*) 'time=',tfinal,' tstep=',tsteps
       write(7,*) 'source=',Bo,' Htot=',Htot
      write(7,*)
       write(7,*) 'time(sec) ','b(M) ','c(M)'
      return
      end

      SUBROUTINE bcinitial(n, b, c,mmax, part)
C     initializes the b vector

      INTEGER i, n
      double precision b(mmax), c(mmax), part

      c(1)=0.0
      b(1)=1.0
      do 60 i=2,n
        b(i)=0.0
        c(i)=0.0
60    continue
      return
      END

      subroutine newmat (cmat,dmat,mmax,n)
c     refreshes the cmat matrix for the next band sub

      integer i,j,n
      double precision cmat(mmax,3),dmat(mmax,3)

      do 62 i=1,n
        do 63 j=1,3
          dmat(i,j)=cmat(i,j)
63      continue
62    continue
      return
      end

      SUBROUTINE bopvect(n,bop,b,c,dt,t,mmax,Bon, Boff)
C     uses the currect b vector to produce the b operator vector

      INTEGER i,n,t
      double precision bop(mmax),b(mmax),c(mmax)
      double precision dt
      double precision Bon, Boff
```

```
      bop(1)=b(1)
      do 70 i=2,n-1
        bop(i)=b(i)+Bon*b(i)*c(i)*dt+Boff*c(i)*dt
     &         -Bon*b(i)*dt
70    continue
      bop(n)=b(n)
      return
      END

      subroutine band (cmat, v, nod, mmax)\


      double precision cmat(mmax,3), v(mmax), det
      integer nod, nvarg, iband
      double precision eps, p, piv, pivmax, pivmag, t, theta
      integer mc, nc, nv, icount, nc1, lr, mr, ii, ir
      integer jj, jr, jc, k, ic, ipiv, kr, iv, lc, nr
      integer i

      iband=3
      nvarg=1

      mc=nod
      nc=iband
      nv=nvarg
c       do 135 i=1,nod
c         print *, i,cmat(i,1),cmat(i,2),cmat(i,3)
c 135   continue

c
c     ***** initialize det  *****
c
      eps=1.0e-15
      icount=0
      det=1.0
c
c         *** prepare the matrix c for processing by shifting undefined   ***
c         *** elements out of the upper-left-hand corner and inserting    ***
c         *** zeros in the lower right-hand-corner                        ***
c
      nc1=nc+1
      lr=nc1/2
      mr=lr-1
      ii=mc+1
      do 133 ir=1,mr
        ii=ii-1
        nr=lr-ir
        jj=nc1
        do 132 jr=1,nr
          do 131 jc=2,nc
            p=cmat(ir,jc)
            k=jc-1
            cmat(ir,k)=p
```

```
 131      continue
          cmat(ir,nc)=0.0
          jj=jj-1
          cmat(ii,jj)=0.0
 132    continue
 133  continue

c      do 136 i=1,nod
c        print *, i,cmat(i,1),cmat(i,2),cmat(i,3)
c 136   continue

c
c        *** use row operations to eleminate the lower triangular part of a ***
c        *** apply these same operations to the right-hand-sides          ***
c
     do 400 ic=1,mc
        ipiv=ic
        piv=cmat(ic,1)
        pivmax=abs(piv)
        kr=ic+1
        if(kr.gt.lr)go to 140
c
c        ***** find the largest possible pivot in the current column.
c
        do 134    ir=kr,lr
          pivmag=abs(cmat(ir,1))
          if(pivmax.ge.pivmag)go to 134
          ipiv=ir
          pivmax=pivmag
 134    continue
        piv=cmat(ipiv,1)
c
c        ***** check the pivot magnitude *******
c
 140    continue
        if(pivmax.ge.eps)go to 150
c
c        **** a nonzero pivot smaller than eps has been found ****
c
        write(6,*) ' zero pivot ', piv
        return
c
c        **** if necessary , swap row ipiv with row ic ****
c
 150    continue
        if(ipiv.eq.ic)go to 200
        det=-det
        do 160 jc=1,nc
          t=cmat(ic,jc)
          cmat(ic,jc)=cmat(ipiv,jc)
          cmat(ipiv,jc)=t
 160    continue
        t=v(ic)
        v(ic)=v(ipiv)
```

```
      v(ipiv)=t
c
c        ***** update the determinant value *****
c
 200    continue
      if(abs(det).ge.1.0e+25)icount=icount+1
      if(abs(det).ge.1.0e+25)det=det/abs(det)
      det=det*piv
c
c        ***** normalize the pivot row *****
c
      theta=1./piv
      do 220 jc=2,nc
        cmat(ic,jc)=cmat(ic,jc)*theta
 220    continue
      v(ic)=v(ic)*theta
c
c        *** eliminate the lower triangular elements in the current column ***
c
      if(kr.gt.lr)go to 400
      do 380 ir=kr,lr
        t=cmat(ir,1)
        do 230 jc=2,nc
          k=jc-1
          cmat(ir,k)=cmat(ir,jc)-t*cmat(ic,jc)
 230      continue
        cmat(ir,nc)=0.0
        v(ir)=v(ir)-t*v(ic)
 380    continue
      if(lr.eq.mc)go to 400
      lr=lr+1
 400  continue
c
c        ***** triangularization is complete *****
c
c
c        ***** back-substitute to compute the solution vector(s) ******
c
     kr=2
     lc=mc-1
     do 480 ic=1,lc
       iv=mc-ic
       ii=iv
       do 440 jc=2,kr
        ii=ii+1
        v(iv)=v(iv)-cmat(iv,jc)*v(ii)
 440    continue
       if(kr.eq.nc) go to 480
       kr=kr+1
 480  continue
c
c        ****** the matrix equation is solved ******
c
     return
```

```
      end

      SUBROUTINE newb(n, t, bop, b, Bom, Bo, mmax, dt, Bot,
     &              part)

      INTEGER n, t, i
      double precision b(mmax), bop(mmax)
      double precision  Bo,  Bom, dt, Bot,part

      b(1)=1.0-Bom*((t*dt)/(Bot+(t*dt)))
      do 80 i=2,n
        b(i)=bop(i)
80    continue
      if (abs(b(2)).gt.1000000) then
         print *,t, '   KABOOM'
        stop
      endif
      return
      END


      SUBROUTINE  newc(n, t, b, c, dt, mmax,Con, Coff)

      INTEGER n, t, i
      double precision b(mmax), c(mmax)
      double precision dt,Con, Coff

      do 90 i=1,n
        c(i)=c(i)+dt*(Con*(b(i)-c(i)*b(i))-Coff*c(i))
90    continue
      return
      END

      SUBROUTINE store (n,b,c, mmax,t,tin,din,carr,barr,
     &              dx, space, step,delt,Htot,Bo,part)

c         Outputs the sink concentration to file "difinal", and stores internal
c         profile data

      INTEGER i, n,t,tin,din,tcount,ncount,step
      double precision b(mmax),c(mmax),carr(10,200),barr(10,200),
     &              space(200)
      double precision dx, delt,Htot,Bo,part

105   format(4e11.4)
      if (mod(t,step).eq.0) then
c        write(*,*) 'check ',t
        write(7,105) t*delt,Bo*b(n),Htot*c(n)
      endif
      if (mod(t,tin).eq.0) then
        tcount=int(t/tin)
c       write(*,*) tcount,din,tin
        do 110 i=1, n
c          write(*,*) i,n,din
```

```
c         ncount=int(i/din)
c         write(*,*) ncount
          space(i)=i*dx
          barr(tcount,i)=b(i)
          carr(tcount,i)=c(i)
110     continue
      endif
      return
      END

      SUBROUTINE output(n,tfinal,barr,carr,len,dx,dt,
     &                  din,tin,space)

c         Outputs internal complex and free profiles to "difresc" and "difresb" respectively

      integer tcount,ncount,n,tin,din
      double precision tfinal,dx,dt,len
      double precision carr(10,200),barr(10,200),space(200)

      open(unit=5, file='difresb')
      open(unit=6, file='difresc')
120   format(6e10.3)
      do 130 ncount=1,n
        write(5,120)  space(ncount),barr(1,ncount),barr(2,ncount),
     &              barr(3,ncount),barr(4,ncount),barr(5,ncount)
        write(6,120)  space(ncount),carr(1,ncount),carr(2,ncount),
     &              carr(3,ncount),carr(4,ncount),carr(5,ncount)
130   continue
      return
      end
```

Bibliography

1. Sporn, M. B. and A. B. Roberts. ed. 1991. The Multifunctional Nature of Peptide Growth Factors. 3-15. in Sporn and Roberts: Peptide Growth Factors and Their Receptors I. Springer-Verlag, New York.

2. Kefalides, N. A., R. Alper and C. C. Clark. ed. 1979. Biochemistry and Metabolism of Basement Membranes. 167-168. in Bourne and Danielli: International Review of Cytology. Academic Press, New York.

3. Yurchenco, P. D. and J. O'Rear. ed. 1993. Supramolecular Organization of Basement Membranes. 20-45. in Rohrbach and Timpl: Molecular and Cellular Aspects of Basement Membranes. Academic Press, Inc., San Diego.

4. Chan, F. L., S. Inoue and C. P. Leblond. 1993. Cryofixation of Basement Membranes Followed by Freeze Substitution or Freeze Drying Demonstrates that They are Composed of a Tridimensional Network of Irregular Cords. The Anatomical Record. **235**: 191-205.

5. Goldberg, M. and F. Escaig-Haye. 1986. Is the Lamina Lucida of the Basement Membrane a Fixation Artifact? European Journal of Cell Biology. **42**: 365-368.

6. Timpl, R., S. Fujiwara, M. Dziadek, M. Aumailley, S. Weber and J. Engel. ed. 1984. Laminin, Proteoglycan, Nidogen, and Collagen IV : Structural Models and Molecular Interactions. 25-43. in Porter and Whelan: Basement Membranes and Cell Movement. Pitman, London.

7. Yurchenco, P. D. ed. 1990. Assembly of Basement Membranes. 195-213. in Fleishmajer, Olsen and Kuhn: Structure, Molecular Biology and Pathology of Collagen. New York Academy of Sciences, New York.

8. Haskin, C. L., I. L. Cameron and D. H. Rohrbach. ed. 1993. Role of Water of Hydration in Filtration Function of Proteoglycans of Basement Membrane. 107-117. in Rohrbach and Timpl: Molecular and Cellular Aspects of Basement Membranes. Academic Press, Inc., San Diego.

9. Dohlman, C. and Balazs. 1955. Chemical Studies on Descemet's Membrane of the Bovine Cornea. Archives of Biochemistry and Biophysics. **57**: 445-457.

10. Labermeier, U., T. A. Demlow and M. C. Kenney. 1983. Identification of Collagesn Isolated from Bovine Descemet's Membrane. Experimental Eye Research. **37**: 225-237.

11. Kleppel, M. M., W. Fan, H. I. Cheong and A. F. Michael. 1992. Evidence for Separate Networks of Classical and Novel Basement Membrane in Collagen. Journal of Biological Chemistry. **267**: 4137-4142.

12. Sawada, H., H. Konomi and K. Hirosawa. 1990. Characterizatio of the Collagen in the Hexagonal Lattice of Descemet's Membrane: It s Relation to Type VIII Collagen. The Journal of Cell Biology. **110**: 219-227.

13. Kapoor, R., P. Bornstein and E. H. Sage. 1986. Type VIII Collagen from Bovine Descemet's Membrane: Structural Characterized of a Triple-Helical Domain. Biochemistry. **25**: 3930-3937.

14. Ljubimov, A. V., R. E. Burgeson, R. J. Butkowski, A. F. Michael, T. Sun and M. C. Kenney. 1995. Human Corneal Basement Membrane Heterogeneity: Topographical Differences in the Expression of Type IV Collagen and Laminin Isoforms. Laboratory Investigation. **72**: 461-473.

15. Sawada, H. 1982. The Fine Structure of the Bovine Descemet's Membrane with Special Reference to Biochemical Nature. Cell and Tissue Research. **226**: 241-255.

16. Madri, J. A., B. M. Pratt, P. D. Yurchenco and H. Furthmayr. ed. 1984. The Ultrastructural Organization and Architecture of Basement Membranes. 6-24. in Porter and Whelan: Basement Membranes and Cell Movement. Pitman, London.

17. Folkman, J., M. Klagsbrun, J. Sasse, M. Wadzinski, D. Ingber and I. Vlodavsky. 1988. A Heparin-Binding Angiogenic Protein-Basic Fibroblast Growth Factor-Is Stored Within Basement Membrane. American Journal of Pathology. **130**: 393-400.

18. Gallagher, J. T., M. Lyon and W. P. Steward. 1986. Structure and Function of Heparan Sulfate Proteoglycans. Biochemical Journal. **236**: 313-325.

19. Jackson, R. L., S. J. Busch and A. D. Cardin. 1991. Glycosaminoglycans: Molecular Properties, Protein Interactions, and Role in Physiological Processes. Physiological Reviews. **71**: 481-539.

20. Chakrabarti, B. and J. W. Park. 1980. Glycosaminoglycans: Structure and Interaction. CRC Critical Reviews in Biochemistry. **8**: 225-313.

21. Casu, B. 1991. Structural Features and Binding Properties of Chondroitin Sulfates, Dermatan Sulfate, and Heparan Sulfate. Seminars in Thrombosis and Hemostasis. **17**: 9-13.

22. Linhardt, R., H. Wang and S. Ampofo. 1992. New methodologies in heparin structure analysis and the generation of LMW heparins. Advances in Experimental Medicine and Biology. **23**: 53-80.

23. Kejellen, L. and U. Lindahl. 1991. Proteoglycans: Structures and Interactions. Annual Review of Biochemistry. **60**: 443-475.

24. Nader, H. B., C. P. Dietrich, V. Buonassisi and P. Colburn. 1987. Heparin Sequences in the Heparan Sulfate Chains of an Endothelial Cell Proteoglycan. Proceedings of the National Acadamey of Sciences USA. **84**: 3565-3569.

25. Gallagher, J. T. and A. Walker. 1985. Molecular Distinctions Between Heparan Sulfate and Heparin. Biochemical Journal. **230**: 665-674.

26. Ernst, S., R. Langer, C. Cooney and R. Sasisekharan. 1995. Enzymatic degradation of glycosaminoglycans. Critical Reviews in Biochemistry and Molecular Biology. **30**: 387-444.

27. Lindahl, U., M. Kusche, K. Lidholt and L. Oscarsson. ed. 1989. Biosynthesis of Heparin and Heparan Sulfate. 36-50. in Ofosu, Danishefsky and Hirsh: Heparin and Related Polysaccharides. New York Academy of Sciences, New York.

28. Gallagher, J. T., J. E. Turnbull and M. Lyon. 1992. Patterns of Sulfation in Heparan Sulfate: Polymorphism Based on a Common Structural Theme. International Journal of Biochemistry. **24**: 553-560.

29. Turnbull, J. E. and J. T. Gallagher. 1991. Sequence analysis of heparan sulphate indicates defined location of N-sulphated glucosamine and iduronate 2-sulphate residues proximal to the protein linkage region. Biochemical Journal. **277**: 297-303.

30. Ishihara, M., Y. Guo, Z. Wei, Z. Yang, S. J. Siedler, A. Orellana and C. B. Hirschberg. 1993. Regulation of Biosynthesis of the Basic Fibroblast Growth Factor Binding Domains of Heparan Sulfate by Heparan Sulfate-N-Deacetylase/N-Sulfotransferase Expression. Journal of Biological Chemistry. **268**: 20091-20095.

31. Noonan, B. M. and J. R. Hassell. ed. 1993. Proteoglycans of Basement Membranes. 189-210. in Rohrbach and Timpl: Molecular and Cellular Aspects of Basement Membranes. Academic Press, Inc., London.

32. Kato, M., Y. Koike, S. Suzuki and K. Kimata. 1988. Basement Membrane Proteoglycan in Various Tissues: Characterization Using Monoclonal Antibodies to EHS Low Density Heparan Sulfate Proteoglycan. The Journal of Cell Biolgy. **106**: 2203.

33. Heremans, A., B. Van der Schueren, B. De Cock, M. Paulsson, J. Cassiman, H. Van den Berghe and G. David. 1989. Matrix-associated Heparan Sulfate Proteoglycan: Core Protein-specific Monoclonal Antibodies Decorate the Pericellular Matrix of Connective Tissue Cells and Stromal Side of Basement Membranes. The Journal of Cell Biology. **109**: 3199-3211.

34. Kanwar, y. S. and M. G. Farquhar. 1979. Anionic Sites in the Glomerular Basement Membrane. In Vivo and In Vitro Localization to the Lamina Rarae by Cationic Probes. Journal of Cell Biology. **81**: 137-153.

35. Schittny, J. C., R. Timpl and J. Engel. 1988. High Resolution Immunoelectron Microscopic Localization of Functional Domains of Laminin, Nidogen, and Heparan Sulfate Proteoglycan in Epithelial Basement Membrane of Mouse Cornea Reveals Different Topological Orientations. The Journal of Cell Biology. **107**: 1599-1610.

36. Hassell, J. R., W. C. Leyshon, S. R. Ledbetter, B. Tyree, S. Suzuki, M. Kato, K. Kimata and H. K. Kleinman. 1985. Isolation of Two Forms of Basement Membrane Proteoglycan. The Journal of Biological Chemistry. **260**: 8098-8105.

37. Ledbetter, S. R., B. Tyree, J. R. Hassell and E. A. Horrigan. 1985. Identification of the Precursor Protein to Basement Membrane Heparan Sulfate Proteoglycans. The Journal of Biological Chemistry. **260**: 8106-8113.

38. Klein, D. J., D. M. Brown, T. R. Oegema, P. E. Brenchley, M. A. Dickinson, E. A. Horigan and J. R. Hassell. 1988. Glomerular Basement Membrane Proteoglycans are Derived From a Larger Precursor. The Journal of Cell Biology. **106**: 963.

39. Kato, M., Y. Koike, Y. Ito, S. Suzuki and K. Kimata. 1987. Multiple Forms of Heparan Sulfate Proteoglycan in the EHS Mouse Tumor. The Journal of Biological Chemistry. **262**: 7180.

40. Paulsson, M., P. D. Yurchenco, G. C. Ruben, J. Engel and R. Timpl. 1987. Structure of Low Density Heparan Sulfate Proteoglycan Isolated From a Mouse Tumor Basement Membrane. Journal of Molecular Biology. **197**: 297-313.

41. Noonan, D. M., A. Fulle, P. Valente, S. Cai, E. Horigan, M. Sasaki, Y. Yamada and J. R. Hassell. 1991. The Complete Sequence of Perlecan, a Basement Membrane Heparan Sulfate Proteoglycan, Reveals Extensive Similarity with Laminin A Chain, Low Density Lipoprotein-Receptor, and the Neural Cell Adhesion Molecule. The Journal of Biological Chemistry. **266**: 22939-22947.

42. Kallunki, P. and K. Tryggvason. 1992. Human Basement Membrane Heparan Sulfate Proteoglycan Core Protein: A 467-kD Protein Containing Multiple Domains Resembling Elements of the Low Density Lipoprotein Receptor, Laminin, Neural Cell Adhesion Molecules, and Epidermal Growth Factor. The Journal of Cell Biology. **116**: 559-571.

43. Murdoch, A. D., G. R. Dodge, I. Cohen, R. S. Tuan and R. V. Iozzo. 1992. Primary Structure of the Human Heparan Sulfate Proteoglycan from Basement Membrane (HSPG2/Perlecan). The Journal of Biological Chemistry. **267**: 8544-8557.

44. Baird, A. and P. Bohlen. ed. 1991. Fibroblast Growth Factors. 369-418. in Sporn and Roberts: Peptide Growth Factors and Their Receptors I. Springer-Verlag, New York.

45. Basilico, C. and D. Moscatelli. 1992. The FGF Family of Growth Factors and Oncogenes. Advances in Cancer Research. **59**: 115-165.

46. Baird, A., F. Esch, P. Mormede, N. Ueno, N. Ling, P. Bohlen, S. Ying, W. B. Wehrenberg and R. Guillemin. ed. 1986. Molecular Characterization of Fibroblast Growth Factor: Distribution and Biological Activities in Various Tissues. 143-200. in Greep: Recent Progress in Hormone Research. Academic Press, Inc., Orlando.

47. Cardin, A. D. and H. J. R. Weintraub. 1989. Molecular Modeling of Protein-Glycosaminoglycan Interactions. Arteriosclerosis. **9**: 21-32.

48. Baird, A., D. Schubert, N. Ling and R. Guillemin. 1988. Receptor- and Heparin-Binding Domains of Basic Fibroblast Growth Factor. PNAS. **85**: 2324-2328.

49. Seno, M., R. Sasada, T. Kurokawa and K. Igarashi. 1989. Carboxyl-Terminal Structure of Basic Fibroblast Growth Factor Significantly Contributes to Its Affinity for Heparin. 1990. **188**: 239-245.

50. Presta, M., M. Statuto, A. Isacchi, P. Caccia, A. Pozzi, A. Gualandris, M. Rusnati, L. Bergonzoni and P. Sarmientos. 1992. Structure-Function Relationship of Basic Fibroblast Growth Factor: Site-Directed Mutagenesis of a Putative Heparin-Binding

and Receptor-Binding Region. Biochemical and Biophysical Research Communications. **185**: 1098-1107.

51. Eriksson, A. E., L. S. Cousens, L. H. Weaver and B. W. Matthews. 1991. Three-dimensional Structure of Human Basic Fibroblast Growth Factor. PNAS. **1991**: 3441-3445.

52. Zhang, J., L. S. Cousens, P. J. Barr and S. R. Sprang. 1991. Three-dimensional structure of human basic fibroblast growth factor, a structural homolg of interleukin 1β. PNAS. **88**: 3446-3450.

53. Zhu, X., H. Komiya, A. Chirino, S. Faham, G. M. Fox, T. Arakawa, B. T. Hsu and D. C. Rees. 1991. Three-dimensional Structures of Acidic and Basic Fibroblast Growth Factors. Science. **251**: 90-93.

54. Faham, S., R. E. Hileman, J. R. Fromm, R. J. Linhardt and D. C. Rees. 1996. Heparin Structure and Interactions with Basic Fibroblast Growth Factor. Science. **271**: 1116-1120.

55. Habuchi, H., S. Suzuki, T. Saito, T. Tamura, T. Harada, K. Yoshida and K. Kimata. 1992. Structure of a Heparan Sulfate Oligosaccharide That Binds to Basic Fibroblast Growth Factor. Biochemical Journal. **285**: 805-813.

56. Turnbull, J. E., D. G. Fernig, Y. Ke, M. C. Wilkinson and J. T. Gallagher. 1992. Identification of the Basic Fibroblast Growth Factor Binding Sequence in Fibroblast Heparan Sulfate. The Journal of Biological Chemistry. **267**: 10337-10341.

57. Ishihara, M., D. J. Tyrrell, G. B. Stauber, S. Brown , L. S. Cousens and R. J. Stack. 1993. Preparation of Affinity-Fractionated, Heparin-Derived Oligosaccharides and Their Effects on Selected Biological Activities Mediated by Basic Fibroblast Growth Factor. The Journal of Biological Chemistry. **268**: 4675-4683.

58. Tyrrell, D. J., M. Ishihara, N. Rao, A. Horne, M. C. Kiefer, G. B. Stauber, L. H. Lam and R. J. Stack. 1993. Structure and Biological Activities of a Heparin-Derived Hexasaccharide with High Affinity for Basic Fibroblast Growth Factor. The Journal of Biological Chemistry. **268**: 4684-4689.

59. Gospodarowicz, D. and J. Cheng. 1986. Heparin Protects Basic and Acidic FGF From Inactivation. Journal of Cellular Physiology. **128**: 475-484.

60. Saksela, O., D. Moscatelli, A. Sommer and D. B. Rifkin. 1988. Endothelial Cell-derived Heparan Sulfate Binds Basic Fibroblast Growth Factor and Protects It from Proteolytic Degradation. The Journal of Cell Biology. **107**: 743-751.

61. D'Amore, P. A. 1990. Modes of FGF Release In Vivo and In Vitro. Cancer and Metastasis Reviews. **9**: 227-238.

62. Gajdusek, C. M. and S. Carbon. 1989. Injury-Induced Release of Basic Fibroblast Growth Factor From Bovine Aortic Endothelium. Journal of Cellular Physiology. **139**: 570-579.

63. Brooks, R. A., J. M. Burrin and E. M. Kohner. 1991. Characterization of Release of Basic Fibroblast Growth Factor From Bovine Retinal Endothelial Cells in Monolayer Cultures. Biochemical Journal. **276**: 113-120.

64. McNeil, P. L., L. Muthukrishnan, W. Warder and P. A. D'Amore. 1989. Growth Factors Are Released by Mechanically Wounded Endothelial Cells. The Journal of Cell Biology. **109**: 811-822.

65. Witte, L., Z. Fuks, A. Haimovitz-Friedman, I. Vlodavsky, D. S. Goodman and A. Eldor. 1989. Effects of Irradiation on the Release of Growth Factors from Cultured Bovine, Porcine, and Human Endothelial Cells. Cancer Research. **49**: 506-5072.

66. Mignatti, P., T. Morimoto and D. B. Rifkin. 1992. Basic Fibroblast Growth Factor, a Protein Devoid of Secretory Signal Sequence, Is Released by Cells via a Pathway Independent of the Endoplasmic Recticulum-Golgi Complex. Journal of Cellular Physiology. **151**: 81-93.

67. Moscatelli, D. 1987. High and Low Affinity Binding Sites for Basic Fibroblast Growth Factor on Cultured Cells: Absence of a Role for Low Affinity Binding in the Stimulation of Plasminogen Activator Production by Bovine Capillary Endothelial Cells. Journal of Cellular Physiology. **131**: 123-130.

68. Moscatelli. 1988. Metabolism of Receptor-bound and Matrix-bound Basic Fibroblast Growth Factor by Bovine Capillary Endothelial Cells. The Journal of Cell Biology. **107**: 753-759.

69. Rapraeger, A. C., A. Krufka and B. B. Olwin. 1991. Requirement of Heparan Sulfate for bFGF-Mediated Fibroblast Growth and Myoblast Differentiation. Science. **252**: 1705-1708.

70. Yayon, A., M. Klagsbrun, J. D. Esko, P. Leder and D. M. Ornitz. 1991. Cell Surface, Heparin-like Molecules Are Required for Binding of Basic Fibroblast Growth Factor to Its High Affinity Receptor. Cell. **64**: 841-848.

71. Nugent, M. A. and E. R. Edelman. 1992. Kinetics of Basic Fibroblast Growth Factor Binding to Its Receptor and Heparan Sulfate Proteoglycan: A Mechanism for Cooperativity. Biochemistry. **31**: 8876-8883.

72. Fannon, M. and M. A. Nugent. 1996. FGF binds its receptors, is internalized and stimulates DNA synthesis in Balb/c3T3 cells the absence of heparan sulfate. J. Biol. Chem. **271**: 17949-17956.

73. Jaye, M., J. Schlessinger and C. A. Dionne. 1992. Fibroblast Growth Factor Receptor Tyrosine Kinases: Molecular Analysis and Signal Transduction. Biochimica et Biophysica Acta. **1135**: 185-199.

74. Gospodarowicz, D., N. Ferrara, L. Schweigerer and G. Neufeld. 1987. Structural Characterization and Biological Functions of Fibroblast Growth Factor. Endocrine Reviews. **8**: 95-114.

75. Burgess, W. H. and T. Maciag. 1989. The Heparin-Binding (Fibroblast) Growth Factor Family of Proteins. Annual Review of Biochemistry. **58**: 575-606.

76. Baird, A. 1993. Fibroblast Growth Factors: What's In a Name. Endocrinology. **132**: 487-488.

77. Hori, A., R. Sasada, E. Matsutani, K. Naito, Y. Sakura, T. Fujita and Y. Kozai. 1991. Suppression of Solid tumor Growth by Immunoneutralizing Monoclonal Antibody Against Human Basic Fibroblast Growth Factor. Cancer Research. **51**: 6180-6184.

78. Pesenti, E., F. Sola, N. Mongelli, M. Grandi and F. Spreafico. 1992. Suramin Prevents Neovascularisation and Tumor Growth Through Blocking of Basic Fibroblast Growth Factor Activity. British Journal of Cancer. **66**: 367-372.

79. Baird, A. and N. Ling. 1987. Fibroblast Growth Factors are Present in the Extracellular Matrix Produced by Endothelial Cells In Vitro: Implications for a Role of Heparinase-like Enzymes in the Neovascular Process. Biochemical and Biophysical Research Communications. **142**: 428-435.

80. Vlodavsky, I., J. Folkman, R. Sullivan, R. Fridman, R. Ishai-Michaeli, J. Sasse and M. Klagsbrun . 1987. Endothelial cell-derived basic fibroblast growth factor: Synthesis and deposition into subendothelial extracellular matrix. PNAS. **84**: 2292-2296.

81. Globus, R. K., J. Plouet and D. Gospodarowicz. 1989. Cultured Bovine Bone Cells Synthesize Basic Fibroblast Growth Factor and Store it in Their Extracellular Matrix. Endocrinology. **124**: 1539-1547.

82. Bashkin, P., S. Doctrow, M. Klagsbrun, C. M. Svahn, J. Folkman and I. Vlodavsky. 1989. Basic Fibroblast Growth Factor Binds to Subendothelial Extracellular Matrix and Is Released by Heparitinase and Heparin-like Molecules. Biochemistry. : 1737-1743.

83. Jeanny, J., N. Fayein, M. Moenner, B. Chevallier, D. Barritault and Y. Courtois. 1987. Specific Fixation of Bovine Brain and Retinal Acidic and Basic Fibroblast Growth Factors to Mouse Embryonic Eye Basement Membranes. Experimental Cell Research. **171**: 63-75.

84. Vigny, M., M. P. Ollier-Hartmann, M. Lavigne, N. Fayein, J. C. Jeanny, M. Laurent and Y. Courtois. 1988. Specific Binding of Basic Fibroblast Growth Factor to Basement Membrane-Like Structure and to Purified Heparan Sulfate Proteoglycan of the EHS Tumor. Journal of Cellular Physiology. **137**: 321-328.

85. Presta, M., J. A. M. Maier, M. Rusnati and G. Ragnotti. 1989. Basic Fibroblast Growth Factor is Released From Endothelial Extracellular Matrix in a Biologically Active Form. Journal of Cellular Physiology. **140**: 68-74.

86. Rogelj, S., M. Klagsbrun, R. Atzmon, M. Kurokawa, A. Haimovitz, Z. Fuks and I. Vlodavsky. 1989. Basic Fibroblast Growth Factor Is an Extracellular Matrix Component Required for Supporting the Proliferation of Vascular Endothelial Cells and the Differentiation of PC12 Cells. The Journal of Cell Biology. **109**: 823-831.

87. Flaumenhaft, R., D. Moscatelli, O. Saksela and D. B. Rifkin. 1989. Role of Extracellular Matrix in the Action of Basic Fibroblast Growth Factor: Matrix as a Source of Growth Factor for Long-Term Stimulation of Plasminogen Activator Production and DNA Synthesis. Journal of Cellular Physiology. **140**: 75-81.

88. Vlodavsky, I., P. Bashkin, R. Ishai-Michaeli, R. Chajek-Shaul, R. Bar-Shavit, A. Haimovitz-Friedman, M. Klagsbrun and Z. Fuks. ed. 1991. Sequestration and Release of Basic Fibroblast Growth Factor. in Baird and Klagsbrun: The Fibroblast Growth Factor Family. New York Academy of Sciences, New York.

89. Saksela, O. and D. B. Rifkin. 1990. Release of Basic Fibroblast Growth Factor-Heparan Sulfate Complexes from Endothelial Cells by Plasminogen Activator-mediated Proteolytic Activity. The Journal of Cell Biology. **110**: 767-775.

90. Ishai-Michaeli, R., A. Eldor and I. Vlodavsky. 1990. Heparanase Activity Expressed by Platelets, Neutrophils, and Lymphoma Cells Releases Active Fibroblast Growth Factor From Extracellular Matrix. Cell Regulation. **1**: 833-842.

91. Flaumenhaft, R., D. Moscatelli and D. B. . Rifkin. 1990. Heparin and Heparan Sulfate Increase the Radius of Diffusion and Action of Basic Fibroblast Growth Factor. The Journal of Cell Biology. **111**: 1651-1659.

92. Dabin, I. and Y. Courtois. 1991. In Vitro Kinetics of Basic Fibroblast Growth Factor Diffusion Across a Reconstituted Corneal Endothelium. Journal of Cellular Physiology. **147**: 396-402.

93. Flaumenhaft, R. and D. B. Rifkin. 1992. The Extracellular Regulation of Growth Factor Action. Molecular Biology of the Cell. **3**: 1057-1065.

94. Vlodavsky, I., G. Korner, A. Eldor, R. Bar-Shavit, M. Klagsbrun and Z. Fuks. ed. 1993. Extracellular Matrix-Resident Growth Factors and Enzymes. 463-489. in Zern and Reid: Extracellular Matrix. Marcel Dekker Inc., New York.

95. Phillies, G. D. J. 1989. The Hydrodynamic Scaling Model for Polymer Self-Diffusion. Journal of Physical Chemistry. **93**: 5029-5039.

96. Ogston, A. G., B. N. Preston and J. D. Wells. 1973. On the Transport of Compact Particles Through Solutions of Chain-Polymers. Proceedings of the Royal Society of London. **333**: 297-316.

97. Peppas, N. A. and C. T. Reinhart. 1983. Solute Diffusion in Swollen Membranes. Journal of Membrane Science. **15**: 275-287.

98. Phillips, R. J., W. M. Deen and J. F. Brady. 1989. Hindered Transport of Spherical Macromolecules in Fibrous Membranes and Gels. AIChE Journal. **35**: 1761-1769.

99. Brady, J. 1994. Hindered Diffusion. AICHE Annual Meeting. 320.

100. Johnson, E. M., D. A. Berk, R. K. Jain and W. M. Deen. 1995. Diffusion and Partitioning of Proteins in Charged Agarose Gels. Biophysical Journal. **68**: 1561-1568.

101. Ogston, A. G. 1958. The Spaces in a Uniform Random Suspension of Fibers. Transactions of the Faraday Society. **54**: 1754-1757.

102. Fanti, L. A. and E. D. Glandt. 1990. Partitioning of Spherical Particles into Fibrous Matrices. Journal of Colloid and Interface Science. **135**: 385-395.

103. Carslaw, H. S. 1906. Fourier's Series and Integrals. Macmillan, New York.

104. Daynes, H. A. 1920. The Process of Diffusion through a Rubber Membrane. Proceedings of the Royal Society of London. **97A**: 286-307.

105. Edelman, E. R., M. A. Nugent and M. Karnovsky. 1993. Perivascular and Intraveneous Administration of Basic Fibroblast Growth Factor: Vascular and Solid Organ Deposition. PNAS. **90**: 1513-1517.

106. Riley, B. R., M. P. Savage, K. Simandl, B. B. Olwin and J. F. Fallon. 1993. Retroviral expression of FGF-2 (bFGF) affects patternin in chick limb bud. Development. **118**: 95-104.

107. Slack, J. M. W. and H. V. Isaacs. 1994. The role of fibroblast growth factor in early *Xenopus* development. Biochemical Society Transactions. **22**: 585-589.

108. Handler, M., P. D. Yurchenco and R. V. Iozzo. 1997. Developmental expression of perlecan during murine embryogenesis. Developmental Dynamics. **210**: 130-145.

109. Farndale, R. W., D. J. Buttle and A. J. Barret. 1986. Improved Quantitation and Discrimination of Sulphated Glycosaminoglycans by Use of Dimethylmethylene Blue. Biochimica et Biophysica Acta. **883**: 173-177.

110. Bradford, M. M. 1976. A rapid and sensitive method for the quantitation of microgram quantities of protein utilizing the principle of protein-dye binding. Analytical Biochemistry. **72**: 248-254.

111. Forsten, K. F., N. A. Courant and M. A. Nugent. 1997. Endothelial Proteoglycans Inhibit bFGF Binding and Mitogenesis. Journal of Cellular Physiology. **172**: 209-220.

112. Conrad, H. E. ed. 1995. Beta Elimination for Release of O-linked Glycosaminoglycans from Proteoglycans. 17.15.1-17.15.3. in Chanda: Current Protocols in Molecular Biolgy. J. Wiley and Sons,

113. Wasteson, A. 1971. A Method for the Determination of the Molecular Weight and Molecular-Weight Distribution of Chondroitin Sulfate. Journal of Chromatography. **59**: 87-97.

114. Bitter, T. and H. M. Muir. 1962. A Modified Uronic Acid Carbazole Reaction. Analytical Biochemistry. **4**: 330-334.

115. Jakus, M. A. 1956. Studies on the Cornea. II. The Fine Structure of Descemet's Membrane. Journal of Biophysical and Biochemical Cytology. **2**: 243-250.

116. Morton, K., C. Hutchinson, J. C. Jeanny, I. Karppouzas, Y. Pouliquen and Y. Courtois. 1989. Colocalization of Fibroblast Growth Factor Binding Sites With Extracellular Matrix Components in Normal and Keratoconus Corneas. Current Eye Research. **8**: 975-987.

117. Wormer, W., K. Sames and J. W. Rohen. 1979. Histochemiche Untersuchungen uber Struktur und Alternsveranderungen der Descemetschen Membran beim Rind. Albrecht v. Graefes Arch. klin. exp. Opthal. **211**: 271-278.

118. Murphy, C., J. Alvarado and R. Juster. 1984. Prenatal and Postnatal Growth of the Human Descemet's Membrane. Investigative Ophthalmology and Visual Science. **25**: 1402-1415.

119. McManas, J. F. A. 1946. Histological Demonstration of Mucin after Periodic Acid. Nature London. **158**: 202.

120. Hascall, V. C. and K. J. H. ed. 1982. Proteoglycans: Isolation and Purification. 769-800. in Cunningham and Frederiksen: Methods in Enzymology. Academic Press, New York.

121. Whitelock, J. M., A. D. Murdoch, R. V. Iozzo and P. A. Underwood. 1996. The Degradation of Human Endothelial Cell-Derived Perlecan and Release of Bound basic Fibroblast Growth Factor by Stromelysin, Collagenase, Plasmin, and Heparanases. Journal of Biological Chemistry. **271**: 10079-10086.

122. Reubsael, F. A. G., J. P. M. Langeveld and J. H. Veerkamp. 1985. Glycosaminoglycan content of glomerular and tubular basement membrane of various mammalian species. Biochimica et Biophysica Acta. **838**: 144-150.

123. Fujiwara, S., M. Dziadek, H. Wiedemann, R. Timpl, A. Lustig and J. Engel. ed. 1985. Structure, Interaction and Immunological Characterization of Heparan Sulfate Proteoglycans from a Mouse Tumor Basement Membrane. 49-60. in Shibata: Basement Membranes. Elsevier Science Publishers B. V. (Biomedical Division), Amsterdam.

124. Hassell, J. R., P. G. Robey, H. Barrach, J. Wilczek, S. I. Rennard and G. R. Martin. 1980. Isolation of a Heparan Sulfate-Containing Proteoglycan from Basement Membrane. Proc. Natl. Acad. Sci. USA. **77**: 4494-4498.

125. Kato, M., H. Wang, M. Bernfield, J. T. Gallagher and J. E. Turnbull. 1994. Cell Surface Syndecan-1 on Distinct Cell Types Differs in Fine Structure and Ligand Binding of Its Heparan Sulfate Chains. Journal of Biological Chemistry. **269**: 18881-18890.

126. Moscatelli, D. 1992. Basic Fibroblast Growth Factor (bFGF) Dissociates Rapidly from Heparan Sulfates by Slowly from Receptors. The Journal of Biological Chemistry. **267**: 25803-25809.

127. Chintala, S. K., R. P. Miller and C. A. McDevitt. 1994. Basic Fibroblast Growth Factor Binds to Heparin Sulfate in the Extracellular Matrix of Rat Growth Plate Chodrocytes. Archives of Biochemistry and Biophysics. **310**: 180-186.

128. Krause, A. C. 1934. The Biochemistry of the Eye. The Johns Hopkins Press, Baltimore.

129. Coster, L., C. Cintron, S. P. Damle and J. D. Gregory. 1983. Proteoglycans of Rabbit Cornea: Labelling in Organ Culture and in vivo. Experimental Eye Research. **36**: 517-530.

130. Gregory, J. D., L. Coster and S. P. Damle. 1982. Proteoglycans of Rabbit Corneal Stroma. The Journal of Biological Chemistry. **257**: 6965-6970.

131. Malmsten, M. 1995. Ellipsometry studies ofthe effects of surface hydrophobicity on protein adsorption. Colloids and Surfaces B: Biointerfaces. **3**: 297-308.

132. Suzawa, T. and H. Shirahama. 1991. Adsorption of Plasma Proteins onto Polymer Latices. Advances in Colloid and Interface Science. **35**: 139-172.

133. Karlstrom, G. and O. Engkvist. ed. 1997. Theory of Poly(ethylene glycol) in Solution. 16-30. in Harris and Zalipsky: Poly (ethylene glycol) Chemistry and Biological Applications. American Chemical Society, Washington ,DC.

134. Amiji, M. and K. Park. 1992. Prevention of Protein Adsorption and Platelet Adhesion on Surfaces by PEO/PPO/PEO triblock copolymers. Biomaterials. **13**: 682-690.

135. Sofia, S. J. and E. W. Merrill. ed. 1997. Protein Asorption on Poly(ethylene oxide)-Grafted Silicaon Surfaces. 342-360. in Harris and Zalipsky: Poly (ethylene glycol) Chemistry and Biological Applications. American Chemical Society, Washington ,DC.

136. Sofia, S. J. and E. W. Merrill. 1998. Grafting of PEO to polymer surfaces using electron beam irradiation. Journal of Biomedical Materials Research. **40**: 153-163.

137. Regnier, F. E. and R. Noel. 1976. Glycerolpropylsilane Bonded Phases in the Steric Exclusion Chromatography of Biological Macromolecules. Journal of Chromatographic Science. **14**: 316-320.

138. Poitevin, E. and P. Wahl. 1988. Study of the Translational Diffusion of Macromolecules in Beads of Gel Chromatography by the FRAP method. Biophysical Chemistry. **31**: 247-258.

139. diGiovine, F. S. and G. W. Duff. 1990. Interleukin 1: The First Interleukin. Immunology Today. **11**: 13-20.

140. Clore, G. M. and A. M. Gronenborn. 1991. Comparison of the Solution Nuclear Magnetic Resonance and X-ray Crystal Structures of Human Recombinant Interleukin-1β. Journal of Molecular Biology. **221**: 47-53.

141. Moy, F. J., A. P. Seddon, P. Bohlen and R. Powers. 1996. High-Resolution Solution Structure of Basic Fibroblast Growth Factor Determined by Multidimensional Heteronuclear Magnetic Resonance Spectroscopy. Biochemistry. **35**: 135221-13561.

142. Neufeld, G. and D. Gospodarowicz. 1987. Protamine sulfate inhibits mitogenic activities of the extracellular matrix and fibroblast growth factor, but potentiates that of epidermal growth factor. Journal of Cellular Physiology. **132**: 287-294.

143. Kim, J. H., K. Green, M. Martinez and D. Paton. 1971. Solute Permeability of the Corneal Endothelium and Descemet's Membrane. Experimental Eye Research. **12**: 231-238.

144. Fatt, I. 1969. Permeability of Descemet's Membrane to Water. Experimental Eye Research. **8**: 340-354.

145. Chrambach, A. and D. Rodbard. 1971. Polyacrylamide Gel Electrophoresis. Science. **172**: 440-451.

146. Ticha, M., B. Zelezna, V. Jonakova and K. Filka. 1994. Immobilization of Heparin on Polyacrylamide Derivatives. Journal of Chromatography B: Biomedical Applications. **656**: 423-426.

147. Miura, R. O., S. Yamagata, Y. Miura, T. Harada and T. Yamagata. 1995. Analysis of Glycosaminoglycan-Degrading Enzymes by Substrate Gel Electrophoresis (Zymography). Analytical Biochemsitry. **225**: 333-340.

148. Gong, H., K. Brown, M. Johnson, R. D. Kamm and T. F. Freddo. 1997. Hydraulic conductivity of juxtacanalicular connective tissue using quick-freeze/deep-etch. The Association for Research in Vision and Ophthalmology. **384**: S564.

149. Raphael, B. and B. J. McLaughlin. 1990. Adsorptive and fluid phase endocytosi by cultured rabbit corneal endothelium. Current Eye Research. **9**: 249-258.

150. Noske, W., M. Fromm, B. Levarlet, K. M. Kreusel and M. Hirsch. 1994. Tight junctions of the human corneal endothelium: morphological and electrophysical features. German Journal of Ophthalmology. **3**: 253-257.

151. Tripathi, R. C., S. C. Borisuth and B. J. Tripathi. 1992. Detection, Quanitfication, and Significance of Basic Fibroblast Growth Factor in the Aqueous Humor of Man Cat Dog and Pig. Experimental Eye Research. **54**: 447-454.

152. Wolpert, L. 1971. Postional information and pattern formation. Current Topics in Developmental Biology. **6**: 183-224.

153. Child, C. M. 1941. Patterns and Problems of Development. University of Chicago Press, Chicago.

154. Reichsman, F., L. Smith and S. Cumberledge. 1996. Glycosaminoglycans can modulate extracellular localization of the wingless protein and promote signal transduction. Journal of Cell Biology. **135**: 819-827.

155. Binari, R. C., B. E. Staveley, W. A. Johnson, R. Godavarti and R. Sasisekharan. 1997. Genetic evidence that heparin-like glycosaminoglycans are involved in wingless signaling. Development. **124**: 2623-2632.

156. Sayle, R. 1995. RasMol.

157. Abola, E. E., F. C. Bernstein, S. H. Bryant, T. F. Koetzle and J. Weng. 1987. Protein Data Bank, in Crystallographic Databases-Information Content, Software Systems, Scientific Applications. Allen, Bergerhoff and Sievers. Data Commission of the International Union of Crystallography, Bonn/Cambridge/Chester.

158. Bernstein, F. C., T. F. Koetzle, G. J. B. Williams, E. F. Meyer, M. D. Brice, J. R. Rodgers, O. Kennard, T. Shimanouchi and M. Tasumi. 1977. The Protein Data Bank: a Computer-based Archival File for Macromolecular Structures. Journal of Molecular Biology. **112**: 535-542.